Politecnico di Milano
Dipartimento di Elettronica e Informazione
Dottorato di Ricerca in Ingegneria dell'Informazione

Study of an Anthropomorphic Artificial Arm for application in Humanoid Robotics

Sviluppo di un arto artificiale superiore antropomorfo per applicazioni nel campo della Robotica Umanoide

Tesi di dottorato di:
Michele Folgheraiter

Relatore:
Prof.ssa Giuseppina Gini
Tutore:
Prof. Marco Colombetti
Coordinatore del programma di dottorato:
Prof. Stefano Crespi Reghizzi

XVI ciclo

Politecnico di Milano
Dipartimento di Elettronica e Informazione
Piazza Leonardo da Vinci 32 I 20133 — Milano

Politecnico di Milano
Dipartimento di Elettronica e Informazione
Dottorato di Ricerca in Ingegneria dell'Informazione

Study of an Anthropomorphic Artificial Arm for application in Humanoid Robotics

Ph.D. Dissertation of:
Michele Folgheraiter

Advisor:
Prof.ssa Giuseppina Gini
Tutor:
Prof. Marco Colombetti
Supervisor of the Ph.D. Program:
Prof. Stefano Crespi Reghizzi

XVI edition

Acknowledgements

I owe a huge debt of gratitude to my advisor, Prof.ssa Giuseppina Gini. She made my enrollment at the Ph.d program possible by offering the financial support and continuing to support me during the studies.

I would like to thank Barbara Webb for the time spent in reading this manuscript and for the comments and suggestions that she gave me to improve the thesis.

A big thank also to my tutor Prof. Marco Colombetti, the Ph.d program coordinator Prof. Stefano Crespi Reghizzi, Prof. Andrea Bonarini and all the Artificial Intelligence and Robotics group. I want also to remember Prof. Marco Somalvico for his encouragements and teachings; he will remain in my memory.

I am thankful to all my friends and especially to Antonietta.

Finally a big big thank to my family which fully support all my decisions and dreams.

Summary

The main goal of this research was the development of a human-like artificial arm for application in the field of humanoid robotics. Because of its multidisciplinary nature, the research focused on many tasks. A kinematic and dynamic model of the arm was formalized. A neurally-inspired control, emulating the spinal cords circuits, was implemented and tested on the model. The efficacy of a reflex module, in controlling the single joint position and stiffness was demonstrated, and results compared with those of a human limb. The inverse kinematic was implemented using a neural network and the module was integrated with an high level control system based on the actual knowledge of the human cerebellum and motor cortex. A real robotics arm was also designed and developed, and the basic control strategies tested in real time. In comparison with analogous systems, the arm presents a novel three degrees of freedom shoulder and one degree of freedom elbow actuated by seven artificial muscles.

Sommario

Lo scopo principale di questa ricerca é stato quello di studiare e sviluppare un braccio artificiale human-like, per applicazione nel campo della Robotica Umanoide. Questo ha richiesto l'implementazione di un modello cinematico e dinamico del sistema, sul quale poi é stato testato un controllore neurale in grado di emulare i circuiti presenti all'interno della spina dorsale umana. E' stata dimostrata l'efficacia del sistema di controllo nel regolare la posizione e la rigidita' di ogni singolo giunto, e i risultati sono stati comparati con esperimenti analoghi fatti sul braccio umano. La cinematica inversa é stata implementata mediante rete neurale, e il sistema é stato poi integrato con un controllore ad alto livello basato sulle conoscenze attuali sul cervelletto e la corteccia motoria umana. E' stato progettato e realizzato un braccio robotico sul quale sono state testate le strategie di controllo in real-time. Rispetto sistemi analoghi, il braccio artificiale presenta un'innovativa spalla a tre gradi di liberta' e un gomito ad un grado di liberta' attuati mediante sette muscoli artificiali.

Contents

List of Figures

List of Tables

1 Introduction

The goal of this study is to develop an Artificial Arm that mimics the morphology and the functionality of a human limb. The approach that I have adopted is in accordance with the general view of the Biorobotics field. People involved in this Robotics branch, [5], [6], [7], [8], [9], [10] believe that studying and mimicking a biological organism allows us to synthesize a robot with more powerful characteristics and functionalities than a classical robot, as well as to better understand the organism itself. Indeed, if we think of the history of technology, often humans were inspired by nature. Famous are the studies conducted by Leonardo da Vinci between 1487 and 1497 on the flying machines, that were inspired by the birds. This does not mean that observing and studying nature we can find out the best solution for a specific problem. In fact, for example, our technology can synthesize flying machines that are much faster than any biological organism.

In this first chapter I introduce the context of Humanoid Robotics as a subfield of Biorobotics; I also point out the state of the art both in terms of the classical and the bio-mimetic approach in controlling the arm. Finally I explain the methodology followed in this study.

1.1 The Humanoid Robotics Field

"Humanoid Robotics" denotes a particular Biorobotics subfield.
As mentioned before, biorobotics has the main goal to create robots able to mimic some behaviors typical of a biological organism. In Humanoid Robotics the organism to mimic is a human being.
To create an artificial machine with human morphology and behaviors is a very old human dream. There are some historical documents that ascribe to Heron of Alexandria ($\sim 200AD$), the building of some automaton puppets worked by strings, drums and weights. Also Leonardo da Vinci in 1495, inspired by Greek books, designed a mechanical knight able to autonomously move arms and head .
The modern Humanoid Robotics was born in Japan, where in 1973 at

the Waseda University was built the first humanoid robot, WABOT-1 (Figure 1.1). Wabot-1 was able to walk (in statical condition), manipulate simple objects and communicate with a human being using the natural language.

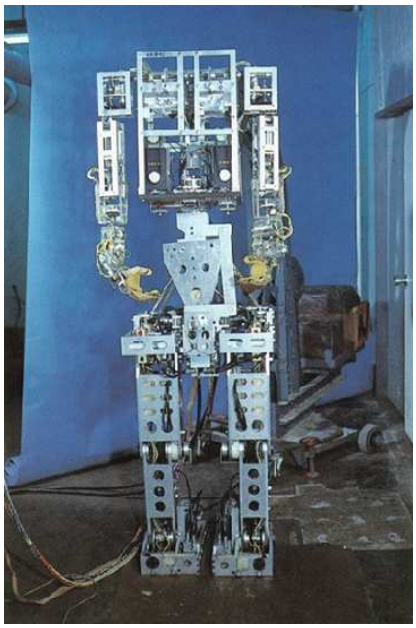

Figure 1.1: Wabot-1 was the first humanoid robot, builded in 1973 at Waseda University, Japan (with permission of Prof. Shigeki Sugano).

Although there are some example of full size humanoid robots, until now build and study such a systems requires a big amount of time and resources. Furthermore it is necessary effort many scientific and technical problems. Therefore many robotic groups, involved in this field, have chose to concentrate their attention on specific sub-problems. For example there are researches on manipulation systems, on walking stability, on vision-manipulation coordination etc.
An important project of intelligent vision-manipulation system started at Massachusetts Institute of Technology (Boston) in 1993. Here Rodney A. Brooks and his team developed "COG" [11] an anthropomorphic robot. The COG(Figure1.2) project has two main goals: the first is to build a general purpose robot and the second is to better understand the mechanism that governs the human perception.

Cog has 21 degrees of freedom (DOF) that permit it to realize movements comparable with those of the human torso. Each joint is controlled

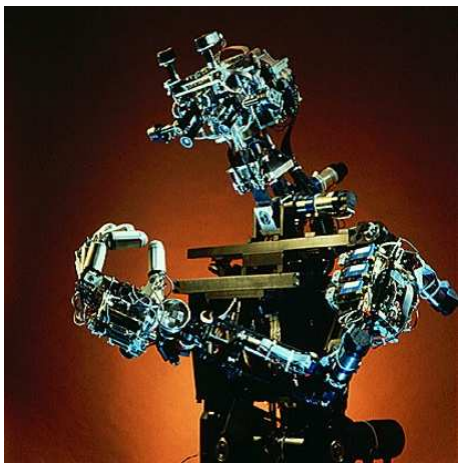

Figure 1.2: The COG robot, MIT, 1993 (with permission of Prof. Rodney A. Brooks)

by an independent electronic circuit that receives commands coming from a higher level controller. The robot's "brain" is located in a computer network that acquires the sensorial data and plans the next action autonomously.
Also the National American Space Agency (NASA) is interested in developing humanoid robots. The main idea of their Robonaut project [12] is to build an autonomous robot able to support astronauts during the extravehicular activities. Presently the robot is operated by a remote station, using sophisticated tele-presence and haptic interfaces. The robot can manipulate tools, and perform a task in collaboration with a human being.

A beautiful example of a full size humanoid robot is "DB"; this system was born from the collaboration between the Japan Science and Technology Corporation and the Sarcos company (Figure1.4). The robot is approximately 1.85 meters tall, weighs 80 kg, and contains 25 linear hydraulic actuators and five rotary hydraulic actuators. It has 30 degrees of freedom: seven in each arm, three in the neck, two in each eye, three in each leg, and three in the trunk. At the moment the robot is sustained by a special structure which allows the robot to remain in the stand up position. Every DOF is equipped with a position sensor and a force sensor except the eye's DOF.
The principal goal pursued by the team working on this robot, is to teach it new movements by demonstration. Indeed the robot can learn a new motion primitive by observing a human being performing it, and subsequently adjusting the learned movement to the task currently per-

Figure 1.3: The Robonaut humanoid robot, NASA.

formed [13]. According to this control strategy, imitation speeds up the learning process, especially in a complex multi-dimensional motor system, such as a humanoid robot.

Not only academic research, but also industrial research is interested in the humanoid robotics field. A well known example is the Honda company that right now with "Asimo" is at its fourth generation humanoid robot. Honda is interested in developing humanoid robots not only for technology prestige, but also because they are convinced that in a near future this kind of system will have practical and useful applications. With other purposes the Sony company developed its small size humanoid robot the "SDR-4X" only for the entertainment market.

1.1.1 Why Emulate Human Body Morphology and Functionalities

An important question is: why emulate the human body? Many scientists involved in this field are convinced that for a robot whose purpose is to work with people, human morphology is necessary. In millions of years the human species has adapted the environment to its needs, developing tools and things that are suitable for its morphology. So, if we want a robot to collaborate with a human being in a unstructured environment, it must have human shape and human-like manipulation capabilities. It is clear that, from a technical point of view, it is not possible, and at the same time not necessary, to reproduce in detail the

Figure 1.4: The DB humanoid robot, Japan Science Technology Corporation and Sarcos company (copyrighted by the ATR/CNS Laboratory)

human body's functionalities and morphology. Instead what is desirable for a futuristic humanoid robot is the same human mobility, manipulation capability and adaptability. Another aspect that justifies research in this field, as well as in the biorobotics field in general, is the utilization of biomimetic robotic systems as a new tool to investigate cognitive and biological questions. Collaboration between neurologists, psychologists and roboticians can be a useful way to improve in each specific field. Engineers can be inspired by neurological and psychological studies in the synthesis of the artificial system, and at the same time, neurologists and psychologists can better understand the biological system analyzing results coming from the experimentation on the artificial system.

1.1.2 An Overview of some Humanoid Robotics Arm Projects

Robotics since its historical origin was involved in replicating human manipulation capabilities. In order to better understand the motivation pushing researchers toward humanoid robotics it is useful to look at the robot arms' history. One of the first robots for research purpose was the Stanford arm, designed in the Stanford Artificial Intelligence Lab. This

robot has 6 DOFs, five revolute joints and one prismatic, therefore it can not be classified as anthropomorphic, nevertheless it was one of the first attempt to reproduce human arm manipulation capabilities.

In the sixties General Motor (the first to apply a robot in industry) financed a research program at MIT that developed another famous robot: the PUMA (Programmable Universal Manipulator for assembly).
This manipulator has 6 rotational DOF's and therefore it is classified as anthropomorphic; we can say that this robot was clearly inspired by biology. Indeed it is possible to compare this robot to a human arm; we can divide the mechanical structure in three principal blocks: the shoulder with two DOF, the elbow with 1 DOF and the wrist with another three DOF. The Puma has a dexterity that is quite near to that of a human arm, even though the human shoulder has more than two DOF. The analogy between the human arm and the PUMA manipulator is true only from a kinematic point of view, because the two systems have completely different performances. We can assert that this robot is more precise than the human arm, but at the same time the human arm can exhibit a compliant behavior that is indispensable to perform certain tasks like use a screwdriver or clean a complex surface.

It is clear that for industrial applications, a classical manipulator is better than a human arm. For example a manipulator is stronger than a human limb. The load for a medium size robot is about 10 Kg, but a human being finds it difficult to move, in every position of the workspace, such a weight. Manipulators are more precise and accurate in positioning the end-effector and furthermore they are free from fatigue problems that affect the human arm during intense activities.
Nevertheless from another point of view, the human arm is superior to robots. It is lighter and therefore it has a big force to weight ratio (100N/20N=5) with respect to an artificial manipulator(100N/3000N=0.03).
Right now, with present technology, we are far away from the possibility to emulate human arm efficiency and functionality. What is lacking today is a system that presents the same flexibility and the same compliant behavior as the human limb. In this context, the applicability of industrial robots remains confined in the factories. Therefore, at the moment, a lot of research in order to bring robot systems also in the household and in the public environments is still needed.
Right now there are many research groups involved in developing humanoid artificial arms; usually the simple robot structure comprises one or two arms, a torso and a head equipped with a vision system. Because light-weight and a compliant behavior is needed for the robot, a lot of research was done on novel actuators able to mimic, at list from the macroscopic point of view, the human muscle.

At the Center for Intelligent Systems (Vanderbilt University) Prof. Kawamura and its group are working on the ISAC humanoid robot (Figure 1.5).

This robot consists of a human-like trunk equipped with two six-DOF arms moved by McKibben artificial muscles [8]. The system has also a four-DOF stereo vision head with voice recognition that permits interaction between the robot and humans.

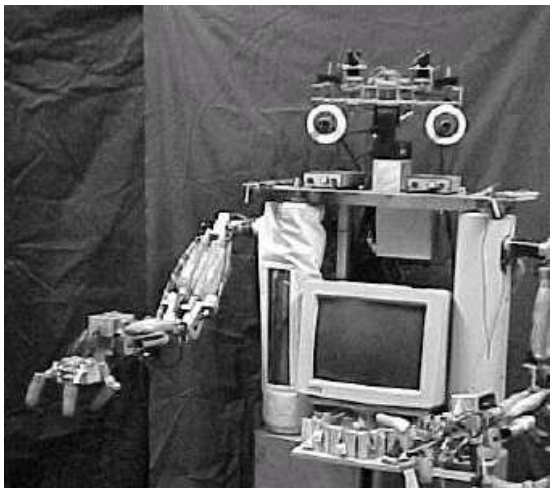

Figure 1.5: Humanoid Robot Isac, Center for Intelligent System, Vanderbilt University (with permission of Prof. K. Kawamura))

Each joint is actuated by two antagonistic actuators that are controlled by a system able to emulate the electromyogram patterns (EMG) of a human muscle. In particular the pressure inside the actuator is governed by a control signal analogous to the tonic and phasic activation of the muscle; it consists in three phases (agonist-antagonist-agonist) that permits the single joint to reach a precise position. The sensorial information are used to correct for misperceived loading conditions and to compensate eventually variations of the physical characteristics of the robot's actuators. The arm, during a fast reaching movement, can avoid an obstacle performing a reflex behavior [14], furthermore the phasic pattern is autonomously adjusted when a reach trajectory doesn't closely match a desired response. The main advantage of this bio-mimetic control architecture is the possibility to reduce the joint stiffness during a movement execution; this permits at the same time to save energy and to perform movements that are not dangerous for human beings.
Another project in the same direction is that one at the Biorobotics Lab-

oratory in Washington University. Here Prof. Hannaford and his team have worked intensely on the emulation of the human arm [15] [7]. The goal of this research is to transfer knowledge from human neuro-musculo-skeletal motion control to robotics in order to design an "anthroform" robotic arm system(Figure1.6). They introduce the new word "anthroform" to describe a robotic arm in which all aspects of its design are specified in terms of emulation of the corresponding functions of the human arm. They tested the elastic property of the McKibben actuators [16] [17] and proposed a more accurate dynamic model. In comparison with experiments conducted on human and animals muscle [18] they show how this type of actuators are, actually, the best choice to implement an anthropomorphic robot arm. Following the bio-mimetic approach they developed also a new kind of sensor [19] [20], whose purpose is to replicate a mammalian muscle spindle cell, that measures the contraction and the muscle velocity.

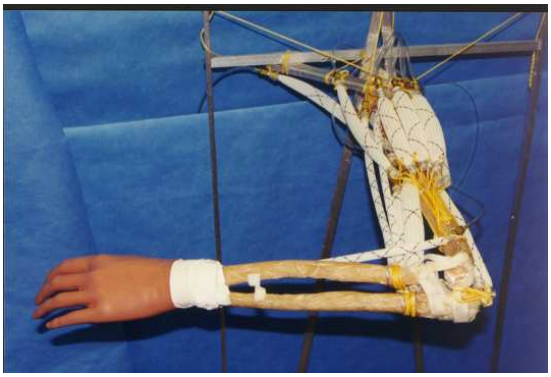

Figure 1.6: "Anthroform" Arm, Biorobotics Laboratory, Washington University (with permission of Prof. Blake Hannaford)

Since they maintain that is very hard to create a realistic model of the human arm, they prefer to make experiments directly on the robotic arm and subsequently compare the data with that of a human limb. They are interested not only in the emulation of the human arm actuation system but also in the emulation of the spinal cord reflexes to control the artefact. Here, in comparison with the Kawamura et al. approach, they based the control system on studies conducted by neurophysiologists on the neural circuits delegated to generate the basic arm reflexes. In order to build a real time controller they implemented the neural circuit in a DSP (Digital Signal Processor) and acquired data coming from the force and position sensor with a dedicated computer (Figure 1.7).

We can see in figure 1.7 that the test bed system takes in account

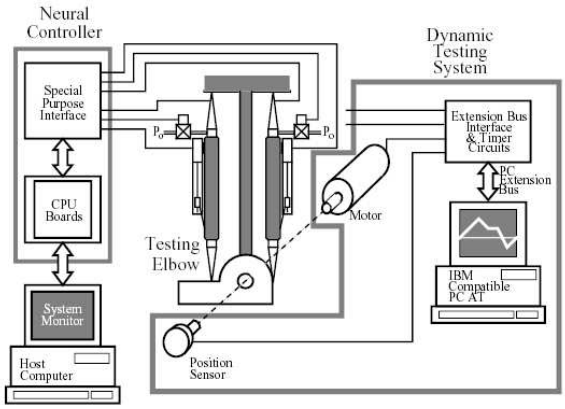

Figure 1.7: Hannaford et al. experimental System (with permission of Prof. Blake Hannaford)

only the elbow movements. The principal experiment conducted on this system was the cyclic application of a noise force on the forearm and the measurements of the joint angle deviation. This was made in many conditions and changing the neural network parameters. After a large amount of experiments they calculate the covariance between the more important variables in order to better understand their correlation. This analysis shows which are the variables and the sub-networks involved in a certain behavior, and allows formalizing hypothesis also on the human limb. The results show that muscle co-contraction and other circuit parameters can regulate the joint stiffness and damping.

1.2 Classical Approaches on the Control of the Robotics Arm

A problem to solve in order to perform a useful task with a manipulator is the generation of the end-effector trajectory. Usually a start and a goal position and orientation for the hand are assigned in cartesian space. Using this information, it is possible to calculate, by the arm inverse kinematic model, the joint positions. When also the hand velocity is imposed we need to take into account the direct and the inverse dynamic model too.
Given the dynamic equations of the robot the aim for the controller is to maintain the dynamic response between a range that a priori is fixed in accordance with a performance criterium. Usually the solution to this

problem is complicated by the inertia, gravity and friction forces and also by the reaction force between the links.
It is possible to model the robot with a multi-inputs multi-outputs (MIMO) non linear dynamic system where the internal state variables are coupled. For industrial manipulators a common way that is followed in order to control the system, is to consider each joint like an independent servomechanism [21]. This simplification is crucial in order to use the classical control theory. Therefore we can assume each joint is like a dynamic linear system (Equation 1.1) and control its position and velocity using a proportional derivative and integrative (PID) controller. The canonical representation for a linear dynamic system is expressed by the following equations.

$$\begin{aligned} \dot{x} &= Ax + Bu \\ y &= Cx + Du \end{aligned} \tag{1.1}$$

where A,B,C and D represent the system matrixes of appropriate dimensions.

This solution works well only if the parameters of the system do not change over time. If this happens the system might worse its performance and in the worst case become instable. A common way to solve this problem is reducing the motion speed, still maintaining the same robot precision in positioning the end-effector. But when also this action is inadequate, it is necessary to consider a more realistic arm dynamic model that takes into account the coupling between the joints, and consequently to synthesize a controller based on this model.
If it is necessary to generate rapid movements the system should compensate the inertia and Coriolis forces and a possible load change. Another unsolved problem is the calibration and re-calibration of the control system [22] due to the wear of the mechanical structure of the robot; in this condition the model assumptions may become increasingly imprecise during operation. This results in an imprecise and unstable behavior of the control system and therefore adaptive methods are required.

1.3 Different approaches to the Bio-Inspired Control of the artificial Arm

It is possible to model a compliant artificial arm with a non linear dynamic system, that in a general form is expressed by equation 1.2

$$\begin{aligned} \dot{x} &= f[x,u,t] \quad x(0) = x_0 \\ y &= g[x,u,t] \end{aligned} \tag{1.2}$$

where f and g are suitable functions. While, for a linear system, there exist many classical techniques in time and frequency domains, this is not true for a non linear system. Nevertheless we can find in literature many successful examples of systems controlled using neural network adaptive controllers [23]. In this section I review some techniques related to the problem of biological motor control.

1.3.1 Model Reference Adaptive Control

This control is based on the reference model M of the plant (in our case the Arm) P and on an algorithm that modifies the feedback gain for the joint actuators of P. In its turn the algorithm bases its output on the error signal calculated by the difference between the output of P and M (Figure 1.8). This technique has many advantages: it does not require a complex dynamic model of the plant, nor the knowledge of the environment (Arm load, frictions etc.)

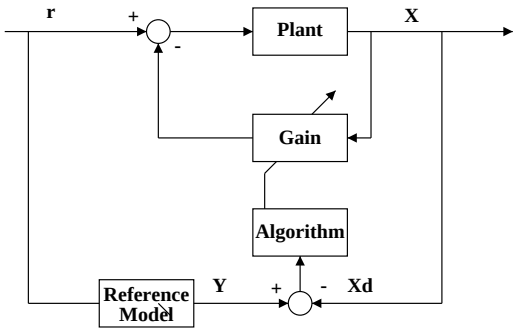

Figure 1.8: Model Reference Adaptive Control (MRAC)

As a reference model it is possible to chose between two alternatives: a dynamic equation with certain characteristics or a neural network. If we adopt the first choice, for each DOF it is necessary to find a time invariant second order differential equation (Equation 1.3), where $y_i(t)$ represents the reference model output and $r_i(t)$ the desired plant output for the i^{th} DOF.

$$a_i\ddot{y}_i(t) + b_i\dot{y}_i(t) + \dot{y}(t) = r_i(t) \tag{1.3}$$

With the a_i and b_i constants it is possible to chose the desired natural frequency and the damping coefficient for the i^{th} robot link.

The alternative is to use, as reference model, a neural network trained with the input-output pairs of the plant that we want to control. Narendra and Parthasarathy [24] describe a method called dynamic back-propagation to train neural networks for indirect adaptive control. Once the forward model performs satisfactory, control errors can be propagated through the forward model to train the controller.

1.3.2 Reinforcement Learning

Reinforcement learning is learning what to do, how to map situations to actions in order to maximize a reward signal. The control system receives a teaching signal that evaluates how good is the current state.

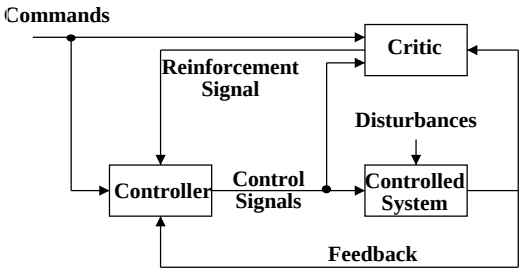

Figure 1.9: Reinforcement Learning Control Schema

Barto [25] notes that: "reinforcement learning involves a conflict between exploitation and exploration". Usually, during the execution of a certain task, the optimal action is unknown. The system can try to perform a randomly selected action and subsequently, from a reward or penalty signal, learn the best control strategy. The controller output (Figure 1.9) is a weighted sum of its inputs (Equation 1.4).

$$s(t) = \sum_{i=1}^{n} w_i(t) x_i(t) \tag{1.4}$$

and produces a random output

$$a(t) = \begin{cases} 1 & \text{with probability } p(t), \\ 0 & \text{with probability } 1 - p(t) \end{cases} \tag{1.5}$$

with $p(t)$ a rising function of $s(t)$. The weights expressed in equation 1.4 are updated according to

$$\Delta w(t) = \eta r(t) a(t) x(t) \tag{1.6}$$

where $r(t)$ is the reinforcement signal, $\eta > 0$ is the learning rate and $x(t)$ the controlled system state.
Reinforcement learning was successfully applied to a biological robot arm [26]. The authors note that it is difficult to apply this method to systems that are redundant (Figure 1.10) , because the cost of the trial and error algorithm is exponential in the dimension of the search domain. For instance, there is an infinite number of possible paths that the hand can follow to obtain the task goal. Even though the path was determined, it can be achieved by different sequences of muscle activations. The authors simplify the problem by considering a subspace of the search domain in which to apply the reinforcement learning algorithm. After the subproblem is solved it is possible to relax the initial constraints.

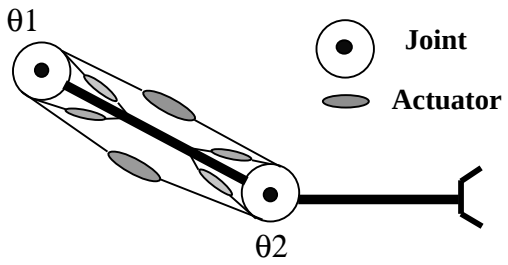

Figure 1.10: Biological Robot Arm Model

The authors demonstrate by simulations, that given a goal hand position in a 2D cartesian space, the controller after 1000 trials is able to reach the target following a straight line.

1.3.3 Memorized Motor Program and Learning by Demonstration

The main idea of this approach is to observe and memorize a motor program executed by a "Teacher". In order to be adapted to different tasks the memorized motor program should be parameterized by the control system.
In the Dynamic Brain Project (M. Kawato, S. Schaal et al) the DB robot [27] stores an explicit representation of a movement trajectory

in memory. When the robot needs information, for example, on how to pitch a baseball, it finds the appropriate tape or template in memory and then executes it. It is possible to make the system more sophisticated by considering the combination of more tapes to produce the movement. According to the authors, human-like learning from demonstration (LFD) should greatly reduce the cost of programming these complex systems.

In the human being LFD requires the mapping of a perceived action from an external frame of reference, suitable to describe the environment, into a different internal frame of reference that is able to manage the neurons that control the muscle activity during motion. Another important feature during the learning of a new task is the prior knowledge. The knowledge necessary to approach this new task can be obtained from previously learned tasks, or it can be acquired by the imitation of a teacher [28].
A problem still open, different from the approach of Kawamura et al., is how enable the robot to fill in missing information using learning from practice. Indeed many things are hard or impossible to perceive in a demonstration, such as muscle activations or responses to errors that do not occur in the demonstration.

A different approach is that one of Gorinevsky [29]; in his system the motor programs for training trajectories is not acquired from a human being, but generated by an algorithm that iteratively optimizes a criterion function to minimize trajectory errors. In the algorithm there is also an estimate and memorization of the sensitivity of parameters with respect to the final trajectory errors. The learned data can be used in a second time to generate new motor programs.

1.3.4 Hierarchical and Modular Neural Networks

In nature, modularity, is an intensely used strategy. We can define modularity as a subdivision of a complex object into simpler objects. Usually in humans each cognitive task can involve different brain processes simultaneously. Humans are able to perform certain tasks in parallel and other only singularly. For example most people have no problems with reading and listening music at the same time; whereas they find listening to two different speakers at the same time very difficult. This means that tasks which can be processed in different brain "modules" can be done easily in parallel, whereas tasks which need the same neural "module" are difficult to execute concurrently.
Like in the human brain it is possible to organize the artificial neural control system in a modular fashion, where each module is expert for a specific behavior (Figure 1.11).

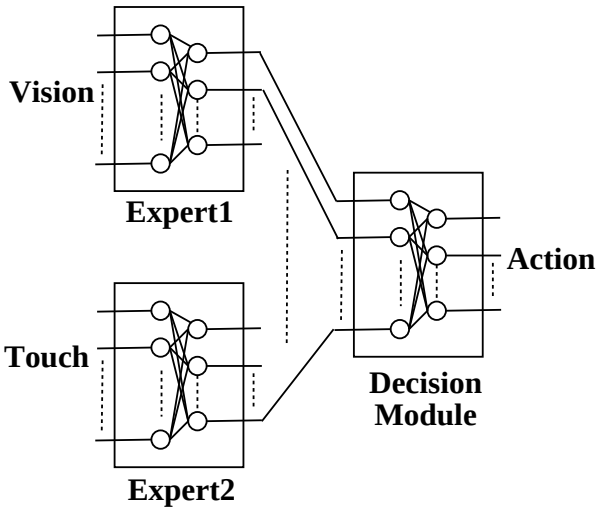

Figure 1.11: Example of Modular Neural Network

To control a robot arm Jordan et all. [30] and Gomi et all. [31] used a modular neural network. Both papers approach the problem that the manipulator dynamic changes during the manipulation of an object so causing a degradation of the robot performance. Each modular control network was trained to learn the dynamics of single objects, while the gating network learned to recognize the manipulated object. Kawato in his works [32], argues that the hierarchical network can be used to model the human brain, but also as efficient robotic controller. He demonstrated the ability of a hierarchical and parallel network in improving the artificial arm trajectory and the force regulation [33]. In the control system there are two module which compute the inverse dynamic of the arm: the first compensates for noise forces and the second for Coriolis and centrifugal forces.

1.4 My Approach and Methodology

After the introduction of some projects and methodologies relevant for this study, in this section, I want to clarify my approach to the problem of designing and controlling a human-like artificial arm. Before starting this study, we had [34], [35] experience with the design an construction of a human-like artificial hand "Blackfingers". This study was useful, not only to familiarize us with the biology of the human hand and ner-

vous system, but also to get involved in solving technical and scientific problems deriving from the goal to mimic as much as possible a complex system like the human hand.

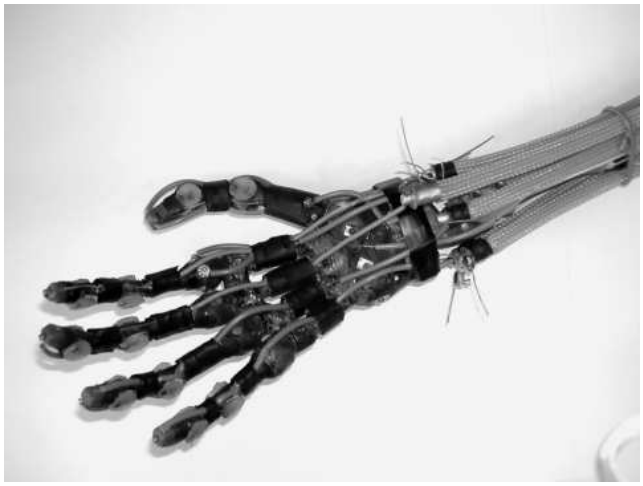

Figure 1.12: Our first prototype of artificial hand, Blackfingers, AirLab, Politecnico di Milano

In the first stage of this project we intensively studied, with the collaboration of biologists and experts in the field, the human hand anatomy and physiology. In the second stage we were involved in the design of the mechanical structure of the artificial hand. In particular in our design we tried to replicate the DOF's and the tendon structure of the human limb. What was immediately clear, in this first experience, is that designing an artificial system on the basis of biological information, allows engineers to take advantages of solutions that nature has found out in millions of years. But also, that nature can only "inspire" the designer; even if the biological system that we want to mimic is well understood each aspects, the problem of how to reproduce it artificially with state-of-art technologies remains unsolved. The bio-robotic engineer is therefore pushed to reach a compromise on the base of available technologies and level of emulation of the natural system.
Returning to this study, to design the bio-inspired artificial arm, I again looked with enthusiasm at biology but with the consciousness that it is necessary to find out technical and scientific solutions that sometime are far away from the solutions adopted by nature.

The goals of this work are both scientific and technological:

- Anatomical and physiological study of the human limb in order to find out specifications for the artificial arm

- Implementation of a kinematical and dynamic model for the artificial arm, in particular solving the problem of a singular three degrees of freedom (spherical) shoulder joint moved by five artificial muscles.
- Design, realization and testing of a novel humanoid arm using a bio-mimetic approach
- Design and experimentation of new kind of sensors and actuators suitable for humanoid robotics applications
- Experimentation of a low and high level control systems based on actual knowledge of the circuits located in the human spinal cords, cerebellum and motor cortex.
- Using the simulation results on the control system in order to improve the knowledge of the human limb.
- Compare results with other analogous works and also with the human limb.

Relative to other analogous researches [36], [7], [11] [15], [19], which focus on a particular sub-problem, this work will consider the integration of both low and high level control systems in order to govern a humanoid robotics arm. This considering classical and also new kind of neural networks based on neurophysiology studies [37], [38], [39], [40].
The thesis is organized in four principal areas: study of the human superior limb and central nervous system, kinematic and dynamic modelling of the bio-mimetic arm, study and experimentation of a model able to mimic the human neural circuits involved in reflexes and coordinating movements and experimentation on the real prototype performing simple movements. The approach I adopted to synthesize the neural controller is based on models and studies conducted on primates by neurophysiologists and neurologists. The prototype architecture corresponds, from a macroscopic and functional point of view, to requirements obtained from the human arm. This allows me to reproduce some natural movements and behaviors, as well as to make predictions on the control structure of the human limb itself. Our arm differs from other analogous systems [36], [7], by the presence of a fully actuated 3DOF shoulder joint and a 1DOF elbow joint. The system is moved by seven artificial muscles that are equipped with novel force and contraction sensors. The actuation system, in comparison with Cog's robot [11], permits a more human-like regulation of the joints stiffness. Furthermore, thanks to the employment of light materials, the system can be easily integrated with a whole humanoid robot.

1.5 Organization of the Thesis

The thesis is organized in eight chapters. Chapter 2 discusses the human arm biology and the crucial parts of the central nervous system that are involved in arm control. Particular attention is paid to the musculature and to the part of the control system involved in reflex behaviors. Chapter 3 describes the control architecture adopted in order to control the artificial arm. The model of each single block is formalized in mathematics, furthermore a description of how the different blocks are interfaced is also provided. The fourth chapter proposes the arm model taking into account kinematical and dynamical aspects. The direct kinematic model is described using the homogeneous coordinates and a solution for the inverse kinematic using a neural network is presented. The arm dynamic model is formalized using the Newton-Euler theory and implemented using the Matlab environment. Chapter 5 shows some results that demonstrate how the control system can achieve reflex behaviors comparable with those of a human limb. In Chapter 6 I report some experiments that deal with the overall arm simulation in reaching a target position, and compare with other research results. Chapter 7 reports the description of the arm prototype and some data acquired during a single joint movement. Finally chapter 8 brings the conclusion for this work and proposes possible future developments.

2 The Biological Limb

2.1 Introduction

In this chapter I review human arm biology and the crucial parts of the central nervous system that are involved in arm control. It is not a general study, because only the aspects needed for my purposes are discussed. I start by studying the arm from the osteologic point of view, with particular attention to the shoulder and elbow articulations. Following there is the physiological and functional presentation of the arm musculature. I focus on the mechanical and kinematical aspects that are involved in arm actuation. The third section of this chapter deals with the parts of the human central nervous system that are involved in regulating and planning arm movements. I explain the organization of the nervous motor system, describing the neural circuit anatomy and functionality. Particular attention is dedicated to the motor unit inside the spinal cord, and to the structure and role of the cerebellum in coordinating movements. Some material and redraw anatomical sketches are based on text-books [41], [42], [43], [44], [45].

2.2 Arm Anatomy and Physiology

2.2.1 The Arm Skeleton and Articulations

The arm's bones constitute the mechanical structure that support the limb. Their role is to transmit the force and the torques, generated by muscles, in order to support the hand and to perform a task. Starting from the shoulder to the wrist, it is possible to distinguish five bones: clavicle, scapula, humerus, radio and ulna (Figure 2.1). The humerus supports the upper arm and is articulated, in the proximal position, with the scapula and in the distal position with the radius and ulna. The proximal articulation is an enarthrosis (spherical) and permits three degrees of freedom, the distal articulation is trochlear (cylindrical) and permits one degree of freedom. Radius and ulna support the forearm and in the distal position they are articulated with the wrist's bones.

Segment	m (kg)	h (cm)	r (cm)	I/y(kg.cm2)	I/z(kg.cm2)
humeral	1.81	27.4	4.16	121.1	15.7
forearm	1.12	27.13	2.53	70.5	3.6
hand	0.46	11.07	2.46	5.4	1.4
forearm+hand	1.58	38.25	2.36	194.87	4.41
ulnar	0.79	38.25	2.36	97.43	2.21
radial	0.79	38.25	2.36	97.44	2.21

Table 2.1: Physical characteristics of the human arm (Data from [4])

In table 2.1 are reported some physical parameters of a human arm, data are obtained by an average made on a population sample of adult individuals.

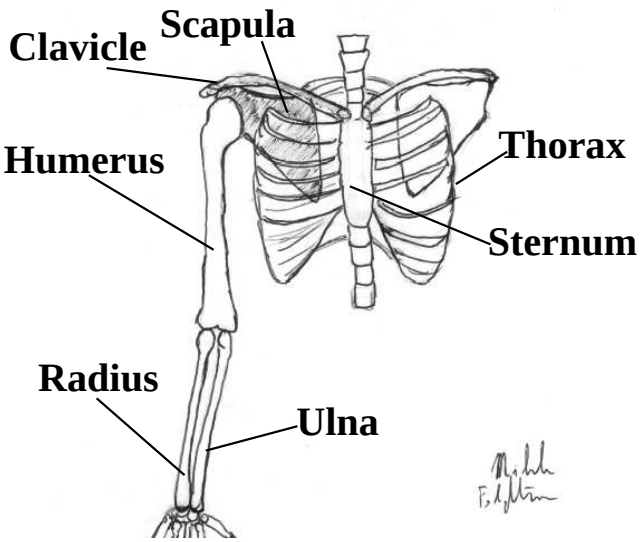

Figure 2.1: The human upper Skeleton

The Shoulder Joint

The shoulder joint is one of the most complicated joints in the body. It is made up of three bones: scapula, clavicle and humerus (Figure 2.1). The joint itself is a ball-and-socket joint [46], the head of the humerus fits into a socket in the outer edge of the scapula. The head of the humerus

is much larger than this socket on the scapula, therefore the shoulder articulation permits a wide range of movements. The clavicula bone itself is not fixed but can slide on the sternum, to extend the movement of abduction. In my model, described in chapter four, I consider only the humerus-scapula articulation, therefore only 3 DOF are permitted.

The Elbow Joint

The elbow joint is situated where the humerus meets the bones of the forearm, the radius and the ulna [47]. The distal part of the humerus is shaped as two rounded surfaces, one of which is coupled with the proximal part of the ulna (the bone that lies on the same side of the thumb), and the other with the proximal part of the radius. When the elbow is straight, a projection in the proximal part of the ulna (the olecranon process) fits against a hollow in the humerus and prevents the joint moving any further; this limits the elbow rotation in a range of about 150^o. If we consider only the humerus-ulna articulation it is possible to model the elbow as a cylindrical joint with only one DOF. The function of the radio is to permit the wrist twisting, however in my model I do not consider this movement and therefore the forearm is represented by a single link with only one DOF.

2.2.2 Arm Muscles Structure

Muscles represent the actuation system of the body [48]. In this section I analyze only the principal muscles that co-work in order to move the shoulder and the elbow articulation. These muscles will be inserted also in the arm's model and in the prototype. For the shoulder movements I consider: pectoralis major, dorsal major, deltoid, supraspinatus and subscapularis. For the elbow rotation I analyze: biceps and triceps.
Muscles located in the forearm actuate the wrist and hand, therefore in this study they are not considered.

Pectoralis Major

Pectoralis Major is a big muscle that is divided in three parts (Figure 2.2): the clavicular head that originates from the medial part of the anterior margin of clavicula, the sternocostal head that originates from the sternal strip and from the cartilages of the 2th and 6th rib, and finally the abdominal head that originates from the cover of the straight muscles.

The pectoralis major has its insertion in the intertubercular groove of humerus. This muscle has a quadrangular shape when the arm is

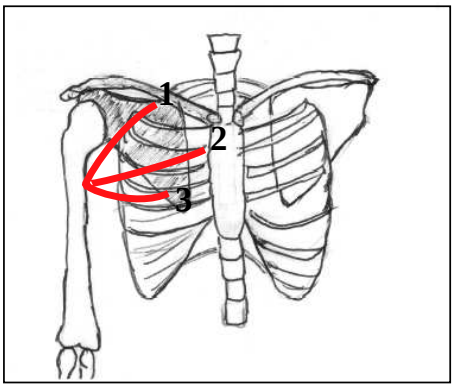

Figure 2.2: Pectoralis Major, 1 clavicular head, 2 sternocostal head, 3 abdominal head

extended to the bottom and is triangular when the arm is lifted.
The mechanical function of this muscle is the flexion, the adduction and medial rotation of the humerus. In our model this muscle has only one "head" that is attached to the front part of the robot, and is inserted in the proximal part of the upper arm under the shoulder joint (for more details see chapters three and four).

Dorsal Major

This muscle is very extended and it is subdivided in many parts (Figure 2.3). The vertebral part originates from the 7th-12th thoracic vertebraes, the iliac part originates from the spine of sacrum and posterior part of iliac crest, the rib part from the 10th-12th ribs and finally the scapular part from the inferior part of scapula. The muscle inserts in the bottom part of the intertubercular groove of humerus. The actions of this muscle are: move down and adduct the arm when it is lifted, move back and rotate inward the arm when the arm is adducted.

In our model, again, the muscle origin from only one point that is located behind the robot body, and is connected at the same point of the Pectoralis insertion by a special tendon (for more details see chapters three and seven)

Deltoid

Deltoid muscle is composed by three parts (Figure 2.4): the clavicular part that originates from the distal part of the clavicle, the acromial part that originates from the acromion of the scapula and the spinal part that originates from the spine of the scapula. Each of these parts are inserted

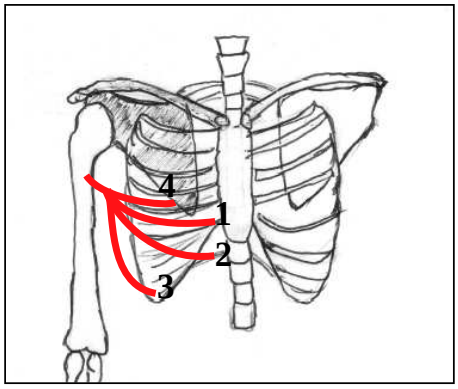

Figure 2.3: Dorsal Major, 1 vertebral part, 2 iliac part, 3 rib part, 4 scapular part

in the deltoid tuberosity of the humerus. Deltoid is the most important abductor of the humerus, the abduction can reach a maximum of 90^o. At the beginning only the acromial part works, but when the abduction has reached the two third of its maximum value also the clavicular and spinal parts cooperate at the movement. The deltoid, opportunely activated, can cooperate also to flex and extend the humerus.

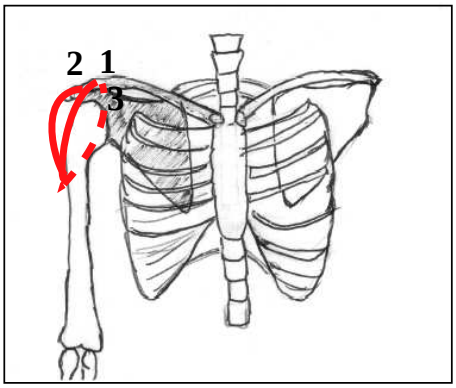

Figure 2.4: Deltoid, 1 clavicular part , 2 acromial part, 3 spinal part

In our model the muscle is composed by only a part that originates from a point on the shoulder joint and is inserted in the distal part of the upper arm.

Supraspinatus

This muscle originates from the supraspinatus fossa of the scapula (Figure 2.5), passes over the articular capsule and inserts on the superior facet on greater tubercle of humerus. It contributes with the rotator cuff muscles to rotate the humerus and to bind the humerus to the scapula. Furthermore, together with deltoid, cooperates to abduct the arm.

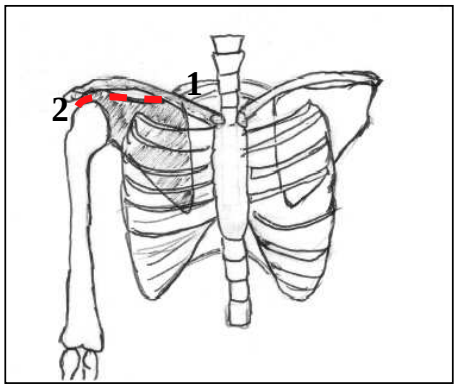

Figure 2.5: Supraspinatus, 1 fossa of the scapula, 2 greater tubercle of humerus

In the model this muscle origins from the opposite side relative to the shoulder joint, in the lower position of the body. This in order to permits a sufficient muscle contraction(this is particular true for the arm prototype). The muscle is connected to a certain point of the shoulder joint by a tendon; this permit to operate the shoulder rotation.

Subscapularis

Subscapularis muscle (Figure 2.6) originates from the subscapular fossa and inserts in the lesser tubercle of humerus. It has two main functions: the medial rotation and the adduction of the arm.

In the model the origin and insertion of this muscle are the same of the supraspinatus muscle, but it rotate the shoulder in the opposite way (for more detail see chapter 7).

Biceps

This muscle has two heads (Figure 2.7): the long head that originates from supraglenoid tubercle of the scapula and the short head that originates from coracoid process of the scapula. This two heads connect together where the deltoid inserts in the humerus. The biceps inserts

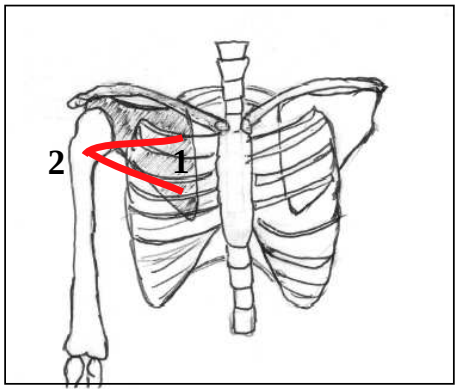

Figure 2.6: Subscapularis, 1 subscapular fossa, 2 lesser tubercle of humerus

with a robust tendon in the tuberosity of the radius. The muscle acts on two articulations simultaneously: the scapula-humerus articulation and the elbow articulation. On the scapula-humerus articulation the long head determines the abduction and the inward rotation of the arm, while the short head determines its adduction. On the elbow articulation the biceps acts as a flexor and supinator. When the forearm is flexed the supinator effect of this muscle is increased.

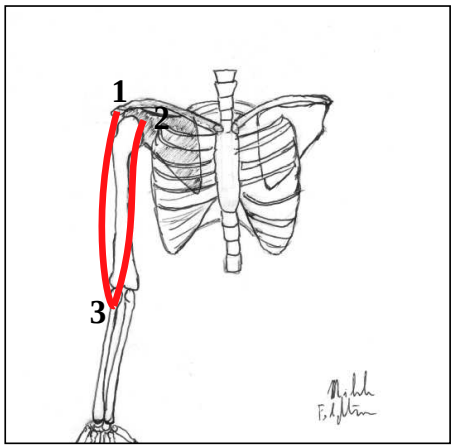

Figure 2.7: Biceps, 1 long head, 2 short head, 3 tuberosity of the radius

In the model this muscle origin from the proximal part of the upper arm and is inserted in the proximal part of the forearm. So a big difference, in comparison with the natural muscle, is that this muscle does not affects the shoulder joint; therefore is a mono-joint actuator.

Triceps

Triceps is formed by three parts (Figure 2.8): the long head that originates from the infraglenoid tubercle of the scapula, the medial head that originates from the posterior surface of humerus below the radial groove and the lateral head that originates from posterior surface of humerus above the radial groove. The three heads connect in a tendinous lamina that inserts in the olecranon process of the ulna. The triceps acts with the long head on two articulations (shoulder and elbow) and with the other two heads only on the elbow articulation. In the elbow articulation the biceps acts as an extensor, while in the shoulder articulation cooperate at the adduction movement.

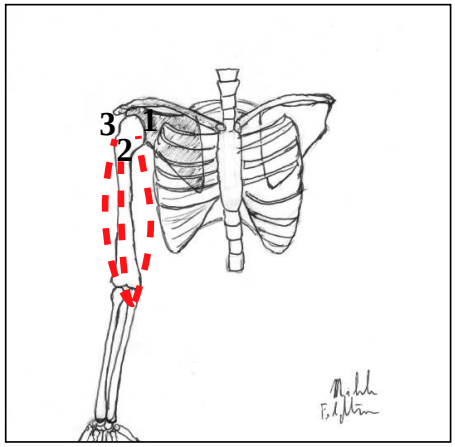

Figure 2.8: Triceps, 1 long head, 2 medial head, 3 lateral head, 4 olecranon process of the ulna

In the model this muscle has the same origin and insertion of the biceps, but it acts in opposite way (extends the forearm).

2.2.3 Muscle Physiology

In this section I analyze the physiology of the skeletal muscle, one of the three types of muscles present in the human body. This kind of muscles are voluntary, therefore they are activated (contracted) by voluntary commands coming from the central nervous system.
The muscle structure is made up by numerous subunits called fascicles surrounded by connective tissue (connective tissue forms also tendons). In its turn each fascicle is composed of numerous muscle fibers (muscle cells) and finally each fiber is made up of many myofibrils. The

membrane of the muscle cell called *sarcolemma*, is comparable with the membrane of a normal neuron, therefore it has a certain potential.

The muscle commands arrive in form of action potentials that originate from motoneurons located in the spinal cord. The impulse crosses the motoneuron's axon and reaches the junction formed by end of the axon and the muscle. This junction works like a synapse in the central nervous system; when the electrical impulse arrives, a chemical transmitter is released and diffuses across the neuromuscular clef. The transmitter molecules fill receptor sites and therefore increment the membrane permeability to sodium. When sodium diffuses in the membrane, its potential become less negative (depolarized) and when a threshold is reached an action potential occurs. At this point the action potential propagates along the muscle cell membrane, and causes its contraction.

Myofibrils are made up by two myofilaments: thick and thin (Figure 2.9). These are organized in a very regular pattern, each thick myofilament being surrounded by six thin myofilaments. These myofibril subunits are called sarcomeres.

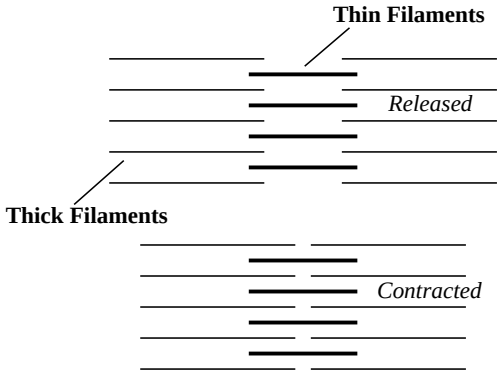

Figure 2.9: Sarcomere Model

Thick myofilaments are composed of a protein called myosin; when the electric impulse travels along the Sarcoplasmic Reticulum some chemical processes happen. From a rough point of view we summarize the process in these steps: the myosin head creates a fixed connection with actin molecule (that lies on the thin filament), then myosin swivels and therefore the entire myofilament moves forward. Combination of many myosin actions causes the sarcomere and therefore the muscle contraction.

From a macroscopic view, it is possible to model the muscle in two main components [49], [50]: the contractile element and the viscose-elastic

element (Figure 2.10).

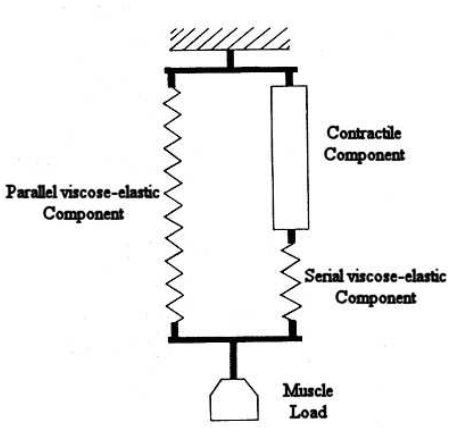

Figure 2.10: Macroscopic muscle model

The viscose-elastic element (due to the connective tissue) is located in series and parallel to the contractile element (due to the myofibrils). The presence of the viscose-elastic element introduces a phase displacement between the sarcomeres and the muscle contraction. This action permits the more gradual increase and decrease of the tension generated by the muscle on the articulation.

Isotonic/Isometric Contraction and Stimulus summation

The muscle is isotonically contracted when its force is greater than the force imposed by the load. It is isometrically contracted when the load force overcomes the force generated by the muscle. During a isometrical contraction the muscle fibers are activated but instead of contracting or releasing they maintain a constant length.
Another important characteristic of the skeletal muscles is the ability to contract to varying degrees; the degree of contraction depends on the number of motor units being stimulated (the motor unit is composed by a motoneuron and all the muscle fibers it innervates). Skeletal muscles are made up by numerous motor units and, therefore, stimulating more motor units causes a stronger contraction.
The strength of contraction depends on the frequency of muscle stimulation; the higher the frequency and the more the strength of contraction is increased. With rapid stimulation, a muscle fiber is stimulated while there is still some contractile activity, resulting in a summation of the contractile force.

Dependence of the velocity and force of contraction on the muscle length

The velocity of the muscle contraction depends on the load attached to the muscle. Experimentally was found [1], [51] (Figure 2.11) that the velocity of contraction reaches its maximum value when the load force is null, while it decreases with the increasing of the load. The maximum velocity of contraction depends also on the muscle characteristics; indeed there are muscles (for example the muscles that control the eyelids opening and closure) that are weakens than others, but can contract very rapidly ($100ms$).

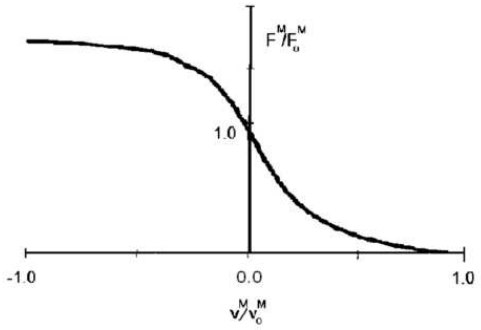

Figure 2.11: Relation between the muscle velocity and muscle load (from Hill (1938) [1])

Studies of muscle force, under isotonic conditions, have shown a bell-shaped curve (Figure 2.12) between force and muscle length. Observing the curve it is possible to see that the tension assumes the minimum value at the two extremes and reaches the maximum value in between. This phenomenon fits well with the sliding filament theory of muscle contraction; according to the theory, when the overlap between the actin and myosin filaments is increased more cross-bridges can be formed, and this causes an increasing of muscle force.

Because of I am interested in developing an artificial arm, in the model I do not considered the physiology of the natural muscle. Nevertheless the study of the natural muscle is useful to obtain some directions in the choice of the proper actuators, like the force that it can develop and its dynamic response. In chapter four I will analyze the static model for a special actuator, the McKibben artificial muscle. In chapter seven I will present some testings on this type of device.

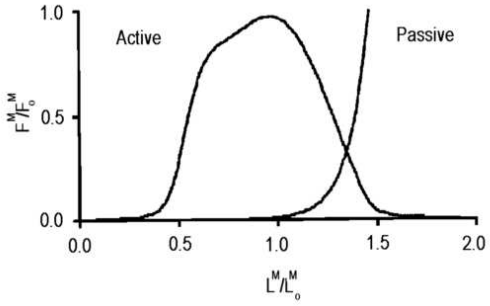

Figure 2.12: Relation between the muscle tension and muscle length (from Hill (1938) [1])

2.3 Basis of the Motor System

In this section I analyze the organization and the neurophysiology of the parts of the central nervous system involved in the arm motor functionalities. Because they are not so relevant for my study, I skip the molecular and chemical aspects of this complex system. This section involves neuroscience field, therefore to avoid erroneous terminology, sometimes I report the same sentences of the author.

2.3.1 Biology of the Neuron

The neuron is the fundamental brick that composes the human nervous system. It is a cell and its key parts are: the cell body, the dendrites, the axon and the synaptic terminal of the axon (Figure 2.13). The neuron can receive input from other similar cells and transmits information via electrical signals that are called action potentials. The axon structure is specialized to transmit information over long distance. Presynaptic terminals permit communication with other cells through the release of specialized molecules, the neurotransmitters.

In order to transmit information, the axon of a neuron can form synapses with dendrites or cell bodies of other neurons. When an action potential occurs in the presynaptic site, neurotransmitters are released and consequently diffuse across the synaptic cleft. These neurotransmitters, in the postsynaptic cell, interact with receptors (particular organs that can establish a chemical connection with the neurotransmitters). The principal effect of a neurotransmitter on its target cell is to change its membrane potential. Depending on the electrical response that neurotransmitters cause on the target cell, they are classified as *excitatory* or *inhibitory*.

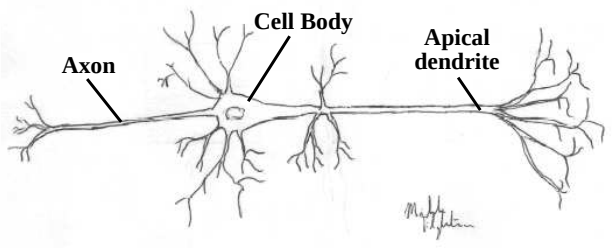

Figure 2.13: Diagram of the structural part of a pyramidal neuron in the cerebral cortex

Neuron inputs are summed and "integrated" over time, setting the level of the membrane depolarization and therefore the neuron's firing rate. When the membrane is not stimulated it is polarized at about -70 mV, this potential is called *resting membrane potential.* The membrane polarization is due to unequal distribution of Na^+ and K^+ ions on the two sides of a nerve cell membrane. An *action potential* is a very rapid change in membrane potential that occurs when the membrane potential overcomes a certain voltage. In particular, the membrane potential goes from the resting potential to some positive value (about +30 mV) in a very short period of time (Figure 2.14).

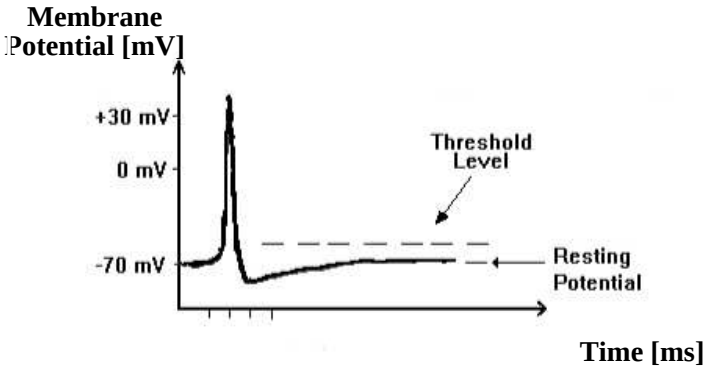

Figure 2.14: Action potential in a neuron

Spatial and Temporal Summation

Usually in the central nervous system (CNS) the stimulation of a single synapse is not powerful enough to depolarize the postsynaptic neuron

and therefore to generate an action potential [52]. Instead, each time a synapse is stimulated , it produces a small depolarization (excitatory) or hyperpolarization (inhibitory); this signal then sums with the signals generated by other synapses. There are two basic processes that involve the summation process (integration): the temporal summation and the spatial summation. According to [52] temporal summation: "is the process through which two input signals that occur sequentially can summate to produce a larger depolarization of the neuron membrane". Spatial summation: "is the process though which the signals generated by different inputs can summate".
Synaptic currents are generated by the opening of the ion channels. When the channel opens the membrane potential shifts to reach an equilibrium potential, characteristic of the ion to which the channel is permeable.

At this point even if other ion channels open they will not influence the membrane potential. For this reason, during an action potential, a second stimulus, near to the first one, will not produce a second action potential (Figure 2.15).

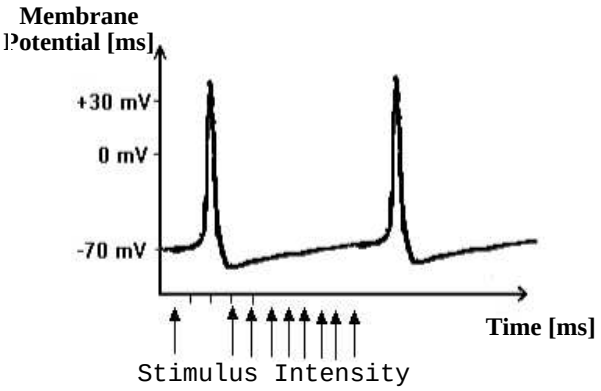

Figure 2.15: Non Linear Summation of the neuron (arrows represent the stimulus)

In chapter three I will present a realistic model for the natural neuron, that preserves its membrane dynamical behavior.

2.3.2 Anatomical Organization of the Motor System

The human motor system is hierarchically organized in the sense that higher level circuits control lower level circuits. Nevertheless there are

also many local circuits that influence sensory motor integration.
This complex system comprises:

- motor neurons in the spinal cord and cranial nerve nuclei in the brain stem that directly innervate striate muscle
- segmental circuitry that controls motor neurons
- structures in the brainstem, midbrain, and motor cerebral cortex that provide descending pathway input to the motor neurons

2.3.3 Descending Pathway of the Motor system

Muscle are innervated by motoneurons, that have their cell bodies in the ventral horn of the spinal cord and cranial nerve nuclei in the brainstem. These neurons send their axon to the muscles via the ventral roots (toward the belly) and cranial nerves.
There are two types of motoneurons:

***alpha* motoneurons** which regulate the muscle contraction;

***gamma* motoneurons** which regulate the contraction of the intrafusal muscle fibers, an internal organ of the *muscle spindle*;

It is necessary to make another motoneurons distinction:

***lower* motoneuron** neuron that directly innervate the muscles;

***upper* motoneurons** neurons that provide descending inputs to the lower motoneurons; these neurons are located in the motor cortex and brainstem.

Each individual muscle fiber receives input from one and only one motor axon, but a single motoneuron can innervate a group of muscle fibers. It is possible to define as a *motor unit* the set composed by an individual motoneuron and all the muscle fibers that it contacts. Motoneurons within the spinal segment are organized according to the muscle groups that they innervate. We can distinguish two main rules:

Proximal-distal rule motoneurons innervating proximal musculature are located medially in the ventral horn; motoneurons innervating distal musculature are located laterally.

Flexor-extensor rule motoneurons innervating extensor muscles lie ventral (anterior) to those innervating flexors.

Motoneurons in the spinal cord receive direct input from: descending pathway interneurons within the spinal segment, sensory afferents, and interneurons in near segments. The descending pathway terminates directly on the motoneurons and the interneurons. These pathways originate from the cerebral cortex (*corticofugal pathways*)and the brainstem pathway (*brainstem pathways*).

Corticofugal Pathway

In its turn the corticofugal pathway divides in:

1. *Corticospinal tract (CST)* which projects to motoneurons in the spinal cords
2. *Corticobulbar tract* which project to motoneurons in the medulla, pons, and midbrain

There are also other important projections to nuclei in the midbrain and brainstem that in turn give rise to the descending pathway:

1. *Corticorubral tract* which projects to the red nucleus
2. *Corticoreticular fibers* which project to the part of the reticular formation that gives rise to medial brainstem pathway

The CST is formed by the axons of the large pyramidal neurons of the primary motor cortex (Brodmann's area 4) and also from the axons of pyramidal neurons in Brodmann's areas 1, 2 and 3 of the somatosensory cortex. The CST system is divided into lateral and medial components. The fibers of lateral CST innervate motoneurons that stimulate distal muscles and flexors. The fibers of medial CST stimulate motoneurons and interneurons in the medial and ventral portion of the ventral horn where are located motoneurons that supply proximal and extensor muscles.
The corticobulbar tract is, from the functionality point of view, similar to the CST. These pathways contact the lower motor neurons in cranial nerve nuclei, and therefore they control muscles of the head and face.

Brainstem Pathway

There are medial and lateral brainstem pathways. Medial brainstem pathways originate from the vestibular nuclei and terminate on interneurons and motoneurons that innervate axial musculature. These are important for controlling musculature that maintains balance and posture.

The lateral brainstem pathway (rubrospinal tract) originates from the red nucleus and projects to the spinal cord via the lateral column. These circuits receive input from motor cortex and also from the *cerebellum*.

2.3.4 Proprioceptors

Proprioceptive information is very important for motor control. These information is required for initiating a movement: starting position of the limb (joint receptors), load of the muscles(stretch receptors), and feedback about the trend of the movement. In this section we analyze only two types of receptors that are important to acquire information about the muscle state: muscle spindles and Golgi tendon organs.

Muscle Spindles

Muscle spindles (Figure 2.16) are organs located inside the muscle. Each organ is surrounded by 10 to 12 very small muscle fibers (intrafusal muscles) that in turn are covered by a sheath of connective tissue. Inside this "sheets" there is the end of a sensory nerve that functions as a stretch receptor (**Ia** fiber). The sensitivity of the stretch receptor depends on the tension of the intrafusal muscle fibers which are regulated by the gamma motoneurons.
There are two types of stretch receptors: the *primary spindles* and the *secondary spindles*. The primary spindles provide dynamic and static information about the muscle stretch. These kind of receptors are rapidly adapting sensorial organs, therefore if the stretch stimulus continues the rate of firing decreases. Instead the firing rate of secondary spindles depends only on the amount of stretch applied. They are slow adapting receptors: when a stretch is applied the firing rate increases and remains high for the entire period of stretch application. We can assert that the muscle spindles, because of they are connected in parallel with the muscle's fibers, measure the muscle contraction (primary spindles) and the velocity of contraction (secondary spindles). In our arm prototype the behavior of this kind of receptors is performed by a flexible sensor fixed with the external shell of the actuator (for more detail see chapter seven).

Golgi Tendon Organs

Golgi tendon organs are located at the junction between the muscle fibers and the tendon. These receptors are in series with the muscle (whereas muscle spindles are in parallel) and sense the amount of tension in the

muscle (Force sensors). Golgi tendon organs are innervated by **Ib** afferent fiber that transports tension information to the spinal cords.

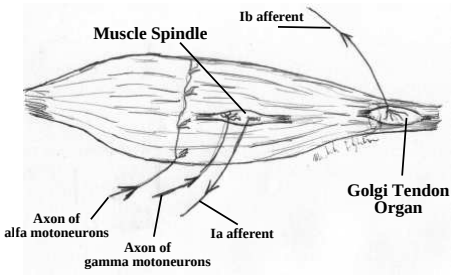

Figure 2.16: Muscle Spindle and Golgi Tendon Organs

In the arm prototype this kind of receptors are substituted by force sensor that are connected between the actuator and its point of insertion.

2.3.5 Segmental Reflexes

The sensor information coming from the muscle receptors regulates the spinal reflexes (called also segmental reflexes). Reflexes are involuntary and have afferent and efferent components. The efferent component is the output of the motoneurons, and the afferent component is the input from the muscle and pain receptors.
We can distinguish three types of segmental reflexes: the myotatic reflex (or stretch reflex), the inverse myotatic reflex (or Golgi tendon organ reflex) and the flexion-withdrawal reflex.

Myotatic Reflex

Ia afferent fibers (from primary spindles) form excitatory synaptic connections with the alpha motoneurons that innervate the same muscle (Figure 2.17). The Ia afferents innervate also inhibitory interneurons whose axons go to motoneurons that stimulate the antagonist muscle. If the muscle is stretched Ia afferents are activated and this increase the firing rate of the corresponding motoneuron that produces inhibition of motoneurons supplying antagonist muscles.

The myotatic reflex has an important role in regulating normal muscle tone. Gamma motoneurons control intrafusal muscle fibers; contraction of these increases the sensitivity of the stretch receptors. This is transduced into a stronger response of the Ia afferent fibers to a muscle stretch. Gamma activity is controlled by descending pathways, therefore superior neural centers can regulate muscle tone, and therefore the articulation

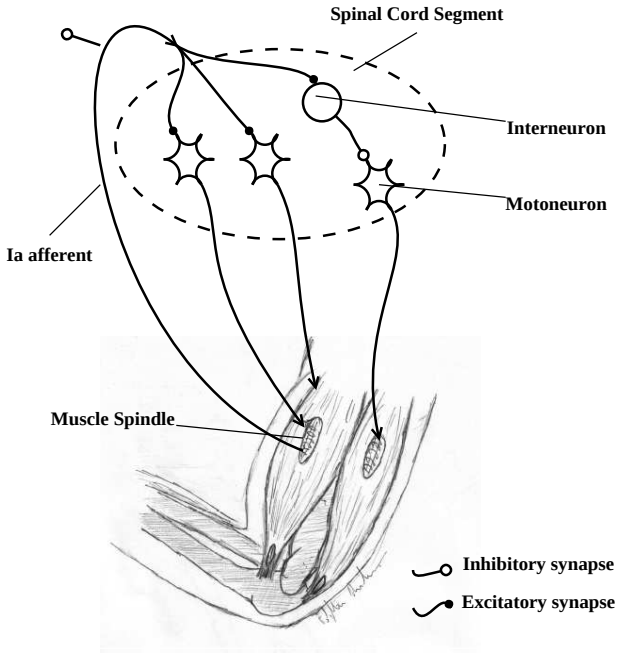

Figure 2.17: The Myotatic Reflex Circuit

stiffness.
Thanks to the mechanism that increases the contraction of agonist muscle and release of antagonist muscle, the myotatic reflex can compensate also for external forces that could alter the joint position.

Inverse Myotatic Reflex

When the muscle is stretched, the tension on the Golgi tendon organ increases, and this will increase the firing of the Ib afferent fiber. Ib afferent fibers innervate interneurons in the spinal cord that inhibit the synergic muscles (Figure 2.18) and excite the motoneuron that controls the antagonist muscles. Therefore when this reflex acts the synergic muscle is released and the antagonist muscle is contracted. This reflex is useful to avoid damage to muscle and tendon when they are overloaded, therefore it has a safety function.

Flexion-Withdrawal Reflex

The function of the flexion-withdrawal reflex (Figure 2.19) is to rapidly withdrawn the limb from a painful stimulus (therefore it has a safety

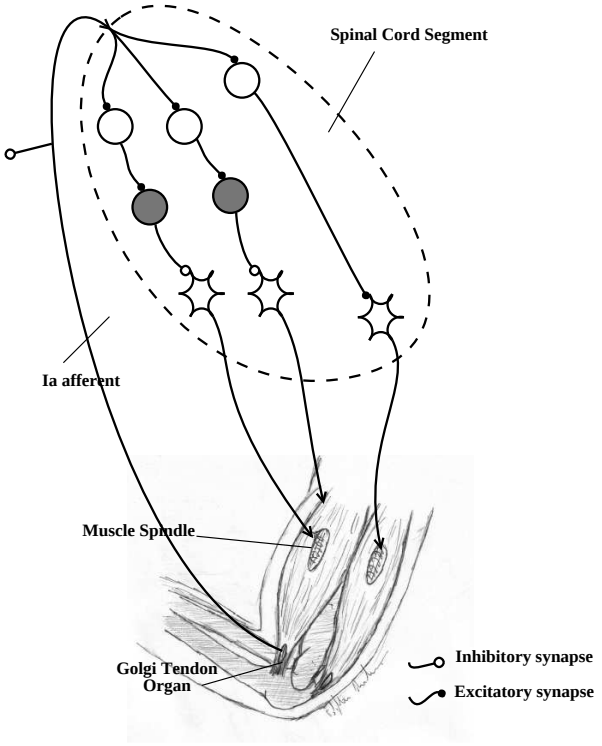

Figure 2.18: The Inverse Myotatic Reflex Circuit

function). The reflex starts from fibers coming from cutaneous pain receptors; these in turn project to the spinal cord and create synapses with interneurons that control activities of motoneurons. If a painful stimulus occurs the pain receptors activate the flexor motoneurons that govern the limb affected by the painful stimulation and this will cause the flexion of the limb. If the painful stimulus is strong there is also a polysynaptic activation of extensor motoneurons on the contralateral side of the body. This is also called *crossed extensor reflex*; for the upper limb this reflex will cause a pushing response that brings the body away from the cause that produces the pain. Unlike the myotatic reflex the flexion-withdrawal reflex can be suppressed by voluntary command. Probably, the reflex inhibition is possible thanks to descending pathway that inactivate interneurons that block transmission along the polysynaptic circuits.

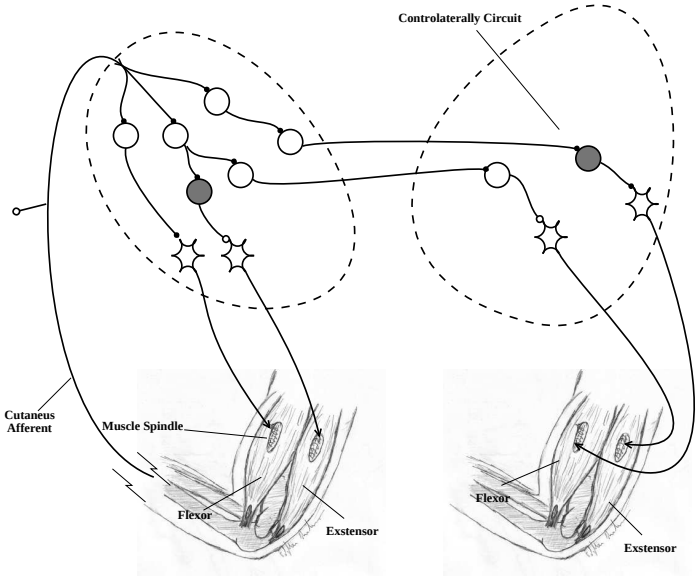

Figure 2.19: The Flexion-withdrawal Reflex

2.3.6 Supraspinal Control of Movement

The functions that require coordination such as voluntary motor activities, postural control, and locomotion depend on higher levels of the nervous system.

Postural Control

Postural control and balance depend on circuits whose function is to regulate muscles that compensate for the gravity force. The principal muscles involved in this control are those of the trunk and the extensor muscles of the limb.
Important components of this circuitry include the reticulospinal and vestibulospinal tracts [53], regulated by descending inputs from the cerebral cortex and cerebellum. Descending input from the reticulospinal tract activates *gamma motoneurons* that increase the sensitivity of the muscle spindle and therefore the tonic activation of the extensor muscles. The activity of the reticulospinal pathway is controlled by input coming from the cerebellum, the cerebral cortex and from ascending somatosensory pathway. "The input of cerebral cortex is important for postural adjustment in anticipation and during the execution of volun-

tary movements" [52]. For example, any voluntary movement of the limb must be accompanied by postural adjustments to maintain body balance. The other medial brainstem pathway that regulates posture is the vestibulospinal tract. It acts, with the reticulospinal tract, to govern the extensor musculature. The vestibulospinal tract output regulates the activities of gamma and also alpha motoneurons. This means that the vestibulospinal pathway can operate both via the gamma loop or by directly controlling the alpha motoneurons activity. The principal inputs to the vestibulospinal pathway are from the vestibular labyrinth, projections from the cerebellar cortex and the deep cerebellar nuclei. In particular projections from the cerebellar cortex are inhibitory. Damage to the cerebellar cortex causes a disinhibition of the neurons that project to the vestibular nuclei. Vestibular neurons in turn project to alpha motoneurons, where they form excitatory synapses. Therefore, the increase in activity of vestibular neurons causes an activation of the alpha motoneuron serving the extensor muscles (the muscles are permanently hyper-extended).

Locomotion

Locomotion depends on spinal circuits that produce stepping and walking movements. Spinal pattern generators are local circuits that can operate autonomously, nevertheless their activity is regulated by descending pathways and sensory inputs. Important evidence for this came from experimental studies conducted on animals that demonstrated that the stimulation of an area located in the mesencephalon produced stepping, and that the rate of stepping depended on the intensity of stimulation.

Voluntary motor activities

During the execution of a voluntary movement usually there is an interaction between the organism and its environment. To perform the movement the organism requires knowledge of the environment, knowledge about the position of its body with respect to elements in the environment, and the planning of the motor action in order to efficiently achieve the objective. The information to perform voluntary movements is integrated together by means of the cerebral cortex. Different parts of the cortex are involved in voluntary movements: the *primary motor cortex* is responsible for controlling segmental circuitry, the *premotor cortex* and *supplementary motor areas* are involved in planning the motor strategy, the *posterior parietal cortex* integrates spatial information for the planning of the motor activity.

I do not study in depth these parts of the brain, instead I can concentrate on the role of another important organ of the brain involved in motor functions, *the cerebellum.*

2.3.7 Role of the Cerebellum in Motor Functions

According to many neuroscientists [54], [55], [56], the overall function of the cerebellum is that it operates as a comparator. It compares data coming from the output of motor centers (intended movement) and sensory information about the actual results (actual movement). After this comparison the cerebellum projects its outputs to the nuclei in the brainstem. Nuclei output, in turn, gives rise to descending pathway to the spinal cord and to nuclei in the thalamus [57], that controls the activity in the motor cortex.
The cerebellum is thought to be very important for complex movements involving multiple joints, especially for tasks that require fine dexterity. Another function of the cerebellum is as a motor predictor in fast reaching movement. Furthermore, physiological studies, have suggested that the lateral cerebellum plays a key role in triggering the final output of the primary motor cortex. For this reason lesions of the cerebellum are thought to introduce delay in initiating a movement.
The cerebellum [41] is made up of a *cortex* and a core that contains a series of nuclear groups called the *deep cerebellar nuclei.* The cerebellar cortex contain five types of neurons (Figure 2.20): Purkinje cells, granule cells, Golgi cells, stellate cells, and basket cells. Purkinje cells form the output pathway of the cerebellum, while the other cells types project within the cerebellar cortex and control the activity of the Purkinje cells. In particular granule cells form excitatory synapses with Purkinje cells, whereas Stellate cells, Golgi cells, and basket cells are interneurons that give rise to inhibitory synapses.

Purkinje Cells Inputs

The principal inputs for the Purkinje cells come from granule cells. The granule cell's axon goes to the molecular layer, then bifurcates and forms a fiber; all these fibers run parallel one to each other, and therefore this particular cerebellum structure is called *parallel fibers.* It is estimated that each Purkinje cell receives up to 200.000 parallel fiber synapses. The activity of one synaptic connection is not able to depolarize the purkinje cell membrane, therefore to initiate an action potential considerable signal summation must occur.
The other excitatory synaptic input to Purkinje cells is the *climbing fibers*

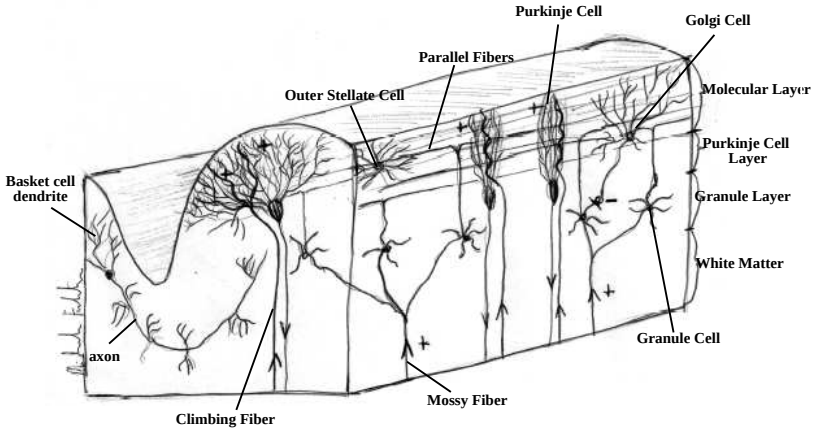

Figure 2.20: Cellular Organization of the Cerebellar Cortex

input, which originates from the *inferior olivary nucleus*. In adult individuals, each Purkinje cell is innervated by one and only one climbing fiber. However, a single climbing fiber can innervate up to 10 Purkinje cells. It is known that each action potential in a climbing fiber powerfully activates the Purkinje cell.
Stellate and basket cells are innervated by parallel fibers and their axon inhibit Purkinje cells. In particular the axon from stellate cells terminates on Purkinje cell dendrites, while the axon from basket cells terminates on Purkinje soma.
Golgi cells are also *inhibitory* interneurons; the axon from Golgi cells inhibits the granule cells.

Cerebellum Input and Output Pathway

The cerebellar input and output pathway enters and leaves the cerebellum via the cerebellar peduncles. The inputs are:

Spinocerebellar pathway , carrying proprioceptive information, which enters the cerebellum via the inferior peduncles

Vestibular pathway , constituted by the axons coming from the vestibular nucleus and vestibular labyrinth, these also arriving via the inferior cerebellar peduncle

Pontocerebellar , transporting information relative to the output of neurons located in the pontine nuclei, which in turn receives input from corticopontine pathway.

Olivocerebellar pathway , originated from neurons in the inferior olivary nucleus and entering the cerebellum via the inferior cerebellar peduncle

The input pathway of the cerebellum is composed of two types of fibers: the mossy fibers that terminate in the granule cells, and the climbing fibers that climb along dendrites of Purkinje cells. In particular each mossy fiber innervates several granule cells, and each granule cell receives input from several mossy fibers.
The axon of the Purkinje cells constitutes the output of the cerebellum. Most of these fibers go to inhibit the activity of neurons in the deep cerebellar nuclei.

3 The Bio-mimetic Control Architecture

3.1 Introduction

In this chapter I explain the architecture of the control system for the artificial arm. I start with a brief introduction of the arm prototype, in order to better understand the motivations that conduct me to the actual control structure. In Section 3 I describe the control system organization, with particular attention to the integration between the modules. The fourth Section explains the model for the neural circuits that are involved in the emulation of the spinal reflexes. Section 5 describes the module responsible in generating the muscle trajectory in order to move the artificial muscle from the initial length to the target length. Finally the last section proposes a possible model of the artificial cerebellum, whose purpose is to learn how to compensate for joints dynamic influence during fast movements.

3.2 Prototype Overview

In this section I introduce the arm prototype in order to better understand and justify the bio-inspired control architecture I adopted. A more detailed description is presented in chapter 7 where I show also some initial experimental results.
The arm we built in our laboratory (Figure 3.1), is intended to be the natural test-bed for testing the control system architecture proposed in this work and for developing new technologies applicable to humanoid robotics. The arm, without considering the wrist and hand that are still under development, has two joints for a total of four degrees of freedom. The shoulder consists in a spherical joint with 3 DOF, and the elbow is a rotational joint with 1 DOF. Joints are moved by tendons connected with McKibben artificial muscles, which in turn are bonded with the support structure and the upper arm. Each muscle is equipped with a force sensor mounted in series to the actuator (comparable, from a functional

point of view, with the Golgi tendon organ in the human arm) and of a position sensor located in parallel to the external shell that covers the artificial muscle (comparable, from a functional point of view, with the muscle spindle in the human arm). The elbow joint has also an angular sensor that measures the joint position and velocity with more precision. Sensor signals are conditioned and gathered by dedicated boards and sent to a PC A/D card. The control system runs in real time on a target PC, and its output are converted in appropriate signals that feed the actuation system.

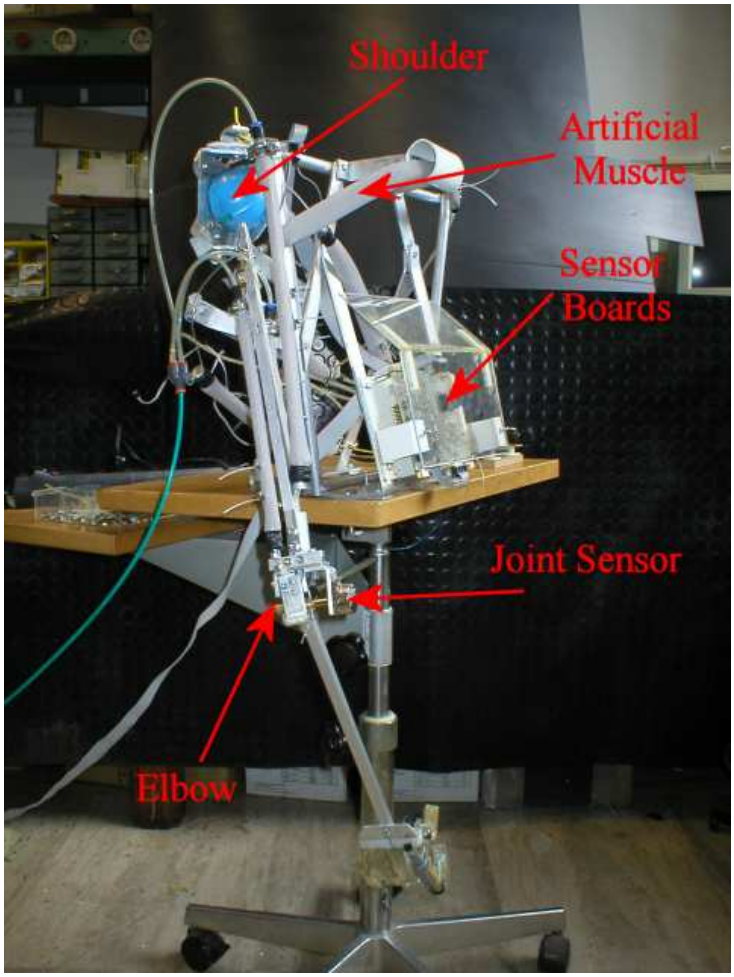

Figure 3.1: The Arm Prototype, MaximumOne, Artificial Intelligence and Robotics Laboratory, Politecnico di Milano

As it is possible to see in the prototype picture (Figure 3.1), this

arm has an anthropomorphic design. In particular, during the design, I have tried to reproduce the human arm dimensions and proportions, the articulation mobilities, the muscle structure, and the same sensorial capabilities. The actuation system is composed of seven muscles (Figure 3.2): five actuate the shoulder joint and two the elbow. This permits me to fully actuate the joints but at the same time to have a minimal architecture. The five shoulder actuators emulate the function of: pectoralis major, dorsal major, deltoid, supraspinatus and subscapularis muscles. The two elbow actuators emulate the function of biceps and triceps muscles.

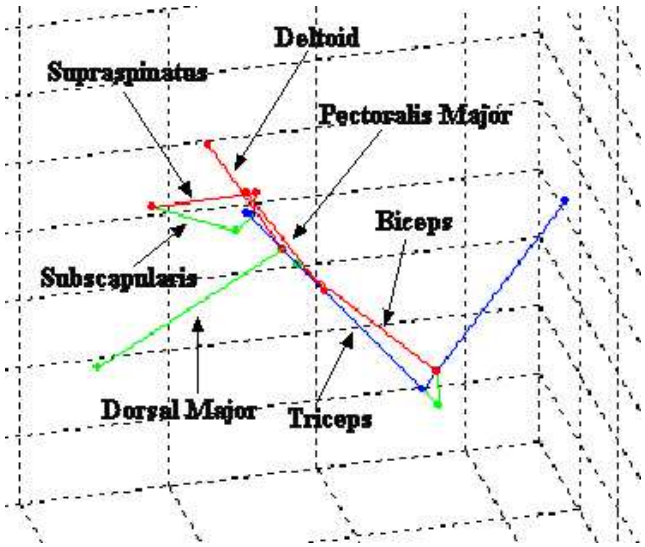

Figure 3.2: Artificial Muscles Configuration

In comparison with the human arm musculature, the actuation system of our prototype is quite different, for example the biceps and triceps artificial muscles are mono-articular in the sense that they are dedicated only for the elbow actuation. Shoulder actuators are placed in order to use the maximum length excursion. In order to conduct intensive experimentation, I have also implemented a realistic model of the prototype (for more details see chapter four) that catches the principal kinematic and dynamic characteristics of the real arm such as: links mass and inertia, joints mobility and friction, actuator dimension and statical response.

3.3 Entire Control System Architecture and Modules Integration

The control system of the arm is organized in a modular and hierarchical fashion. At the bottom level (Figure 3.3) there are the artificial reflex modules that govern the actuator's contraction and force. These modules receive inputs from the joint path generator, which in turn is fed by the inverse kinematic module that computes the target actuators lengths. The reflex modules also receive inputs from the cerebellar module whose function is to regulate the path generator outputs. The cerebellum module, as inputs, receives signals from the path generator modules and the error signals from the reflex modules. The inputs of the entire control system are: the final hand position in the cartesian space, the GO signal that scale the speed of movement and the P signal that scales the level of artificial muscles co-activation (simultaneously activation of the muscle that govern the same joint).

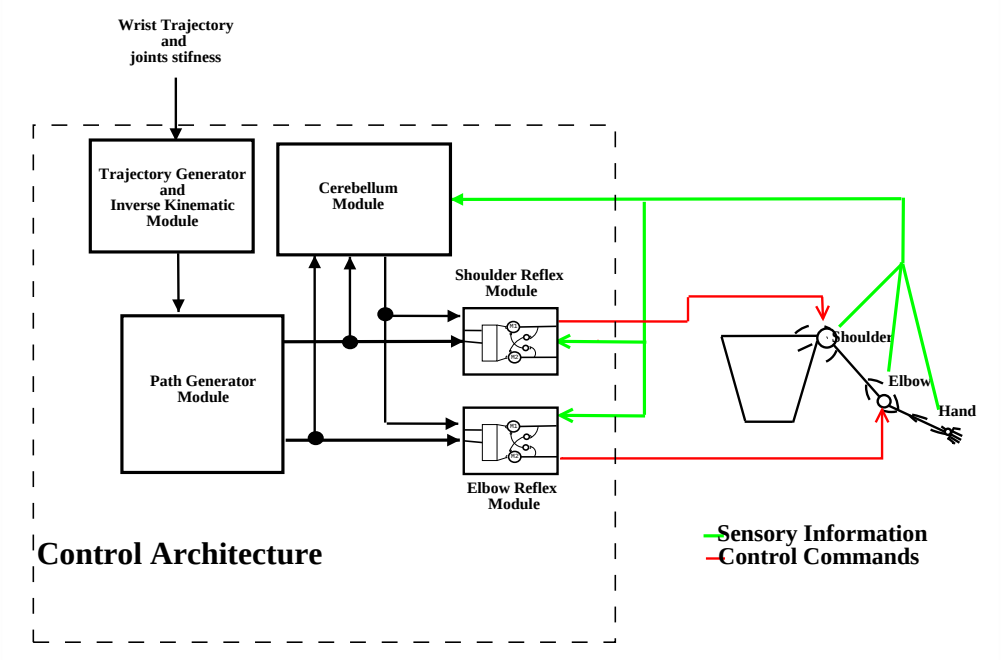

Figure 3.3: Control System Architecture

From a hierarchical point of view, we can distinguish three principal levels:

High level controller :composed of the Inverse Kinematic and the cere-

bellum modules that cooperate in parallel to control the path generator activity

Medium level controller :composed of the path generator module

Low level controller :composed of the reflex modules that control the artificial muscles activities

The signals transmitted from one module to another are expressed in a vectorial form, where each vector component corresponds to one of the seven artificial muscles that compose the actuation system. Therefore L_T represents the target lengths vector for the actuators, V_T represents the target velocity vector for the actuators, E_L represents the length vector error of the actuators, C_S is the signal vector generated by the cerebellum module, and P is the stiffness command vector. At the level of each single module these signals are decomposed in their components and sent to the appropriate submodules.

3.4 The Reflexes Control Modules

Reflex behaviors are accomplished by two modules that implement a simplified model of the natural circuits present in the human spinal cord. With respect to other models in literature [58], [59], [60], [61], or to hardware solutions [62] I decided to neglect the spike behavior of the neuron for all the artificial cells, instead I concentrated my attention on modelling its membrane potential. From an information point of view the spiking behavior in the neuron is not so crucial. In a living organism the action potential mechanism permits to convert an information, represented by the neuron potential (analog signal), into an impulsive signals. In such a manner the information is transmitted modulating the frequency of the impulsive signal. This is particulary useful when the signal (of few mV) is transmitted over a long distance, for example from the arm receptors (peripheral nervous system) to the central nervous system. In our system (arm prototype) the entity of the sensor signals are in the order of some volts, and all the information are processed in a normal CPU, so it is not efficient convert the analog signals into a impulsive signals.
One module is dedicated to the control of the artificial muscles activities that govern the shoulder joint, the other takes under control muscles that actuate the elbow joint. Since the artificial muscle is constituted by only one functional fiber the biological organization of the natural muscle in motor units is neglected in my model. The artificial muscle activity is

therefore regulated by only one motoneuron. The same consideration can be done also for the sensorial system in the muscle, that in this case is constituted by only one artificial spindle organ and only one artificial Golgi tendon organ.

3.4.1 Elbow Module Architecture

The reflex module that governs the elbow muscle is represented in figure 3.4. It implements an opponent force controller whose purposes are to attempt to implement the path generator module commands, measure movements error and return error signals when the execution is different from the desired movement.
In figure 3.4 M_6 and M_7 are the motoneurons that control the contraction rate and force of the triceps and biceps actuators respectively. I_a6 and I_a7 are the interneurons that receive the error signals from the artificial spindles and project, with inhibitory synapses, to the motoneurons of the antagonist muscles M_7 and M_6 respectively. R_6 and R_7 represent the Renshaw cells that receive the error signals from spindles and inhibit the corresponding motoneuron and I_a cell, they are important to reduce oscillations of the joint around the target angular position. I_b6 and I_b7 are interneurons that receive the signals coming from the artificial Golgi tendon organs (that in this system are represented by a normalized force measurements). $I_{nc}6$ and $I_{nc}7$ are interneurons whose purpose is to integrate information coming from the cerebellum (signals C_s6 and C_s7) and from the $I_{ns}6$ and $I_{ns}7$ interneurons, thanks to these cells the cerebellum module can apply its influence on the overall joint movement. $I_{ns}6$ and $I_{ns}7$ are the interneurons that integrate information of stiffness and target length commands.
Finally M_s6 and M_s7 represent the artificial muscle spindle receptors. As inputs they receive the muscle velocity command, the muscle target length command and the actual muscle length and in turn excite the corresponding motoneuron and I_a interneurons.

3.4.2 Shoulder Module Architecture

The reflex module for the shoulder acts on five muscles, therefore the neural circuit is more complex. Since as we know, there are not precise neurophysiology studies that show how this circuit works in governing the shoulder musculature, I design the system making some biological hypotheses and technical speculations.
At first it is possible to make a substantial simplification by considering the muscles action on the upper arm. We can divide the five muscles in

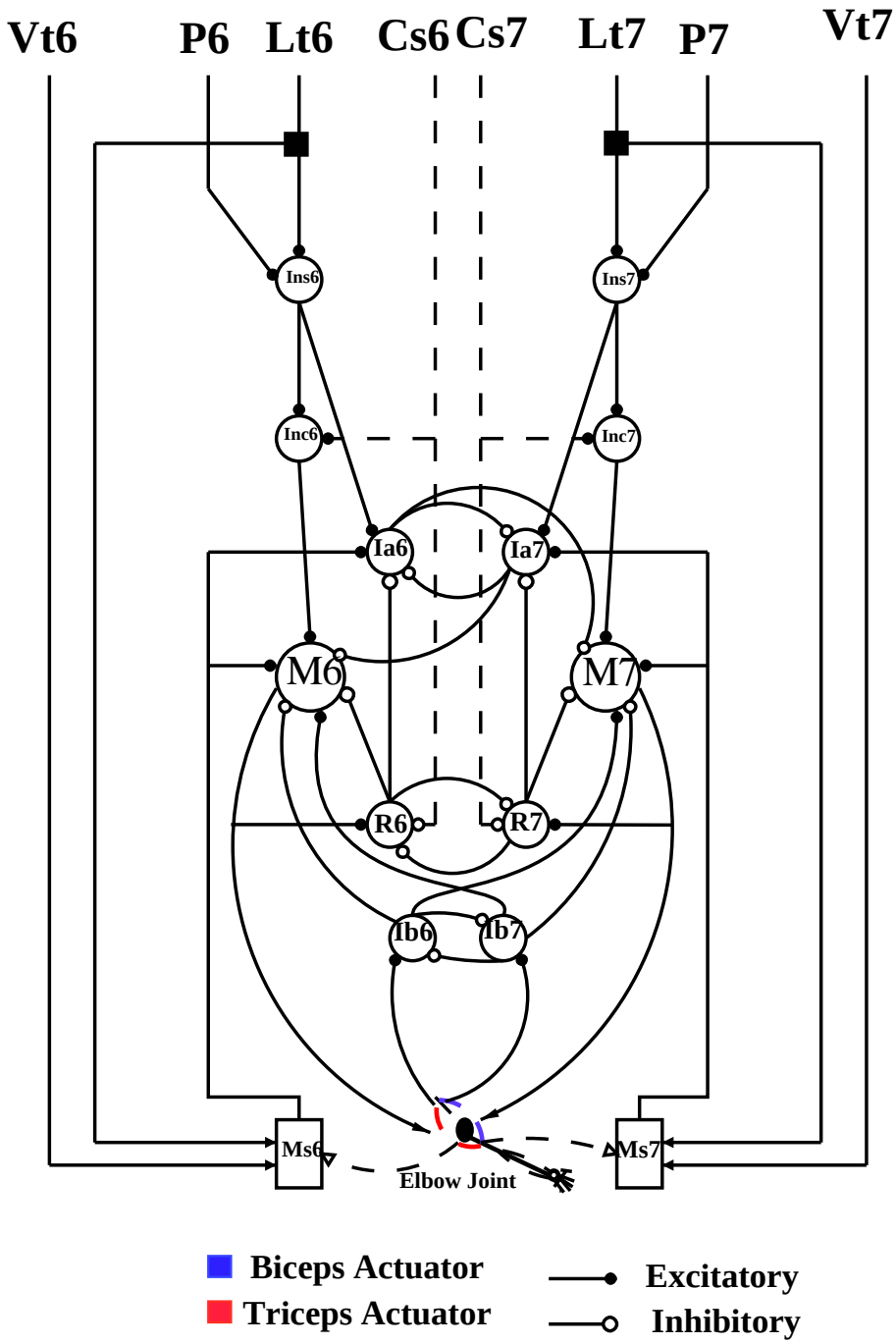

Figure 3.4: Architecture of the Elbow Reflex Module

two groups: the supraspinatus and subscapularis that work together in order to rotate the shoulder (as rotation I intend the rotation around an axis longitudinal to the upper arm link) , and the pectoralis major, dorsal major and deltoid that co-operate to flex-extend and adduct-abduct the upper arm. This subdivision takes in account the synergy between the muscles.
The assumption that I make, is that the mechanical action of these two groups is separated. This means that the rotation of the upper arm does not influence the muscles that govern the adduction-abduction and flexion-extension movements and, in the same way, that any activity of the muscles of the second group cannot influence the muscles that rotate the shoulder. This assumption, confirmed also by experiments conducted on the prototype, has a substantial consequence on the architecture of the reflex module that will govern the artificial muscles of the shoulder. Because of these considerations, we can divide the module in two submodules: one that controls the activity of supraspinatus and subscapularis actuators, and one that controls the contraction of the other three artificial muscles. The first circuit is identical to the one presented in the prior section, indeed it has to govern two antagonist actuators like the triceps and biceps. More complicated is the circuit that governs the pectoralis, dorsal and deltoid actuators, because the actions of these three muscles are coupled. From a system point of view, we can say that the position of the shoulder, specified by two coordinates (for example the Euler coordinates), depends on the three actuator positions.

$$\begin{bmatrix} \alpha \\ \beta \end{bmatrix} = f \begin{bmatrix} L_{M1} \\ L_{M2} \\ L_{M3} \end{bmatrix} \tag{3.1}$$

Where f is a function that I will analyze in the next chapter. Moment by moment the three muscles can be divided in the agonist and antagonist groups. For example when we want to extend the arm the deltoid will be contracted and the dorsal and pectoral actuators released.

If we want extend and adduct the arm at the same time, the pectoralis and deltoid must be contracted while the dorsal is released. The contraction grade of these muscles should be regulated by a second reflex module(Figure 3.4). As it is possible to see, the circuit is an expansion of the architecture presented to control only two antagonistic muscles. Here we have three motoneurons that feed the corresponding muscles, and the number of interneurons is increased. In particular for the $I_a i$, R_i and $I_b i$ interneurons the circuit changes in the sense that now each single interneuron inhibits the two interneurons of the antagonistic muscles.

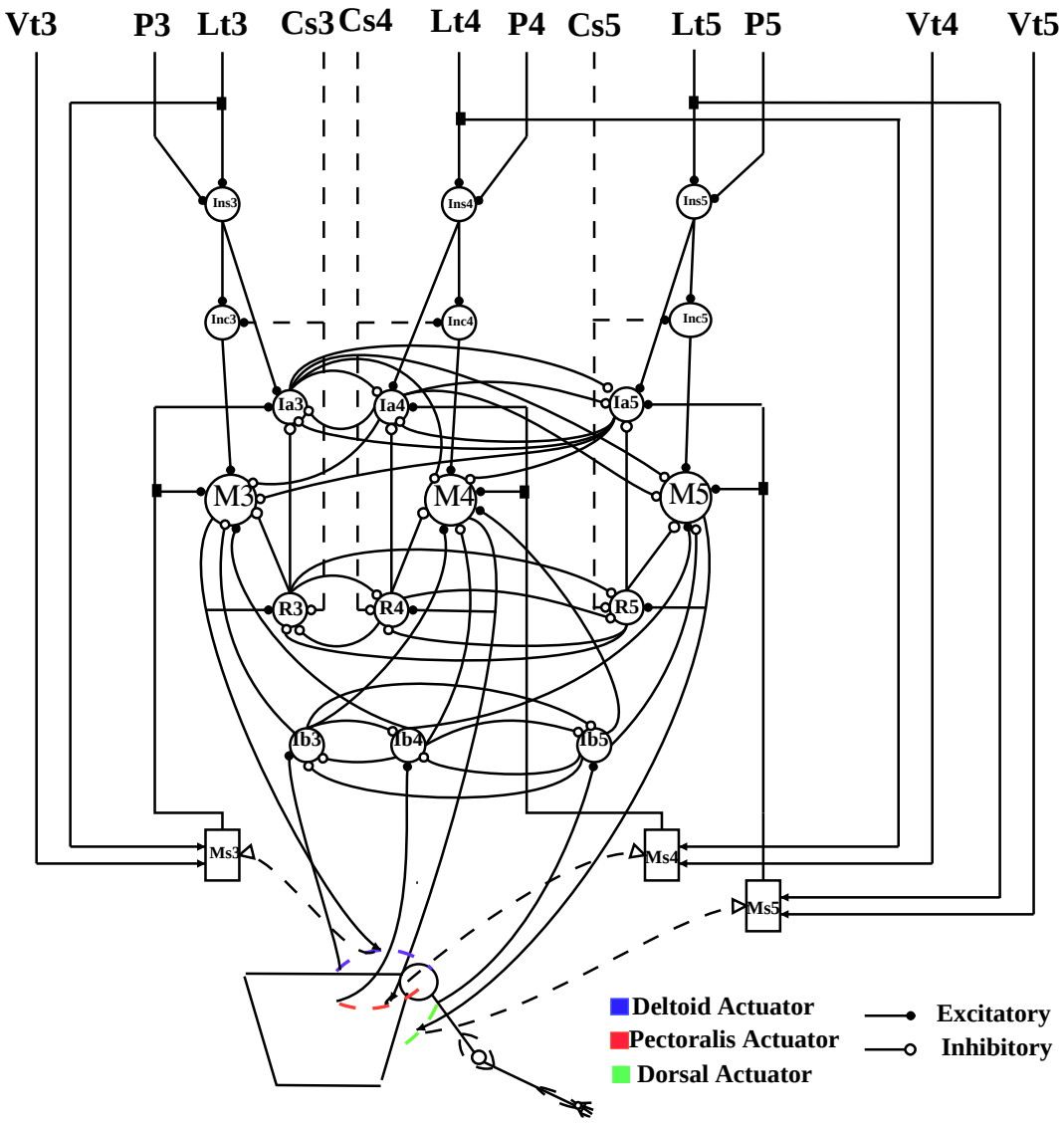

Figure 3.5: Architecture of the Shoulder Reflex Module

This rule is true only for the interneurons of the same type. Furthermore the $I_a i$ interneurons also inhibit the motoneurons of the corresponding antagonist muscles.

3.4.3 Motoneuron and Interneuron Models

In this section I describe the mathematical model for the neurons and the sensorial cells present in the reflex modules. Each neuron is represented by a first order differential equation where the variable is the neuron potential. The potential can change between a minimum and a maximum value, corresponding to the real numbers zero and one. The neuron potential, in turn, is a continuous function of the time and of the neuron's inputs. The output of the neuron is a function of the neuron potential. In my models this is a threshold function. The first model I describe, the motoneuron model, is a general model and can represent quite all the neurons in the circuits. Nevertheless, because of each neuron has different inputs, in order to define the network topology I preferred to instantiate the model for every cell.

Motoneuron Model

The motoneuron receives its inputs from almost all the cells that compose the neural circuit. In equation 3.2 M_i represents the potential (membrane potential) of the motoneuron i.

$$\frac{d}{dt}M_i = (1 - M_i)(exc_i) - M_i(inh_i) \tag{3.2}$$

where the terms exc_i and inh_i are expressed by equations 3.3

$$\begin{aligned} exc_i &= w_1 \cdot E_i + w_2 \cdot Inc_i + \textstyle\sum_{k=1,k\neq i}^{n}(z_k \cdot Ib_k) \\ inh_i &= K + w_3 \cdot R_i + w_4 \cdot Ib_i + \textstyle\sum_{k=1,k\neq i}^{n}(v_k \cdot Ia_i) \end{aligned} \tag{3.3}$$

the motoneuron output is

$$Mo_i = Th(M_i) \tag{3.4}$$

where the threshold function is defined by equations 3.5 :

$$Th(x) = \begin{cases} x & \text{if } 0 \leq x \leq 1 \\ 0 & \text{if } x \leq 0 \\ 1 & \text{if } x \geq 1 \end{cases} \tag{3.5}$$

The first term in the right side of the equation 3.2 is the gain for the excitatory part (**exc**); this gain is a function of the motoneuron potential. Therefore, the more the neuron is actives the smaller the gain will became. This avoids the neuron's potential saturating rapidly when the excitatory synapses are strongly stimulated. The second part of the equation 3.2 gathers the inhibitory signals that feed the motoneuron (**inh**). In the (**inh**) term the inhibitory signals are multiplied by the corresponding synapse's gain w_i and v_k, and added together. It is clear, that the gain for the excitatory part 3.2will decrease when the motoneuron potential increases. This contributes to maintain the neuron activation confined under the maximum value. The summation in the (**inh**) part, takes in account of the inhibitory action of the antagonistic Ia_i, the summation is extended to **n**, the number of motoneurons that constitute the reflex circuit (n=2 for the elbow reflex circuit and 3 for the shoulder reflex circuit).
The term K represents the leaky current of the neuron membrane. When the neuron is not excited its potential will decrease thank to this term. Finally E_i is the error signal coming from the spindle cell Ms_i.

Model of the Ia Interneuron

The Ia interneuron potential model is described by equation 3.6:

$$\frac{d}{dt}(Ia_i) = (1 - Ia_i)(exc_i) - Ia_i(inh_i) \tag{3.6}$$

where the terms exc_i and inh_i are expressed by equations 3.7

$$\begin{aligned} exc_i &= w_1 \cdot E_i + w_2 \cdot Ins_i \\ inh_i &= K + \textstyle\sum_{k=1,k\neq i}^{n}(v_k \cdot Ia_k) + w_4 \cdot R_i \end{aligned} \tag{3.7}$$

the interneuron output is

$$Iao_i = Th(Ia_i) \tag{3.8}$$

Where the threshold function $Th(\cdot)$ is defined as in equation 3.3. As it is possible to see in the second term of the second equation 3.7, it depends by the output of the R cell of the corresponding side of the circuit and by the activities of the antagonistic cells Ia_k.

Model of the R Interneuron

The Renshaw cells model is formalized by equation 3.9:

$$\frac{d}{dt}(R_i) = (1 - R_i)(exc_i) - R_i(inh_i) \tag{3.9}$$

where the terms exc_i and inh_i are expressed by equations 3.10

$$\begin{aligned} exc_i &= w_{i1} \cdot M_i \\ inh_i &= K + \sum_{k=1,k\neq i}^{n}(R_k) + w_2 Cs_i \end{aligned} \tag{3.10}$$

the interneuron output is

$$Ro_i = Th(Ro_i) \tag{3.11}$$

As is expressed in the second equation 3.10 the Renshaw cell potential, like the Ia cell potential, depends on the output of the antagonistic Renshaw cells. This cross inhibition has the purpose to let dominate, on the antagonistic counterparts, the cell that has the greater activity. We can interpret this mechanism as a competitive role: the cell more stimulated will dominate the cell less stimulated. From a system point of view the cross connection can not realize excitatory synapses otherwise the global system will tend autonomously to the saturation point.

Model of the Ib Interneuron

The Ib interneuron potential is formalized by the following equations:

$$\frac{d}{dt}(Ib_i) = (1 - Ib_i)(exc_i) - Ib_i(inh_i) \tag{3.12}$$

where the terms exc_i and inh_i are expressed by equations 3.13

$$\begin{aligned} exc_i &= w_i \cdot F_i \\ inh_i &= K + \sum_{k=1,k\neq i}^{n}(Ib_k) \end{aligned} \tag{3.13}$$

Where F_i is the force measure coming from the force sensor of the actuator, and K a forgetting constant.

The interneuron output Ibo_i is

$$Ibo_i = Th(Ib_i) \tag{3.14}$$

In the model I do not consider the model for the Golgi tendon organ, but I consider only a normalized measure of the force.
As it is possible to see in figure 3.5, the Ib interneurons inhibit the motoneuron of the agonistic muscle and excite also the motoneurons of the antagonistic muscles. In the case of the shoulder reflex module, this controls the dorsal, the pectoralis and deltoid actuators. The action of the Ib interneuron permits the inverse myotatic reflex. For example when the arm is forced in a rapid extension, the force in the dorsal and pectoralis actuators will increase rapidly, which will increase the activity in the corresponding Ib interneurons. Ib cells of the dorsal and pectoralis muscles, in turn, go to excite the deltoid's motoneuron. This action permits the arm to follow the external force, and avoid muscle break. Differently from the Grossberg et al. model [39] I do not take in consideration the action of the other interneurons that are innervated by the Ib afferent fibers.

Muscle Spindle and Inc, Ins Interneurons Models

The artificial muscle spindle has the main purpose of computing the errors of position and velocity of the actuator. This model differs from the model proposed by Grossberg et al. [39], [63] because it doesn't take in account the intrafusal muscle contraction. I adopted this model because of the structure of the actuator and contraction sensor. Indeed, in the arm prototype, the contraction of the actuator is measured by an external sensor that flexes when the actuator length decreases. It is not possible to regulate the flexion of the sensor independently by the actuator contraction, therefore it doesn't make sense to use a specific model for the intrafusal muscle.
The model for the muscle spindle Ms is formalized in equation 3.15.

$$Ms_i = K_p(L_i - A_i) + K_v \sqrt[3]{(\frac{d}{dt}L_i - GV_i)} \tag{3.15}$$

Where L_i represents the i^{th} muscle length, A_i is the desired length for the muscle, GV_i the desired muscle linear velocity and finally K_p and K_v are the gains for the position error and the velocity errors respectively.
The output of the artificial muscle spindle constitutes the error feedback for: motoneurons, Ia cells and cerebellum module. This error is represented in equation 3.16

$$E_i = Th(Ms_i) \tag{3.16}$$

The error can assume only positive values, this is in accordance to the fact that all the neurons dynamics can vary between zero and one. When the position or the velocity errors become negative they are neglected by the artificial muscle spindles. This means that the corresponding motoneuron is not stimulated and therefore it decreases autonomously its potential. This acts in decreasing the contraction of the actuator that, in turn, increases its length and contributes to decrease the negative error. The models for the Inc and Ins interneuron are quite simple. These neurons have the function to integrate the information coming from the cerebellum module and from the P (stiffness) commands with the signals coming from the path generator module. For this neuron I decide to implement an algebraic model, and therefore avoid their dynamics.

$$Inc_i = Ins_i + Cs_i \tag{3.17}$$

$$Ins_i = Lt_i + P_i \tag{3.18}$$

where Cs are the signals coming from the cerebellum module and Lt is the command length for the actuators. In both the cells the signals Cs and P will increase their potential. Also for these cells the output is limited between 0 and 1 by the threshold function.

Dynamic Synapse

The reflex neural network must be able to adapt to the dynamic characteristics of the system that needs to be controlled. In order to perform this behavior, neuron weights have to be changed during the system operation. Their values will change until they reach the optimal solution for the control. This means that the error must decrease as fast as possible, and no overshoot can be present in the system response.

In supervised learning, the adjustment of neuron weights happens in concomitance with function minimization; that is significant for the control problem in question. Instead, in unsupervised learning, the neural network improves its performance using a task-independent measure of the control quality.

However, this process usually is difficult to perform in real time, especially if the network has to learn and control the system at the same time. What I have tried to implement in some neuron model is to use dynamic input weighting. In this specific case, the weight is also a dynamic system, and the model in the Laplace domain is presented by the equations 3.19.

$$w_i = Lim(\frac{1}{s} \cdot [K_1 x_i - K_2 w_i])$$

$$\begin{aligned} Lim(V) = V \quad if \quad V_{min} \leq V \leq V_{max} \\ Lim(V) = 0 \quad if \quad V < V_{min} \\ Lim(V) = 1 \quad if \quad V > V_{max} \end{aligned} \tag{3.19}$$

Where K_1 and K_2 are opportunely chosen to set the "correct" learning rate. In fact, if K_1 is too big, the weight saturates rapidly at the maximum value permitted.

It is possible to set these two values empirically; let's suppose that the weight input x_i (spiking signal) has the maximum frequency, we want that, in these initial conditions, the weight increases and reaches the maximum value admissible (one) in about one second. This specification is sufficient to set the K_1 value. In the same mode we can set the K_2 value, but this time we have to consider a null x_i input signal and choose the period of time that the weight needs to pass from the high value to the low admissible value (zero). In equation 3.19 the function Lim is an output limitation, and it regulates the internal status of the weight.

The weighting differs from the Hebbian learning rule [64], because it does not take into account the correlation between the presynaptic and postsynaptic neuron activity. In fact, we can think at this learning rule as a local observer: the weight is reinforced if the input of the neuron is stimulated, and weakened otherwise. In a certain manner each neuron is an independent controller and it realizes the control strategy taking in account only his own inputs. This simplify the network configuration and avoids the weight saturation.

3.5 Path Generator Module

The path generator module is capable of generating desired arm movement trajectories by smoothly interpolating between the initial and the final length commands for the synergetic muscles that contribute to a multi-joint movement. The rate of the interpolation is controlled by the product of two signals: the start signal GO and the output of the V_i cell, that computes the error in the length of the muscle i^{th}. The Go signal is a volitional command that in our case is formalized by the equation 3.20:

$$GO(t) = Go\frac{(t-\tau_i)^2}{k+(t-\tau_i)^2}u[t-\tau_i] \tag{3.20}$$

where parameter Go scales the GO signal, τ_i is the onset time of the i^{th} volitional command, k takes in account the time that the GO signal needs to reach the maximum value and $u[t]$ is a step function that jumps from 0 to 1 to initiate the movement. The V_i cell dynamics is defined

$$\frac{d}{dt}V_i = K(-V_i + Lt_i - A_i) \tag{3.21}$$

where Lt_i is the target length for the i^{th} muscle, the constant K defines the dynamic for the cell and A_i defines the present length command for the i^{th} muscle. The model for the neuron A_i is defined in equation 3.22.

$$\frac{d}{dt}A_i = GO \cdot Th(V_i) - GO\sum_{k=1,k\neq i}^{n} \cdot Th(V_k) \tag{3.22}$$

Where again the Th is the same threshold function used for all the cells of my model. Study of Bullock and Grossberg [65] have demonstrated that this path generator model can be used to explain a large number of robust kinematic features of voluntary point to point movements with a bell-shaped velocity profiles. The architecture for the path generator is presented in figure 3.6. The circuit is suitable for the three muscles of the shoulder joint that permit the upper arm flexion-extension and adduction-abduction. The trajectory generators for the arm's other muscles are quite similar to that one presented. The inputs for the system are the target lengths Lt_i for each muscle and the outputs are the signals A_i that will feed the inputs of the reflex module of each joint.

3.6 The Cerebellar Module

In this section I propose a possible architecture for emulating the human cerebellum; this model is based on the actual knowledge that neurophysiologists have of this organ.
A large number of cerebellar models are described in the literature, some of which are briefly explained in the following section.

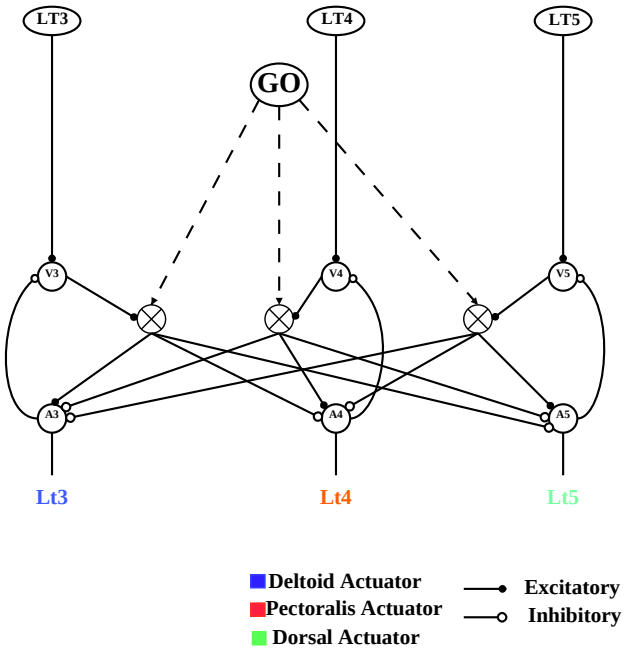

Figure 3.6: Architecture of the Trajectory Generator Module

3.6.1 Computational Cerebellar Models

The regular structure of the cerebellum inspired several early computational models. In 1971 Albus linked the cerebellum to a single perceptron proposed by Rosenblatt in 1962 [66]. In the simple perceptron model, inputs are summed in association units from where they are connected via adjustable weights to an output unit. All units are binary. A simple rule for adjusting the weights will eventually lead to the perceptron generating a desired output for a given input: if the output was correct, increase the weights from active association cells; if the output was incorrect, decrease the weights from active association cells. Another pioneering computational model of the cerebellum was the CMAC (Cerebellar Model Articulation Controller) architecture introduced by Albus in 1975 [67]. The basic architecture of the CMAC (in the implementation of Miller et al. [68]) is depicted in figure 3.7. The first important feature of the CMAC is the discretization of the input signals through the input sensors. Each signal activates a number of input sensors. The input sensors are connected to the state space detectors in a regular fashion;

these detectors are AND-units and therefore their output will assume the value one only when all their inputs are active.

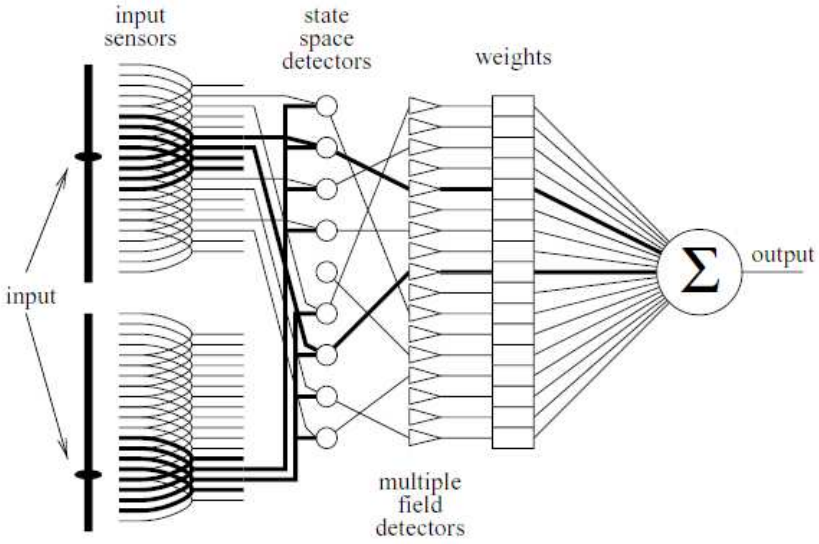

Figure 3.7: The CMAC model of the cerebellum.

The state space detectors are connected to the multiple field detectors via random hashing. These detectors compute the OR function. Finally, the weighted outputs of the multiple field detectors are summed together, constituting the output of the CMAC. CMAC has the advantages of local generalization,incremental training, rapid computation, output superposition and fast practical hardware implementation, but the hash coding could introduce noise and it cannot be guaranteed to learn a low error solution.
Bullock et al. [40] developed a detailed model of the cerebellar circuitry that included all the cell types and connections in the cortex (Figure 3.8). The model was designed to show how the cerebellum could learn timed responses following a conditioned stimulus. Their simulations showed how the Golgi feedback circuit could generate a spectrum of timed activation peaks in granule cells that Purkinje cells could use to time a response. Inhibitory neurons in the cortex (stellate and basket cells) make fixed strength synapses with Purkinje cells, while parallel fiber-Purkinje synapses are excitatory and modifiable. Because stellate cells receive their input from the same parallel fibers that project to the Purkinje cells, this setup allows some granule-Purkinje cell weights to become negative while keeping all the parallel fiber-Purkinje cell weights excita-

tory, making the network more powerful.

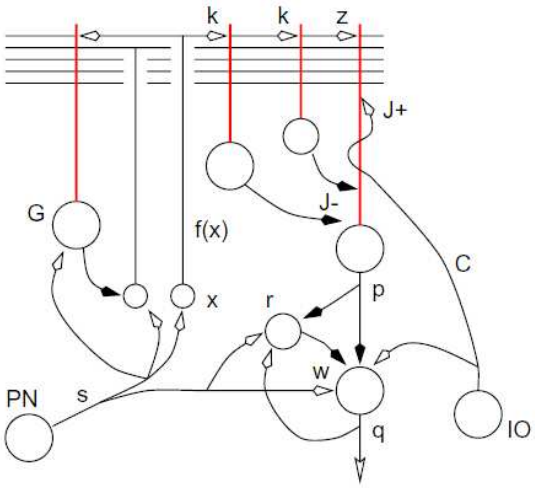

Figure 3.8: Model of cerebellar cortex proposed by Bullock et al.

Others authors have modelled the cerebellum proposing different architectures (Houk at al. [69], Schweighofer-Kawato et al. [70]), Bullock et al. [71], but for brevity they are not reported in this document.

3.6.2 Module Architecture

In order to test a complete control architecture that comprises all the modules presented in this chapter, I decided to implement a simplified version of a cerebellar model that includes the more important aspects of the real organ. In their papers [72], [73], [74], [75], [76] Kawato et al. argue that internal models of the arm are located in all brain regions having synaptic plasticity. Furthermore they maintain that the direct and inverse dynamic model of the arm are located in the cerebellar cortex.
The goal that I want to pursue is the implementation of a system able to learn the inverse dynamic model of the arm, and to adjust, through the regulation of the Inc_i and R_i cells activities , its trajectory during fast movement. The architecture that I adopted is presented in figure (Figure 3.9).

The Gv_i signals generated by the path generator module, that is a vector of 7 elements, in the cerebellum module, constitutes the mossy fiber inputs. These signals (excitatory) feed the granule cell layer (10x10

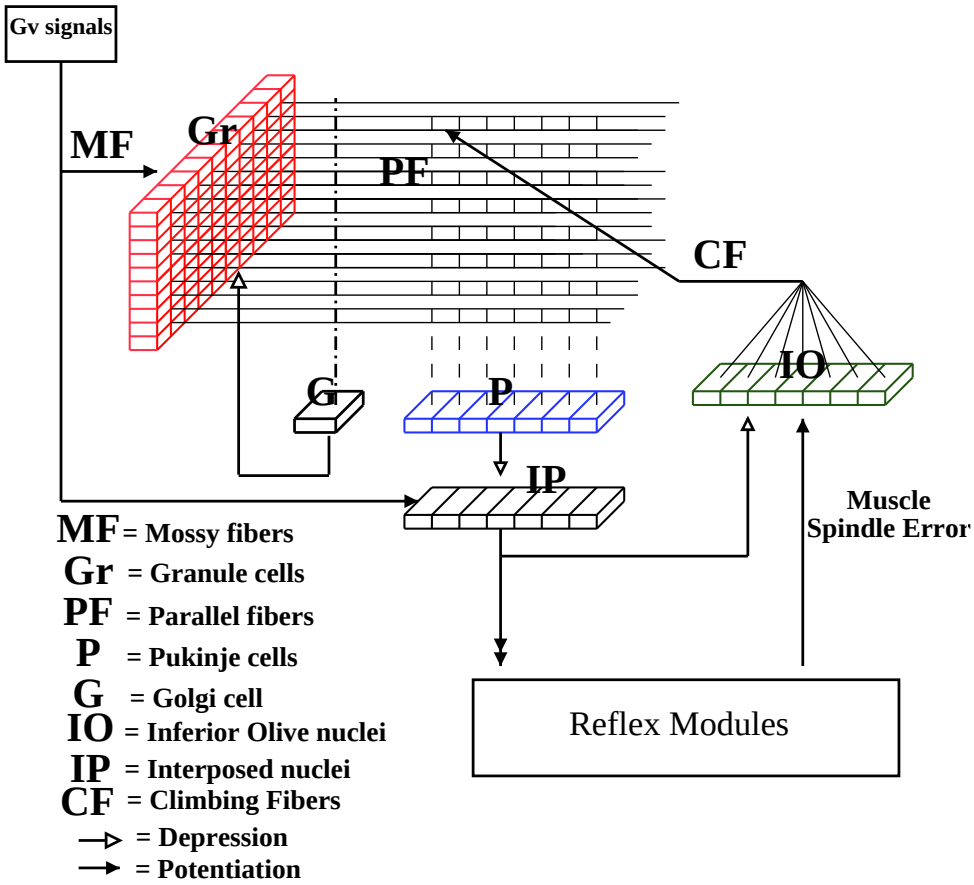

Figure 3.9: Cerebellum Module

cells). In particular, each granule cell receives 4 randomly selected Mfs mossy fibers, in order to implement the sparse code behavior characteristic for these cells. The outputs of the granule cells layer forms, in its turn, the parallel fiber array. The only Golgi cell receives its inputs (excitatory) from all the Mossy fibers, and inhibits all the granule cells. In the Purkinje cells layer (1x7) each cell receives a beam of Mossy Fibers (comprising one third of the Mossy fibers). Each Purkinje cell receives also a single climbing fiber that regulates the weights of the connection between parallel fibers and Purkinje cells. These weights permit the cerebellum to learn the best control strategy in order to correct the arm trajectory during fast movement. Purkinje cell outputs, in turn, go to feed the inputs of the interposed nuclei layer. Each cell of this nuclei receives the output (inhibitory) of a single Purkinje cell and only one

mossy fiber signal (excitatory). In its turn, the output of each cell of the interposed nuclei is sent to the reflex module and to the inferior olive nuclei (inhibitory). The inferior olive's cells receive the other inputs (excitatory) from the reflex modules. These are the 7 error signals coming from the artificial muscle spindles.

3.6.3 Cell Models

In this section I describe the model for each cell type used in the cerebellum module. Each cell is modeled as a leaky integrator, using a first order differential equation. The membrane potential is defined in equation 3.23.

$$\tau \frac{dm}{dt} = -m + u \tag{3.23}$$

where u are the cell inputs opportunely weighted. The cell output, except the output of a inferior olive cell, is a positive real number that represent the instantaneous firing rate, and is defined by the equation 3.24.

$$Y(m) = \frac{1}{1 + exp(-a \cdot (m - b))} \tag{3.24}$$

where a and b are two parameters that define the linear range of the cell and the baseline respectively. For the inferior olive cell output I decided to use a binary signal. Inferior olive cells, in the human cerebellum, are known to fire at very low rates. Spontaneous firing occurs at about 2Hz, while the maximum rate is around 10Hz. The output of this cell is modeled in equation 3.25.

$$Y_{IO}(x) = \begin{cases} 0 & \text{if } m_{io} < V_{th} \\ 1 & \text{if } m_{io} \geq V_{th} \end{cases} \tag{3.25}$$

When $m_{io} \geq V_{th}$ the potential of the inferior olive cell is modified by equation 3.26.

$$m_{io} = m_{io} - 1 \tag{3.26}$$

Granule Cell Model

The granule cell potential is defined in equation 3.27.

$$\tau_{Gr}\frac{d}{dt}(m_{Gr}) = -m_{Gr} - w_G Y_G + \sum_{i\in M}(w_{MF}Y_{MF}) \tag{3.27}$$

where M is the pool of four mossy fibers randomly selected, w_G is the weight for the $G->Gr$ synapse and w_{MF} the weight for the $MF->Gr$ synapse.

Golgi Cell Model

The Golgi cell potential is expressed in the following equations.

$$\begin{cases} \tau_G\frac{d}{dt}(m_G) = -m_G + \sum_{i=1}^{n}(w_{PFi}Y_{PFi}) \\ Y_{PFi} = Y_{GCi} \end{cases} \tag{3.28}$$

where w_{PFi} is the weight for the i^{th} $PF->G$ synapses, and n the total number of parallel fibers (100).

Purkinje Cell Model

The Purkinje cell potential is defined in equation 3.29.

$$\tau_P\frac{d}{dt}(m_P) = -m_P + \sum_{i\in N}(w_{PFCi}Y_{PF}) \tag{3.29}$$

where w_{PFC} is the adaptable synapse regulated by the climbing fibers. The model for this weight is described in the last section of this chapter.

Interposed Cell Model

The model for the potential of the interposed cells is expressed in equation 3.30.

$$\tau_{IP}\frac{d}{dt}(m_{IP}) = -m_{IP} - w_P Y_P + w_{MF}Y_{MF} \tag{3.30}$$

where w_P is the weight for the $P->IP$ synapses, and w_{MF} the weight for the $MF->IP$ synapses .

Inferior Olive Cell Model

The following equation formalizes the potential for the single inferior olive cell.

$$\tau_{IO}\frac{d}{dt}(m_{IO}) = -m_{IO} - w_{IP}Y_{IP} + w_E E \tag{3.31}$$

Where w_{IP} is the weight for the $IP->IO$ synapse and w_E the weight for the error signal E coming from the reflex module.

3.6.4 The Learning Role

A feature of learning in biological systems is that early in the process of adaptation a strategy of high cocontraction (giving higher limb stiffness and improving accuracy) is adopted, but with practice the level of co-contraction is reduced (Ghez [77], [78]). Inferior olive cells are known to fire at very low rates, with spontaneous firing occurring at about 2Hz, while the maximum rate is around 10Hz. This presents a challenge to the model since the entire movement lasts only on the order of 800ms, which would allow for a maximum of 8 error correcting inputs per arm movement. The weight w_{PFC}, in this adaptation, follows the the learning role presented in equation 3.32.

$$\tau_w\frac{d}{dt}(w_{PFC}) = +Y_{PF}(\beta(1 - w_{PFC}) - \alpha \cdot Y_{IO}Y_P) \tag{3.32}$$

where Y_{IO} is the teaching signal, α is a constant that determines the learning rate and β is the constant that regulates the forgetting mechanism. The role is derived from the Hebbian role introduced by Hebb in 1949 [64] with the improvement introduced by Kohonen in 1988 [79], [80] in order to avoid the weight saturation. This rule can be explained in such a statement: *If two neurons on either side of a synapse are activated simultaneously (synchronously), then the strength of that synapse is selectively increased, otherwise the synapse is weakened* [81].
In particular equation 3.32 embodies the hypothesis that long term potentiation LTP will occurs whenever parallel fibers are active without coincident climbing fibers activity. Long term depression requires that both parallel fibers and climbing fibers signals be different from zero [82]. When the system is sufficiently trained it produces a signal similar to the Ia spinal efferents (proportional to muscle errors) which opposes the error and causes improved trajectories.

4 Arm Model

4.1 Introduction

In this chapter I describe the kinematic and the dynamic arm models. These models trace the principal mechanical characteristics of our artificial arm, and are used as a test bed for the control system strategy instead of using the real prototype. Of course, I am conscious that it is quite impossible to take into account all the characteristics of a real system, nevertheless a simplified model will help me to test the overall neural control behaviors. In section 1 I describe the direct kinematic model in homogeneous coordinates; given the vector that describes the joint angle positions, the algorithm will calculate the position of the arm extremity in the Cartesian space. Section 2 deals with the computation of the inverse kinematic model. In order to obtain a fast algorithm a back propagation neural network is trained to perform the inverse computation. In Section 3 I describe the dynamic model for the Arm . The last section elucidates the implementation of the model using the Matlab environment and depicts some testings in order to validate the overall model.

4.2 Direct Kinematic Model

The arm I consider is an open kinematic chain with a total of 4 DOFs, three are inside the shoulder joint and one in the elbow joint. Unlike classical manipulators, where each single joint has only one degree of freedom, the arm I designed has a joint, in the shoulder, with 3 DOFs. This means that the position and the orientation of the upper arm depends on three variables. Nevertheless it is possible, thanks to the disposition of the supraspinatus and subscapularis actuators, to make a simplification. We can consider the rotation actuated by these two muscles (with respect to the axis defined by the upper arm) as independent from the other two shoulder rotations, actuated by the other three muscles. If we think in homogeneous coordinates, to define the upper arm position and orientation , we can do two rotations with respect to an absolute

reference system (fixed at the robot structure) and one rotation about an axis fixed with the upper arm.

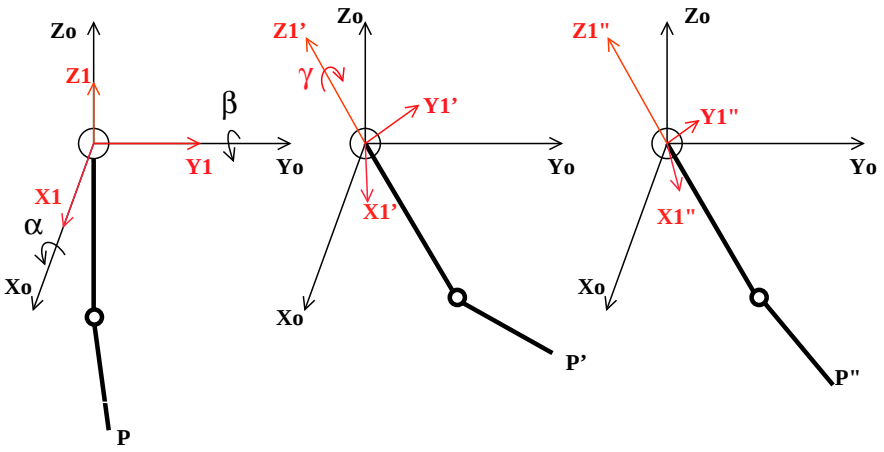

Figure 4.1: Shoulder Rotations

We can represent the first two rotations relatively to the absolute axes X_0 and Y_0 using a single matrix in homogeneous coordinates $H^0_{\alpha,\beta}$: note that the rotation about the X axis is done before the rotation about the Y axis (otherwise a different position is reached).

$$H^0_{\alpha,\beta} = \begin{pmatrix} C\beta & 0 & S\beta & 0 \\ 0 & 1 & 0 & 0 \\ -S\beta & 0 & C\beta & 0 \\ 0 & 0 & 0 & 1 \end{pmatrix} \begin{pmatrix} 1 & 0 & 0 & 0 \\ 0 & C\alpha & -S\alpha & 0 \\ 0 & S\alpha & C\alpha & 0 \\ 0 & 0 & 0 & 1 \end{pmatrix} \tag{4.1}$$

where I have applied pre-multiplication. Now it is possible to execute the third rotation about to the $Z^{1'}$ axis, that is expressed with the equation 4.2.

$$H^{1'}_{\gamma} = \begin{pmatrix} C\gamma & -S\gamma & 0 & 0 \\ S\gamma & C\gamma & 0 & 0 \\ 0 & 0 & 1 & 0 \\ 0 & 0 & 0 & 1 \end{pmatrix} \tag{4.2}$$

Using post-multiplication we can calculate the matrix that defines the direct kinematic for the upper arm (Equation 4.3).

$$H^0_{\alpha\beta\gamma} = H^0_{\alpha,\beta} \cdot H^{1'}_{\gamma} \tag{4.3}$$

Given the three angles $(\alpha\beta\gamma)$ it is possible to calculate the position of the Elbow in the base reference system $sdr0$.

$$P^0_{elbow} = H^0_{\alpha\beta\gamma} \cdot \begin{pmatrix} 0 \\ 0 \\ -L_{UpArm} \\ 1 \end{pmatrix} \tag{4.4}$$

where L_{UpArm} is the length of the upper Arm.
Now we have to consider also the elbow rotation respect a relative reference system (sdr2) fixed with the forearm and with the origin translated along the $Z^{1"}$ axis (see Figure 4.2).

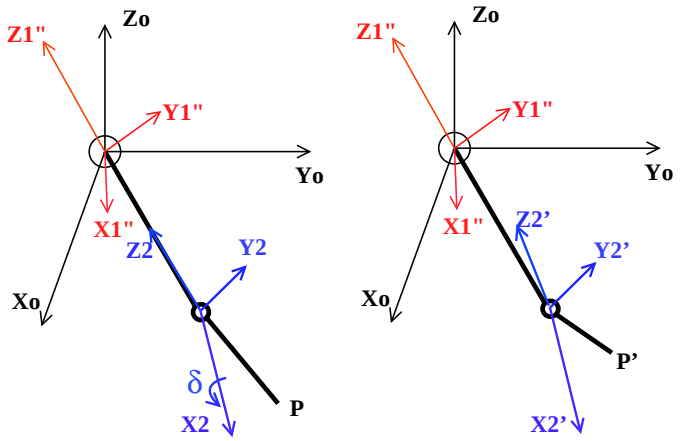

Figure 4.2: Elbow Rotations

The matrix that represents this rotation is :

$$H^{1"}_{\delta} = \begin{pmatrix} 1 & 0 & 0 & 0 \\ 0 & C\delta & -S\delta & 0 \\ 0 & S\delta & C\delta & -L_{UpArm} \\ 0 & 0 & 0 & 1 \end{pmatrix} \tag{4.5}$$

This matrix defines the reference system $sdr2$ expressed in the $sdr1$. The $sdr2$ is rotated about the axis X_1 and translated by the quantity

L_{UpArm} (length of the upper arm). Now we can formalize the arm direct kinematic using the matrix $H^0_{\alpha,\beta,\gamma,\delta}$.

$$H^0_{\alpha,\beta\,\gamma,\delta} = H^0_{\alpha\beta\gamma} H^{1"}_{\delta} \tag{4.6}$$

Therefore given a point relative to $sdr2$ that defines the wrist position and given the four angles $(\alpha, \beta\,\gamma, \delta)$ it is possible to calculate the wrist position relative to the reference system $sdr0$ (that defines the base reference system for the arm).

$$P^0_{wrist} = H^0_{\alpha,\beta\,\gamma,\delta} \cdot P^2_{wrist} = H^0_{\alpha,\beta\,\gamma,\delta} \cdot \begin{pmatrix} 0 \\ 0 \\ -L_{FoArm} \\ 0 \end{pmatrix} \tag{4.7}$$

where L_{FoArm} is the length of the forearm.
It seems that the problem is solved, but this is not true. Indeed the joint positions are fixed by the lengths of the actuators that are connected with the upper and the forearm. Therefore to formalize an appropriate direct kinematic model it is necessary to find a functional relationship F between the actuator lengths and the elbow and wrist positions.

$$P_{wrist} = F \begin{pmatrix} L_1 \\ L_2 \\ L_3 \\ L_4 \\ L_5 \\ L_6 \\ L_7 \end{pmatrix} \tag{4.8}$$

The vectorial field F $(R^7 \rightarrow R^3)$ is not defined for every points $\mathbf{L} \in S$, where S is a subspace of R^7 that includes all the possible combinations of the actuator lengths. This assertion is clear if we think for example at the elbow; we can not fix the triceps and biceps both at the minimum lengths.
It is possible to find the direct kinematics of the arm solving a system of equations, where each equation imposes a constraint on the arm position. The points that I consider in the system of equations are reported in table 4.1.

Actuator	Origin Point	Insertion Point	Actuator Length
Supraspinatus	Osp	Asp	Lsp
Subscapularis	Osc	Asc	Lsc
Dorsal	Odo	Ado	Ldo
Deltoid	Ode	Ade	Lde
Pectoralis	Opc	Apc	Lpc
Triceps	Otr	Atr	Ltr
Biceps	Obi	Abi	Lbi

Table 4.1: Actuators Origin, Insertion and Lengths

4.2.1 Adduction-Abduction of the Upper Arm

The movement of adduction-abduction is governed by the action of three muscles (dorsal, pectoralis, deltoid) and has two degrees of freedom. During the movement we can divide the muscles in two groups: the first comprises the muscles that are contracting (active), the second is composed by the muscles that are releasing (passive). It is possible now, fixed the length of the active muscles, to find the position of the upper arm solving the following system of equations.

$$\begin{cases} (x - Opc_x)^2 + (y - Opc_y)^2 + (z - Opc_z)^2 - Lpc^2 = 0 \\ (x - Odo_x)^2 + (y - Odo_y)^2 + (z - Odo_z)^2 - Ldo^2 = 0 \\ (x - Os_x)^2 + (y - Os_y)^2 + (z - Os_z)^2 - (\|Os - Opc\|)^2 = 0 \end{cases} \tag{4.9}$$

where Os is the point that defines the shoulder position.
In the system the unknown terms x,y,z represent the point of the arm where the pectoralis and dorsal muscles are inserted. The first two equations impose that the distance between the two muscle's extremities are equal to the imposed lengths, the third equation imposes that the distance between the muscle insertion and the shoulder is fixed during the movement. If the lengths imposed for the actuators are admissible values there are two possible solutions for the system, and we can chose one of these. In particular I solved the system in a symbolic form using Matlab. There are other two cases to solve in order to complete all the possible combinations of active muscles; for both of them the systems to solve are very similar to the first one and aren't reported here.

4.2.2 Rotation of the Upper Arm

When the upper arm is positioned in the space we can already fix its rotation. This movement is done by the supraspinal and subscapularis

actuators. At the geometric level this orientation is imposed fixing the point of the shoulder's joint where the two muscles are attached as illustrated in figure 4.3.

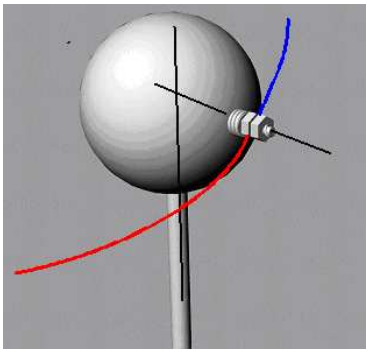

Figure 4.3: Supraspinatus (blue) and Subscapularis (red) Insertions

The segment that connects this point with the center of the joint must be orthogonal to the upper arm. If we fix the length of one of the two muscles (for example the subscapularis) it is possible to find the point where to attach the actuators by the solution of the following system.

$$\begin{cases} (x - Osc_x)^2 + (y - Osc_y)^2 + (z - Osc_z)^2 - Lscc^2 = 0 \\ (x \cdot Oel_x) + (y \cdot Oel_y) + (z \cdot Oel_z) = 0 \\ (x - Os_x)^2 + (y - Os_y)^2 + (z - Os_z)^2 - (\|Os - Asc\|)^2 = 0 \end{cases} \tag{4.10}$$

where Oel defines the elbow position. In the system the first equation imposes that the distance between the insertion and the origin of the subscapularis muscle is equal to Lsc. The second equation imposes the orthogonality between the segment(mentioned before) and the upper arm. And the last equation imposes the distance conservation, between the shoulder origin and the two muscles insertion. The other case (supraspinatus active and subscapularis passive) is quite similar to the first one and therefore is not reported.

4.2.3 Adduction-Abduction of the Forearm

When the elbow position and orientation are already fixed there remains another degree of freedom, the position of the forearm. This is imposed fixing the biceps and triceps lengths. Again we have two possibilities; if we fix the biceps length, the position where the two muscle attach can be found solving the following system of equations.

$$\begin{cases} (x - Obi_x)^2 + (y - Obi_y)^2 + (z - Obi_z)^2 - Lbi^2 = 0 \\ (x \cdot Osc_x) + (y \cdot Osc_y) + (z \cdot Osc_z) = 0 \\ (x - Oel_x)^2 + (y - Oel_y)^2 + (z - Oel_z)^2 - (\|Oel - Abi\|)^2 = 0 \end{cases} \tag{4.11}$$

The meaning of the equations is similar to that introduced before.

4.3 Inverse Kinematic Model

Solving the inverse kinematic problem for the arm, means to find the artificial muscle lengths when a target point for the wrist is known. A necessary, but not sufficient, condition for the existence of the solution, is that the point that we want to reach is inside the arm's workspace. In robotics terminology the manipulator workspace is the portion of the space that is reachable by the robot's hand. If we take in account only the target point and we do not consider the arm orientation when the target is reached, the inverse kinematic problem, in our case, has an infinite number of solutions. This is due to the fact that to reach a point in a three dimensional space only three degrees of freedom (3DOFs) are needed, but our arm has four DOFs. To find a single solution I impose, in the system equations, a constraint on the orientation of the plane formed by the upper and forearm with the robot's sagittal plane. Normally this angle in a human being is about 20 degrees and remains fixed during the arm movement. 4.4.

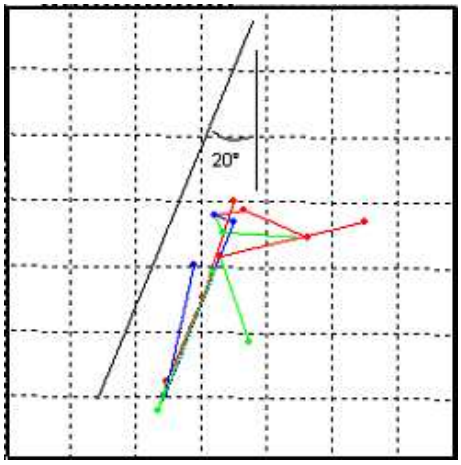

Figure 4.4: Frontal View of the Arm

It is possible to approach the inverse kinematic problem in two ways: using the direct kinematics to generate input-output pairs that can be used to train a neural network, or solving other systems of equations where the wrist position is imposed. I followed the first approach which seems to be more appropriate to this situation.

4.3.1 A Back Propagation Neural Network To Learn the Inverse Kinematics

In order to obtain the input-output pairs necessary to train a neural network, I executed the direct kinematic algorithm on a sufficient set of inputs. Each input was an admissible vector of actuator lengths (as admissible I intend a set of muscle lengths that bring the wrist in a position inside the workspace). To determine the correct intervals for the actuator lengths, I performed some measurements directly on the real arm prototype. In a second step, when this data was known, I created a data set of points each representing a vector of actuators lengths. Finally I calculated the corresponding wrist position.
As a neural network architecture I chose a multilayer perceptron [83] with an input layer of three neurons, two hidden layers of 20 neurons each, and an output layer of seven neurons.

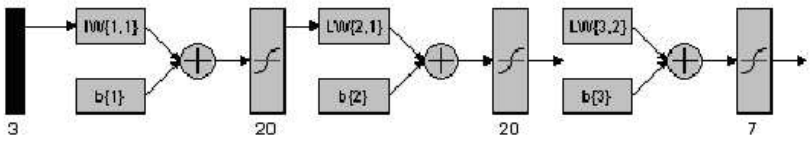

Figure 4.5: Architecture of the Multilayer Perceptron

As an activation function for the neurons I chose a sigmoid, and for the network training the back propagation algorithm. Before training, the input-output pairs were normalized in order to obtain values in the interval (-1,1). I have used a set of 1081 training data, that was obtained using points in the workspace at distances of 5cm. The trend for the medium square error is reported in figure 4.6.

As we see from the graph the error, after 50 epochs, decreases under the value $2 \cdot 10^{-3}$. After 1000 epochs the error reached the value of $1.6 \cdot 10^{-4}$. This required 16 hours of computation on a Pentium-4 (2GHz) equipped with 500 Mb of memory.

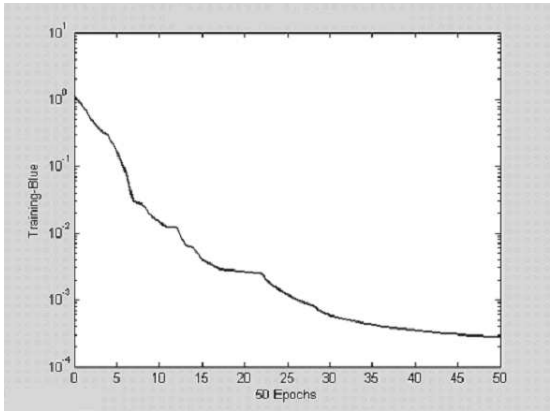

Figure 4.6: Trend of the medium square error after 50 epochs

After the net was trained I conducted a series of tests to understand if the neural network exhibits a generalization behavior. Therefore I gave to the net positions for the wrist that were different from the positions used for training, and I calculated the error of generalization. In figure 4.7 we can see the error for 28 wrist positions.

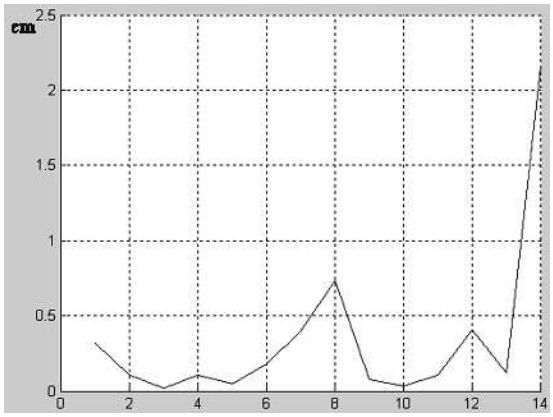

Figure 4.7: The Generalization Error on the wrist position (calculated on 28 points)

The median value in positioning the wrist is about 0.8 cm, which is a good value for my purposes.
The main advantage in using a neural network to compute the inverse kinematics is that we can train the network on values acquired directly on the real arm. This overcame the limitations in using an approximate arm model, and is suitable especially for complex kinematic chains as found

in a humanoid robot. The other advantage is that the time required for the network to compute the inverse kinematic, for a given point in the workspace, is low in comparison with other algorithms. Indeed, when the network is trained, the operations required to calculate the outputs are simple additions and multiplications.

4.4 Direct Dynamic Model

The Arm dynamic model takes into account the dynamic equations that permit to calculate the arm motion. These equations are useful not only to simulate the arm movements, but also to synthesize the best control strategy. In particular there are two principal problems that involve these equations: the direct dynamic problem and the inverse dynamic problem. In the first problem given the forces and the moments applied on the arm it is required to find the arm acceleration, velocity and position. In the second problem given the arm position, velocity and acceleration it is required to find the forces and the moments needed to actuate the system. I will concentrate on the first problem, therefore knowing the forces of the actuators and eventually the external forces I want to calculate the arm acceleration, velocity and instantaneous position. I will not formalize the entire direct dynamic model, but I will focus on the more critical aspects. In particular the model implementation was done using the Matlab tool SymMechanics with the support of the Solidedge software in calculating the inertia matrixes of our arm prototype. This saved a lot time in modelling the system and gave me a full control of each dynamic parameter.
From a mathematical point of view, the arm dynamics can be expressed using the following Newton-Euler formulation:

$$\tau = M(\theta)\ddot{\theta} + V(\theta, \ddot{\theta}) + G(\theta) + T(\theta)F_h \tag{4.12}$$

This equation expresses the joint torques as a function of the motion of the joints [84], where $G(\theta)$ is the matrix of static forces due to gravity. It depends on the arm position; for example the effect of gravity on the joint torques is maximum when the arm is extended in the forward position, and is minimum when the arm is in the rest position. The term $V(\theta)$ contains the centrifugal and Coriolis forces that act due to the relative movement of a joint with respect to the others. The $M(\theta)$ term is known as mass matrix and accounts for the effect of the inertia forces. Finally the term $T(\theta)F_h$ represents the torque generated by an external force applied on the hand F_h.

For a single link it is possible also to define the inertia matrix $J \in M[3 \times 3]$:

$$J = \begin{pmatrix} I_{xx} & I_{xy} & I_{xz} \\ I_{xy} & I_{yy} & I_{yz} \\ I_{xz} & I_{yz} & I_{zz} \end{pmatrix} \tag{4.13}$$

where the diagonal elements of the matrix are the moments of inertia calculated about the principal axes, and the other elements are the products of inertia. This matrix permits to calculate the moment of inertia of a body about a generic axis. The inertia matrices are very important for the dynamic equation 4.12 and furthermore, I need them in order to implement the dynamic model in Matlab. I obtained the inertia matrix for each link using a specific software, (Solidedge). As an input the software needs the 3D design of the arm and the material density. In table 4.2 the principal physical characteristic of the arm prototype are reported.

Link	Length[m]	Section[m^2]	Mass [Kg]
Upper Arm	0.38	$1 \cdot 10^{-4}$	0.21
Forearm	0.28	$1 \cdot 10^{-4}$	0.1
Hand	0.14	$1 \cdot 10^{-3}$	0.2

Table 4.2: Arm's Physical Properties

Link	Matrix of Inertia $[1 \cdot 10^{-6} Kg \cdot m^2]$
Upper Arm	$\begin{pmatrix} 1780 & 0 & 0 \\ 0 & 1780 & 0 \\ 0 & 0 & 13 \end{pmatrix}$
Forearm	$\begin{pmatrix} 590 & 0 & 0 \\ 0 & 590 & 0 \\ 0 & 0 & 4 \end{pmatrix}$
Hand	$\begin{pmatrix} 500 & 0 & 0 \\ 0 & 570 & 0 \\ 0 & 0 & 89 \end{pmatrix}$

Table 4.3: Arm's Inertia Matrices

As it is possible to see, the arm is very light. The overall weight, including the hand mass, is only 0.5 kilogram. This is due to the fact that we chose polycarbonate and aluminium as materials to build the arm's mechanical structure.
The torque vector in the left side of equation 4.12 is a function of the actuator's forces.

$$\tau = D \cdot \mathbf{F} \tag{4.14}$$

where matrix D is function of the joint position of the arm. This matrix like the other terms of equation 4.12 ($V(\theta$,$G(\theta)$) was not calculated directly because it is generated automatically by the SimMechanics software. As inputs, the software needs the kinematic model for the arm and the physical characteristics of each link. Therefore it is necessary to specify the coordinates of each link with respect to a base reference system. When all the quantities are defined, it is possible to choose the parameters for the numerical integration or let the system choose the more appropriate step of integration. This is usually better because the system can choose different steps of integration depending on the actual simulation condition. This reduces errors in the dynamic simulation especially during rapid variations in the motion. In the next sections I will analyze the static and the dynamic models for the other components of the arm: actuators and joints.

4.4.1 Joint Friction and Constraints

Friction modelling is very important for the overall dynamic behavior of the arm. The friction occurs especially in the joints and can be divided in dynamic and static. However in this model I neglected the static friction because of its low relevance for simulation.
Dynamic friction in the joints, called also viscosity friction, depends on the angular velocity and can be expressed by equation 4.15.

$$\tau_{\mathbf{f}}(\mathbf{t}) = K_d \cdot \dot{\vartheta}(\mathbf{t}) \tag{4.15}$$

Where K_d represents the joint's viscosity and $\dot{\vartheta}$ the joint's angular velocity, which for the shoulder is a vector of three components and for the elbow joint is a scalar. In particular for the shoulder the friction is thought to be concentrated in the joint's center of rotation. This introduces a simplification with respect to the arm prototype, where in the real shoulder's joint the friction is distributed on all the spherical surface. The other important thing that I need to model in the arm joint are constraints. Not all the angle positions are allowed during the movements, therefore when these positions are reached it is necessary to implement a constraint reaction force or moment. In order to avoid a brutal collision I introduce a viscoelastic behavior for the joint when it is near to the constraint. This model is expressed by equation 4.16.

$$\tau_{\mathbf{con}}(\mathbf{t}) = K_v \cdot \dot{\vartheta}(\mathbf{t}) + K_e \cdot \vartheta(\mathbf{t}) \tag{4.16}$$

where K_v is the viscosity constant when the joint is near to the constraint, and K_v the elastic constant that implement the constraint's reaction force. It is clear that both the viscosity friction and the constraint reaction force generate a moments opposite to the joint's motion.
The coefficients I chose for the arm model are shown in table 4.4.

Link	$K_f[\frac{Nm}{degres \cdot s}]$	$K_v[\frac{Nm}{degres \cdot s}]$	$K_e[\frac{Nm}{degres}]$
Shoulder	0.01	0.01	0.05
Elbow	0.001	0.001	0.01

Table 4.4: Friction and Constraint Constants

4.4.2 Artificial Muscle Model

In our arm the actuation system is implemented using the McKibben actuator. It was introduced in the 1950s by the physicist J. L. McKibben for the actuation of orthopedic prothesis. Thank to its properties, which are comparable with those of the human muscle, it is also called artificial muscle. In the 60s this kind of actuator was abandoned in favor of the more efficient electrical motors. However recently the interest for it is increased especially for applications in the field of humanoid robotics. The actual success of this kind of actuator is due to its lightness (30g), its cheapness (10 euro), the high ratio of force/weight (300) and its flexibility. It is particular appropriate to actuate human like joints, that require a linear motion.
The McKibben actuator is pneumatic, therefore in order to control its length and its force it is necessary to control the inside pressure. The system is composed by an internal tube made of rubber and an external braided shell made of a polymeric material. When the inside pressure increases, the actuator inflates and at the same time decreases its length . Tondu and Lopez [85] have proposed a good model for this type of actuator, as in the equations 4.17 and 4.18.

$$\begin{aligned} F_i = {} & \pi r_o^2 P_i [a(1 - K\varepsilon_i)^2 - b] - \\ & - [f_k + (f_s + f_k)e^{-\frac{i}{i_s}}] \frac{1}{n} Sco \cdot P_i sign(\dot{x}) \end{aligned} \tag{4.17}$$

$$Sco = 2\pi r_o l_o \frac{\sin \alpha_o}{(1 - k\epsilon)\sqrt{1 - \cos^2 \alpha_o (1 - k\epsilon_i)^2}} \tag{4.18}$$

where F_i is the force generated by the artificial muscle; P_i is the pressure inside the actuator, r_0 and l_0 are its initial radius and length, x is the actuator position, and a ,b, ε, f_k ,f_s are other parameters that characterize the actuator structure and the dynamic friction.
A dynamic model for this kind of actuator is quite complex, furthermore I decided to take into account only the static behavior.
In order to find out the parameters of equation 4.17and 4.18,it is possible to use the virtual works principle applied on a elementary actuator section (Figure 4.8).

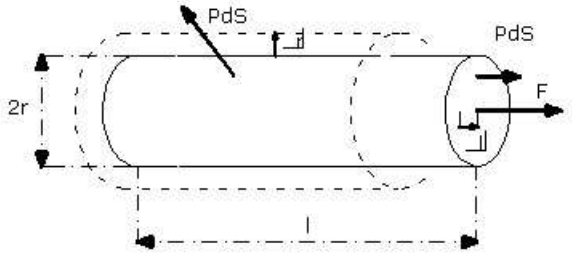

Figure 4.8: A Elementary section of the McKibben pneumatic actuator

Where F is the module of static contraction force for the actuator and δl the elementary variation of the actuator length. I made also the simplifying hypothesis: the pressure inside the inner tube is completely transmitted to the external shell, there are no frictions between the internal tube and the external shell, and furthermore the section of the actuator is cylindrical in each point. Using the virtual works principle we can write:

$$P\delta V = -F\delta l \tag{4.19}$$

where δV is the elementary volume. Therefore :

$$P\delta(A \cdot l) = -F\delta l \Longleftrightarrow Pl\delta A + PA\delta l = -F\delta l \tag{4.20}$$

if we substitute δA and A we obtain

$$P2\pi rl(+\delta r) = (F + P\pi r^2)(-\delta l) \tag{4.21}$$

from which we obtain the actuator force in function of the inside pressure and its length (Eq419).

$$F = 2P\pi rl(-\frac{\delta r}{\delta l}) - P\pi r^2 \tag{4.22}$$

After some algebraical passages it is possible write the equation 4.22 as equation 4.23.

$$F(\epsilon, P) = (\pi r_0^2)P[a(1-\varepsilon)^2 - b] \tag{4.23}$$

where the parameters a and b depend on the actuator characteristic and are equal to:

$$a = \frac{3}{tan^2\alpha_o} \quad and \quad b = \frac{1}{sin^2\alpha_0} \tag{4.24}$$

The variable ϵ is the actuator's rate of contraction and is expressed by equation 4.25.

$$\varepsilon = \frac{l_0 - l}{l_0} \tag{4.25}$$

where l is the actuator length, l_0 the initial actuator length, α_0 the initial angle between the cables of the braided shell and α the actual angle. Observing equation 4.23, we can assert that the force increases with the inside actuator's pressure and decreases with the rate of contraction. Therefore the more the actuator is contracted the less is the force developed. The maximum force is generated when $\epsilon = 0$.

$$F_{MAX} = P\pi r_0^2[a - b] \tag{4.26}$$

It is natural that the actuator can contract only to a given value of its maximum length (usually $15 - 25\%$). When the actuator is completely contracted the force generated is 0. In the following graph I present the test of this model for an actuator with a length of 30cm, an inner tube with a radius of 5mm and parameters a=9 and b=4.

In figure4.9 are reported different characteristics at different pressures; we can observe that the actuator force decreases with the rate of contraction (in chapter seven I will show also same experimental results on a homemade actuator).

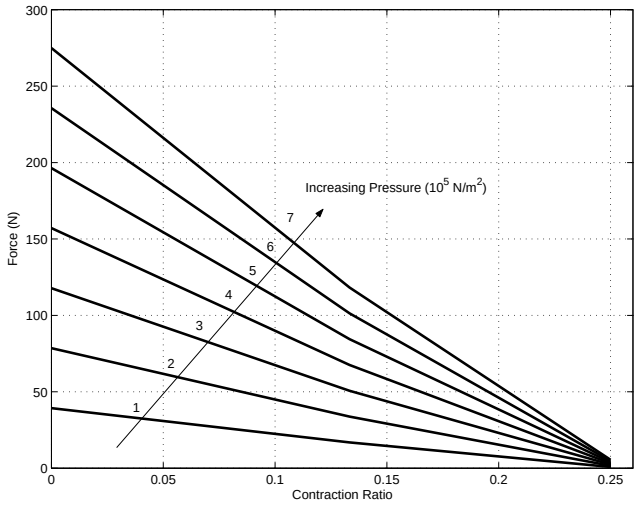

Figure 4.9: McKibben Characteristic from the model simulation

4.5 Simulations of the Arm's Model

In this section I report some results obtained from the simulation of the dynamic arm model. The model that I tested is composed of the structure of the arm, the modules that implement the joint friction and the modules that implement the joint constraints. All the systems were implemented in the Matlab environment.
In order to show the realistic behavior of the model I conducted a simple experiment where the elbow joint was flexed rapidly. To perform this movement I generated artificially (without the actuator dynamic module) a force at the insertion of the biceps actuator and I measured the position, velocity and acceleration for the two arm joints.

The force changes like a step (Figure 4.13) with the maximum value of 30N. In the graphs 4.11, 4.12 and 4.13 are reported the elbow's angular position, velocity and acceleration respectively.

As it is possible to see, the elbow position behaves like a non linear system. The oscillations are damped and this is due to the friction present in the arm joints. The elbow position reach a maximum value of 0.87 radians (0.52^o), therefore the force of 30N is not sufficient to complete the elbow flexion. In figure 4.14 we can see the course of the torque due to the elbow friction, as is possible to note the friction reaches the maximum value when the joint assumes the maximum velocity.

In figures 4.15, 4.16, and 4.17 we can see the angular position, velocity and acceleration of the shoulder joint. As it is possible to see there is

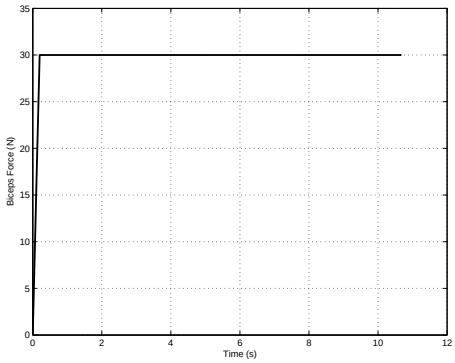

Figure 4.10: Force step applied at the Biceps attach point

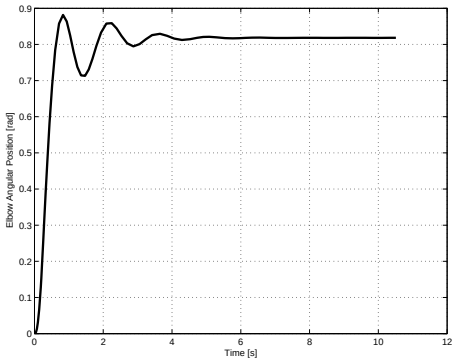

Figure 4.11: Elbow's angular position

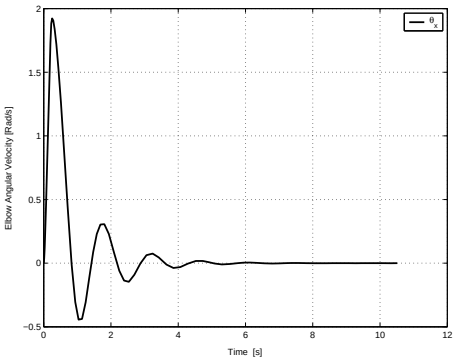

Figure 4.12: Elbow's angular velocity

a rotation with respect to the X axis. This is due to the inertia forces that are transmitted by the forearm to the upper arm during the elbow flexion. In the final position both the elbow and the shoulder are flexed,

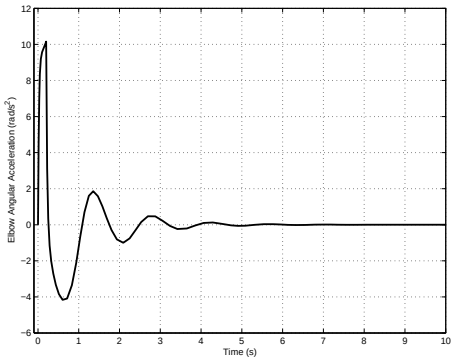

Figure 4.13: Elbow's angular acceleration

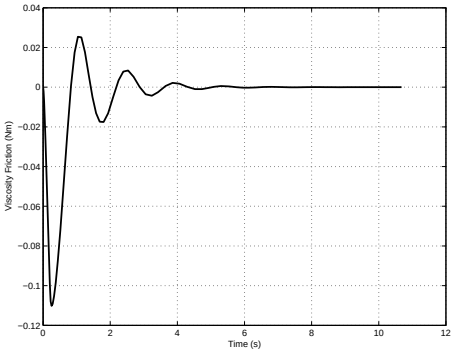

Figure 4.14: Elbow's viscosity friction

this because the arm's barycenter, when the movement is terminated, is positioned in order to guarantee the minimum value for the arm's potential energy.

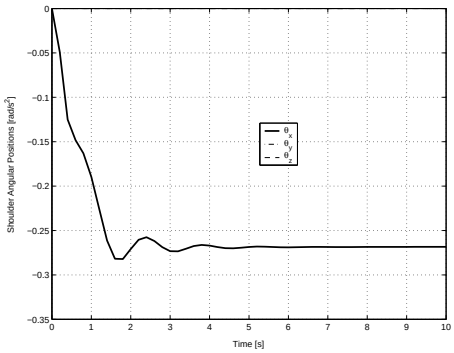

Figure 4.15: Shoulder's angular position

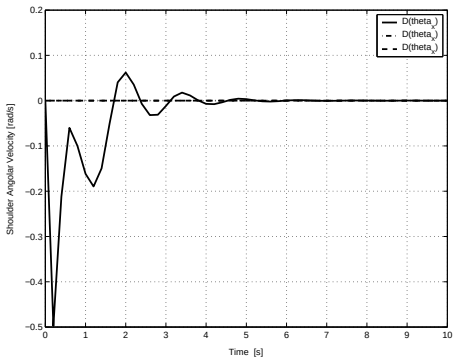

Figure 4.16: Shoulder's angular velocity

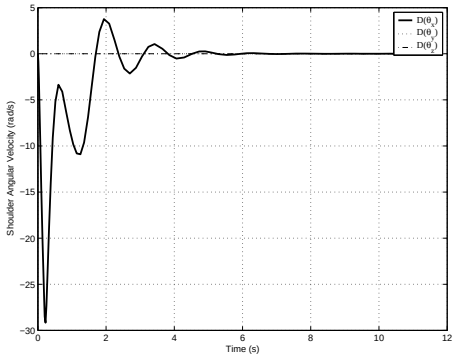

Figure 4.17: Shoulder's angular Acceleration

During the movement the shoulder rotates only about the axis X, and the rotation is opposite to the rotation of the elbow. In the next picture we can see the overall arm movement during the flexion of the elbow. In red are represented the actuators and in green and in blue the upper arm and the forearm respectively. From the picture it is possible to note that some actuators are very short, such as the supraspinatus and subscapularis. This is not true for the real arm prototype, since an artificial muscle can contract only the 20% of its maximum length, we need actuators at least 25cm long in order to perform each movement. Therefore for example for the shoulder rotation the insertions of the supraspinatus and subscapularis do not coincide with that of the model. Instead, in this case, the actuator's representation in the model corresponds with the real tendon that brings the movement from the artificial muscle, situated in the back of the robot, to the shoulder's joint.

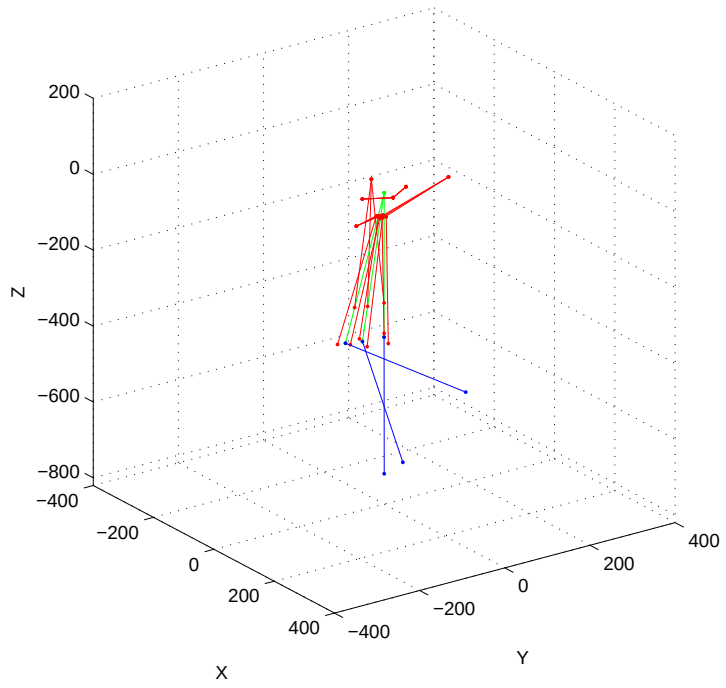

Figure 4.18: Three arm positions during the Elbow Flexion

5 Reflexes Responses and Adaptation

5.1 Introduction

In this chapter I present the results that show how the control system can achieve reflex behaviors comparable to that of a human limb. I will discuss the two principal reflexes that the system can emulate: the myotatic and inverse myotatic reflexes. I will simulate a single joint movement and I will compare the results with an optimal PD controller. I will show the importance of the cross inhibition in the antagonist joint actuators and the effect of an external force on the joint position. In the last section I will explain how the reflex circuits can control the stiffness of a single joint. In particular, stiffness control is very important for a humanoid robot, especially when the robot is required to cooperate with a human being.

5.2 Methods

The simulation of a structured dynamic neural network, like those presented in chapter three, requires substantial attention on the parameter setting. Each parameter can be set between a minimum and a maximum value, for the synaptic weigh this two values are zero and one respectively. Other parameters are constants that fix the dynamic behavior of each neuron.
Because of there are not specific methodologies to set these parameters, I decided to apply an empirical method of trial and error within a prefixed strategy. In order to better understand the behavior of each sub-circuit, it was necessary to start the testing of the control architecture by a initial exclusion of the less essential circuits. This methodology allowed me to adjust the parameters in a simples way than considering the whole system. The simulations started with the testing of the reflex module responsible for the control of the elbow's joint. At first I excluded the action of the interneurons Ia, Ib, R and considered only the

action of the motoneurons. Hence I adjusted the motoneuron synaptic connection with the artificial muscles spindle and the Inc interneurons. Subsequently I added one by one all the other interneurons and adjusted their synapses. In table 5.1 are reported the more important synapse values for the cells present in the elbow reflex module (in chapter three they are reported in a general way w_i).

$Inc_i+>M_i$	$Ia_i->Ia_j$	$Ia_i->M_j$	$R_i->M_i$
0.5	0.1	1	0.6
$M_i+>R_i$	$R_i->R_j$	$Ib_i->M_i$	-
0.6	1	0.5	-

Table 5.1: Synaptic weights for the Elbow Reflex Module

In table 5.2 are reported the neurons's constants.

Neuron	K	Kp	Kv
M_i	0.07	-	-
Ia_i	2	-	-
R_i	0.2	-	-
Ms_i	-	30	10

Table 5.2: Constant values in the Elbow Reflex Module

Note that Kp and Kv constants are so high to adapt the position and velocity errors ($10^{-2} order$) to a value able to influence the artificial muscle spindle's dynamic (that changes between the values zero and one $10^{0} order$). Note also that the muscle's length and velocity are normalized before use by the reflex modules. In performing the simulations I chose a variable step of integration and the Dormand-Pricep integration method. Furthermore, in order to reach a statistic significance, the same simulation was performed many times.

5.3 Myotatic Reflex

In humans the myotatic reflex has the main purpose of regulating the muscle tone and to maintain the articulation position fixed at the length imposed by the high level centers of control.
In our system the artificial reflex should control the actuator pressures in order to regulate the joint position, velocity and stiffness. Furthermore the module should also compensate for disturbance forces that act in altering the joint position. In the next section I will show how the control system can exhibit these behaviors.

5.3.1 Single Joint Movement

The first simulation shows how the elbow reflex module can govern the actuator pressures in order to regulate the joint position. In this simulation the biceps and triceps length commands were manually set, therefore the path generator module, and the inverse kinematic module are not yet connected to the reflex circuit. In figure 5.1 the elbow angular position during the entire motion is reported.

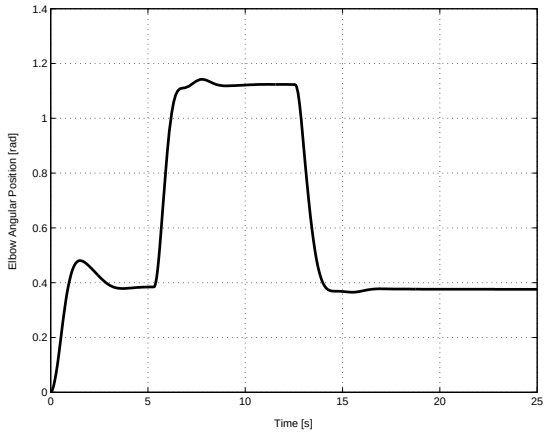

Figure 5.1: The Angular position of the Elbow

We see that the elbow position in the first movement reaches 0.4 radians (24.2^o), with the second movement that starts at the fifth second it reaches 1.15 radians (70^o), and finally the joint is restored to the first position.

Note that in the first movement there is a big over-elongation, partially due to the fact that when the first movement starts all the neurons potentials are set at the minimum value, and it take a certain time for the neurons to reach the operative value. In the arm prototype a minimum motoneuron activity is needed in order to maintain a sufficient pressure inside the artificial muscles. This to avoid the detachment of the inner tube from the external braided shell.
It is possible to note from the graph, that also in the second joint movement there is a certain over-elongation. This behavior is characteristic also for a human movement especially if it is very fast (Figure 5.2). In figure 5.3 and 5.4 the elbow's velocity and acceleration are reported .

From figure 5.3 it is possible to see how the elbow's velocity follows a human bell shape profile, thanks to the smooth control behavior of the motoneurons.
In figure 5.5 are reported the motoneuron and interneuron signals during

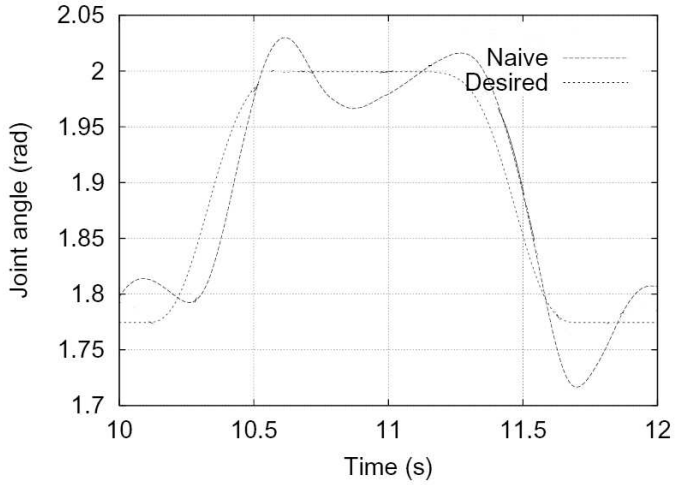

Figure 5.2: Human Elbow's position during a fast movement (from [2], [3])

the elbow flexion.

Starting from the bottom we can see the activities of the artificial spindles Ms_i that measure the length and velocity errors in the biceps and triceps actuators. When the first elbow movement starts, the biceps's spindle increases its activity rapidly this because, in comparison with the length command, the actuator should be shorter. After 0.8 seconds the biceps's Ms decreases its activity to zero , but at the same time there is a burst in the triceps's Ms, due to the fact that the elbow has overcame the target position and therefore the triceps should be contracted. Looking at the axes that report the Ia interneuron outputs, it is possible to note that the activity of this neuron are strictly correlated with those of the Ms. Nevertheless their effect, now, is transmitted on the antagonistic motoneuron. This action is very important for the elbow joint control. Indeed thanks to this cross inhibition a big length or velocity error on an artificial muscle, not only increases its pressure, but decreases at the same time the pressure in the antagonistic artificial muscle. We can see this influence in the motoneurons activities or directly on the actuator force (5.6).

In this first simulation I prevented the action of the R_i (Renshaw cells) interneurons, as it is possible to see in the graph of figure 5.6. They are important to maintain the motoneuron activity under control when the elbow has reached a stable position. From the graph that depicts the actuator force it is possible to note that when each movement is ended

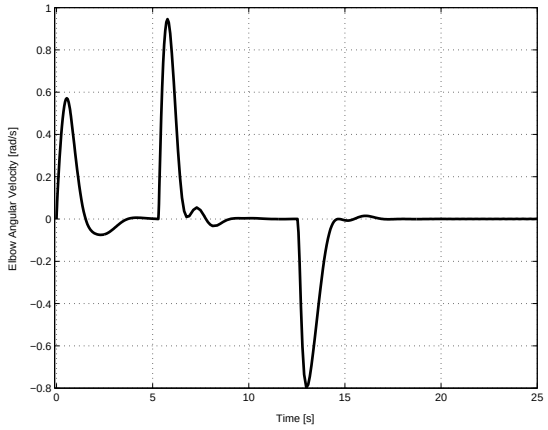

Figure 5.3: The Elbow's angular velocity

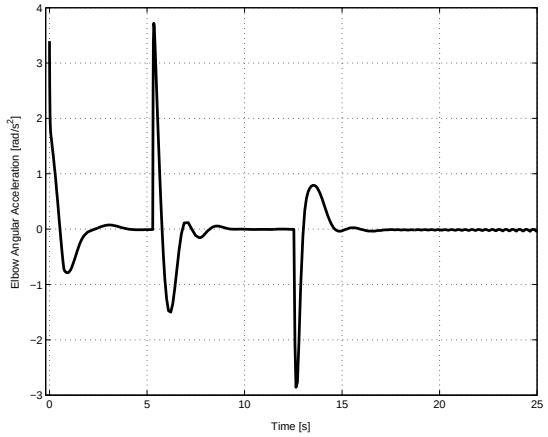

Figure 5.4: The Elbow's angular acceleration

the force increases autonomously in both the motoneurons, this causes a stiffness increasing in the elbow joint. In humans this disease is called hypertonia.
In the following simulation I enabled the R_i interneurons and performed the same movements as the first experiment (Figure 5.7).

This time, even thought the elbow performed the same movements, the actuators force changed. Indeed from the graph in picture 5.8 it is possible to note that after each movement the forces don't increase like in the first experiment.

This behavior is due to the R_i interneurons that limit the motoneurons potential when the elbow doesn't move. We can see their activity in

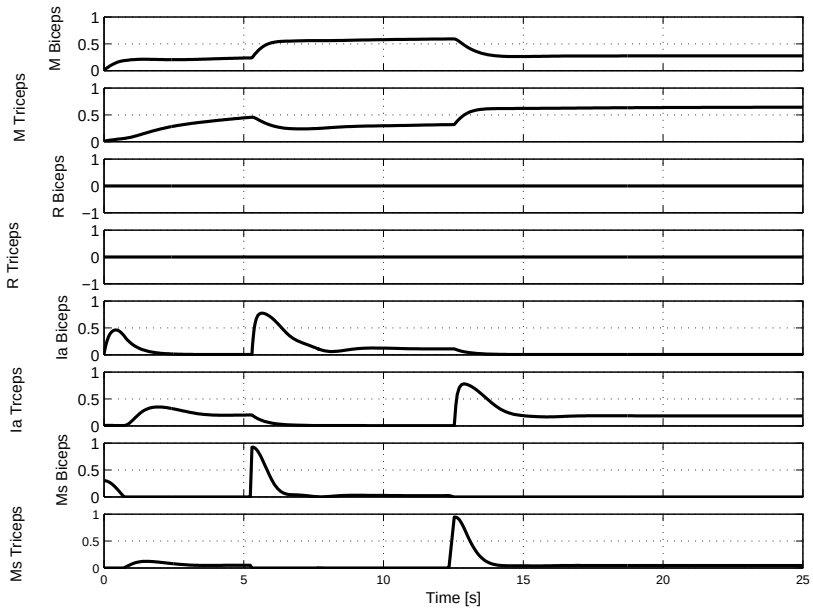

Figure 5.5: Motoneuron and interneurons activities during the Elbow flexion

picture 5.9.

5.3.2 Effects of a Disturbance Force on the Joint Position

The other task for the myotatic reflex control is to compensate for external disturbance forces. In the experiment that I conducted, I applied a force of 0.5N at the hand's barycenter with a direction parallel to the palm of the hand. This force pushes the forearm faraway from the body and requires the elbow to extend. Before applying this force I flexed the forearm to a certain position, in order to increase the pressure, and therefore the force, inside the triceps and biceps actuators. Subsequently I applied a step of force (10^{th} second) and measured the elbow position (Figure 5.10); after eighteen seconds the force was removed.

As it is possible to see from the picture, when the force was applied, for 0.5 seconds the elbow position changed and consequently the elbow extended, but after this period the position was restored to the initial value. We can understand this behavior from the graph that represents the motoneurons and interneurons activities(Figure 5.11); when the force is applied we can see a big activity in the Ms and Ia interneurons of the flexor. This means that the biceps's motoneuron was excited and its antagonist inhibited, in such a way that the increased force of the biceps

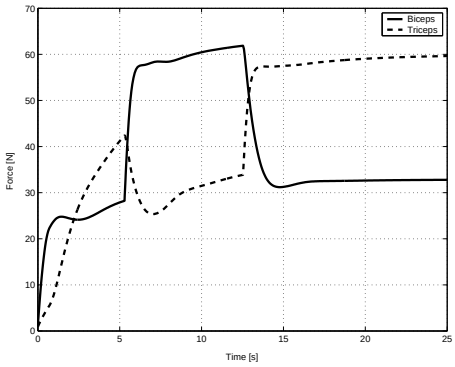

Figure 5.6: The forces generated by the Biceps and Triceps actuators during the elbow movement

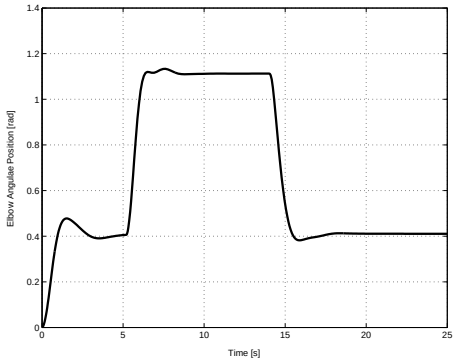

Figure 5.7: The Angular position of the Elbow in the second experiment

actuator and the corresponding decreased force in the triceps compensated the noise force and restored the elbow position at the original value.

After the force was removed we can see that the elbow suffers big over-elongation and under-elongations relative to the final position. This behavior can be observed also in human subjects when they are required to maintain fixed an objects that exercises a force and unexpectedly the force is removed.

5.3.3 Comparison with a PID Controller

In order to understand the merits and the lacks of this bio-mimetic control architecture I performed the experiment of controlling the elbow position using a classical PID (proportional, integrative, derivative) con-

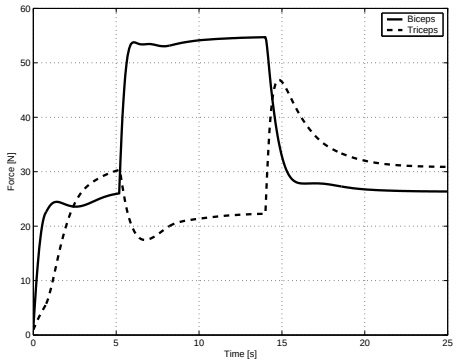

Figure 5.8: The forces generated by the Biceps and Triceps actuators during the second experiment

troller.

$$PID_{out}(t) = K_P(e(t) + \frac{1}{T_I}\int_0^t e(\tau)d\tau + T_D\frac{de(t)}{dt}) \tag{5.1}$$

Because I need to control two actuators it is necessary to use at least 2 PID, because rigorously, according to the control theory, we should apply a matrix of four PID controllers if the system has two variables to control. In this last configuration the PID outside the matrix's diagonal are used to take in account the reciprocal influence that the two control variables have. Nevertheless I neglected this influence and consider a diagonal matrix. The elbow joint that I want to control can be represented by a non linear MIMO system; non linear because the arm and the actuator dynamics are not linear. In the classical control theory to synthesize the controller the following steps are necessary: at first to make a complete dynamic model, and then linearize it around an equilibrium position. Following this methodology in our case is quite complex and tedious, therefore I decided to apply an empirical method in tuning the PID parameters. I used the Ziegler and Nichols method, which consists in closing the control loop and increasing the proportional action $K_P^{'}$ of the PID until the system for a minimum variation in the inputs variables establishes a permanent oscillation of period $T^{'}$ (actuator lengths and joint positions). After this it is possible to set all the three PID's parameters with simple formulas (Equations 5.2).

$$K_P = 0.6K_P^{'} \quad T_I = 0.5T^{'} \quad T_D = 0.12T^{'} \tag{5.2}$$

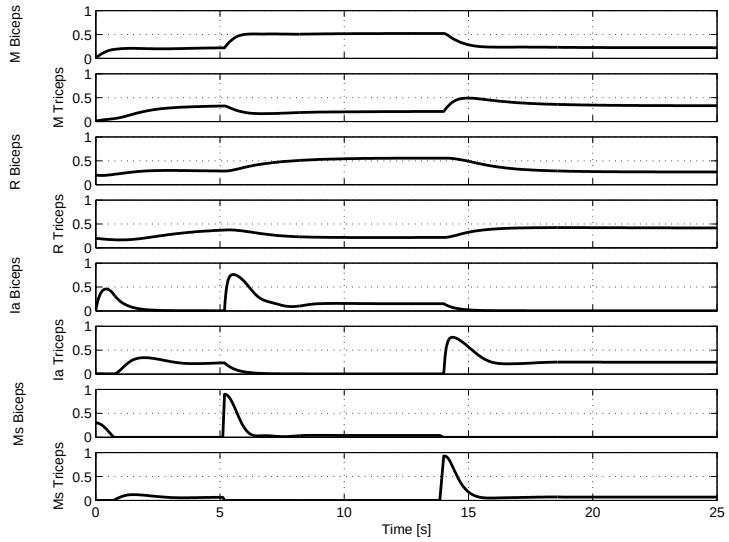

Figure 5.9: Motoneuron and interneurons activities during the second experiment

In our case the two PID were tuned using the same parameters show in table 5.3.

PID	K_P	T_I	T_D
1	55	0.05	0.012
2	55	0.05	0.012

Table 5.3: PID parameters

I decreased the value for the proportional gain K_P with respect to the value calculated with the roles showed in equation 5.2 in order to limit the actuator's force. The result that I obtained in controlling the elbow angular position is in figure 5.12, where the graph reports also the elbow angular velocity.

As it is possible to see the target position is reached in only 0.7 seconds and without over elongations. Nevertheless the force in the actuators is larger relative to the reflex control module, and also it has an impulsive shape (Figure 5.13). This means that to the actuators is required a big stress, and should be dimensioned bigger in comparison with the force specifications obtained from the simulation of the reflex controller.

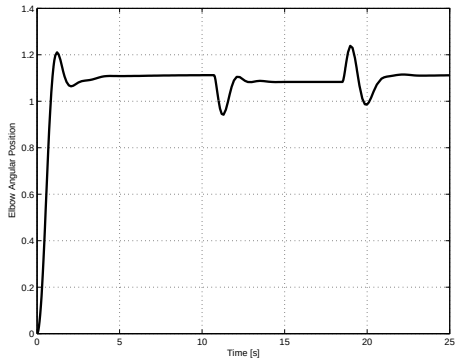

Figure 5.10: The Angular position of the Elbow during the application of a noise force on the hand

5.4 Inverse Myotatic Reflex

The inverse myotatic reflex in human has a safety function and acts when the muscle's force exceed a dangerous value. Usually this reflex becomes hyperactive as a result of disease or injury and therefore it is difficult to observe it. In our reflex module this reflex is due to the presence of the Ib interneurons whose activity becomes important if the actuator force overcomes a pre-settled value $70N$. In the experiment I applied on the hand a force of -3N that will rapidly extend the elbow from a flexed initial position.

This force will increment the bicep's force over a hypothetical dangerous value and therefore the inverse myotatic reflex will act. In figure 5.14 we can see the elbow position before and after the application of the dangerous force. As it is possible to see that final position is different from the start position, because of the inhibition effects of the Ib cells on the agonist motoneurons. It is possible to see this effect in picture 5.15.

As it is possible to see at the eighth second when the force is applied the activity of the biceps's Ib interneuron increases rapidly, and this decreases the activity of the flexor motoneuron. Note that at the same time also the biceps's Ms increases its activity, because of the error in the muscle length, but this is not sufficient to restore the position because of the action of the Ib interneuron. If we look at the graph that reports the muscle's force we can see that they are limited by the inverse myotatic reflex under a maximum value. In a robot the inverse myotatic reflex can be useful in avoiding breaking the tendons that connect the artificial muscle at the joint, and also to prevent damage to the actuators.

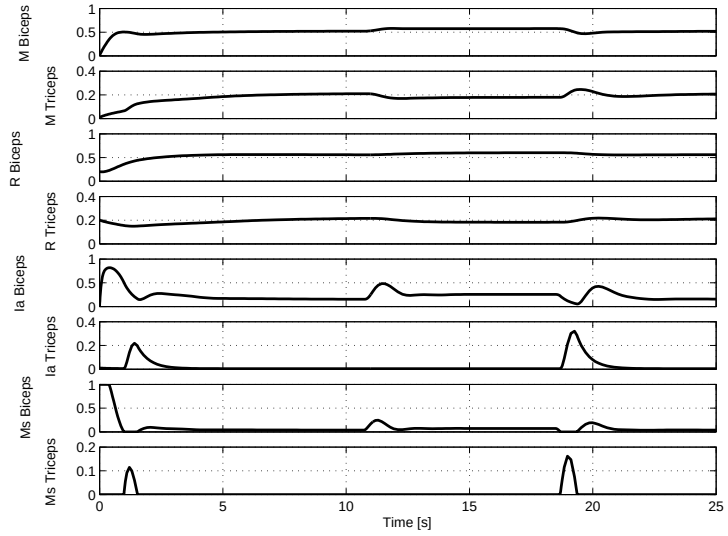

Figure 5.11: Motoneuron and interneurons activities during the third experiment

5.5 Joint Stiffness Regulation

The control of the joint's stiffness is very important during the execution of a certain task with the robot's arm. This is true for industrial robots, but is particulary important for humanoid robots. Usually industrial manipulators operate in a protected environment where humans have a restricted access, in order to guarantee a safe operation for the robot and for the human. It is difficult to control the joint stiffness for an industrial manipulator and even if this is possible the inertia force that acts during the movement can be lethal for a human being hit by the robot. Humanoid robots are expected to operate and collaborate with humans, during a task execution, therefore the robot must not be dangerous; this is in accordance with the first robotics law due to Isaac Asimov: "*A robot may not injure a human being or, through inaction, allow a human being to come to harm* ".
Humans usually can reduce or increase the joint stiffness when they are performing a certain task. For example catching a heavy object that is moving fast requires a stiffness increase of the lower and upper body articulations, while making a caress to someone requires a low stiffness for the arm's articulations. The articulation's stiffness, in turn, is regulated by the muscle cocontraction.
In the reflex modules the stiffness is regulated by the P_i signals that

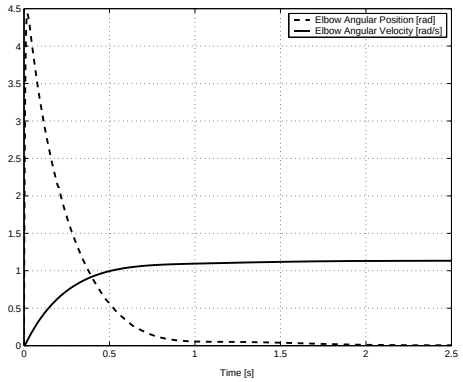

Figure 5.12: Controlling the Elbow position using standard PID

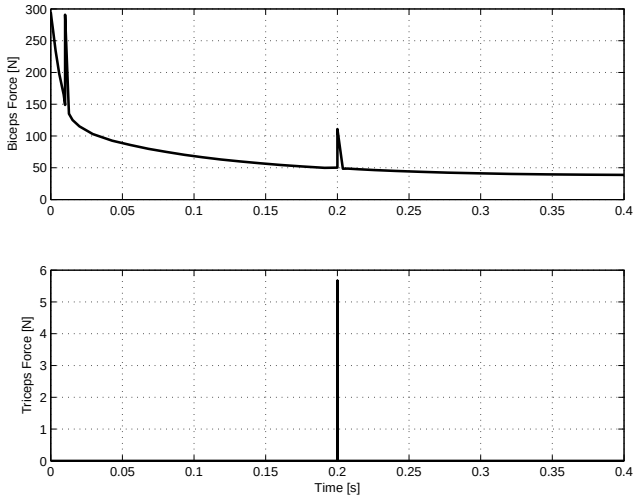

Figure 5.13: Biceps and Triceps force under control of a standard PID

excite the Ins interneurons. In order to demonstrate such a capability in the reflex module I increased the P_i signals for the elbow actuators to the maximum value possible, 1. Picture 5.17 shows the forces increasing due to the P command.

The forces in the biceps and triceps actuators increase at the same time, in order to avoid the joint movement. We can observe also that the triceps increases its force more than the biceps; the important thing is that the total momentum exercised on the elbow joint is equal to zero in order to guarantee its position (Figure 5.18).

As it is possible to note, the elbow position does not change when its stiffness is increased. We can also observe a collateral effect due

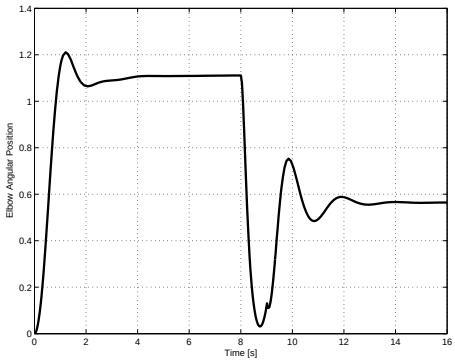

Figure 5.14: The elbow position after the the application of a dangerous force on the hand

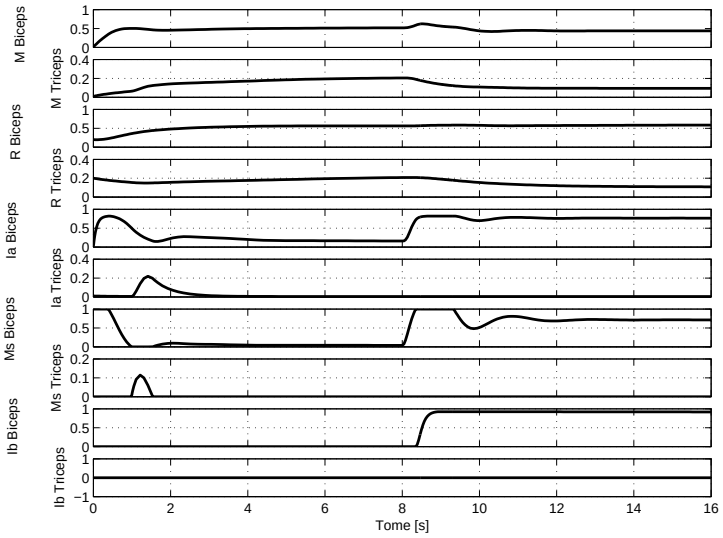

Figure 5.15: Motoneuron and interneurons signals during the action of the inverse myotatic reflex

to the stiffness increasing: for a certain period there are some little oscillations in the elbow joint. Surprisingly this phenomena is present also in humans. When the muscles are very highly co-contracted, a tremor will occur in the arm.

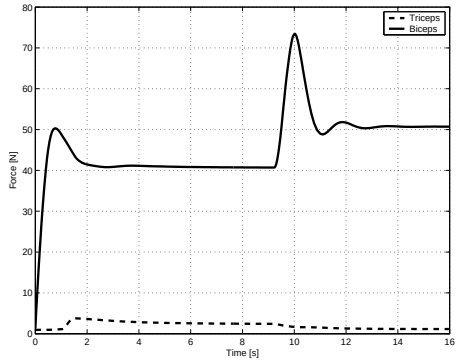

Figure 5.16: Biceps and Triceps forces during the exhibition of the Inverse Myotatic Reflex

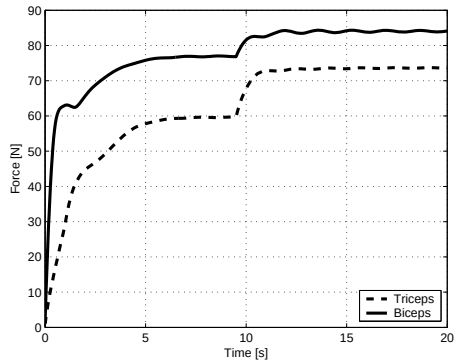

Figure 5.17: Biceps and Triceps forces during the application of a dangerous force to the hand

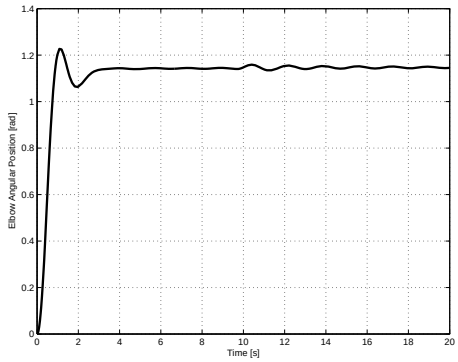

Figure 5.18: Elbow angular position during the increasing of the joint's stiffness

6 Learning Reaching Movements

6.1 Introduction

This chapter explains the results obtained by simulating the whole arm in reaching a target position specified in the Cartesian space. This behavior requires the synergy of the entire arm control system. The pattern generator will compute the straight trajectory, and at each instant, it will send the desired muscle lengths and velocities to the reflex control module. The same data will also be sent to the cerebellar module. The module will integrate this data with the error feedback from the artificial muscles and consequently learn how to modify the command signal to the artificial motoneurons set by the trajectory generator module. A deep study and simulation of the cerebellum module is not discuss in this thesis, but it will be the principal subject of future works.

6.2 Methods

The overall experimentation of the arm control system requires a big care during each single phase of the simulation. Many modules are running at the same time and interact for executing the task. As for the the reflex modules in this case it is necessary to increment the complexity of the control system step by step. The modules that compose the system are:

The Inverse Kinematic Neural Network: given a target point in the workspace it computes the actuator lengths in order to reach that point

The Reflex Modules: they regulate the joint positions and stiffness receiving as inputs the length and velocity command, the stiffness command, and the cerebellum command.

The Path Generator: given the target position it calculates a smooth trajectory for each single artificial muscle.

The Cerebellum Module: during a fast reaching movement it compensates the hand trajectory for inertia and Coriolis forces

I started the experimentation considering at first only the reflex modules: the elbow reflex module and the shoulder reflex module. The shoulder reflex module, in turn, is composed of two submodules, one that controls the shoulder rotation and the other that controls the upper arm flexion-extension and adduction-abduction. The overall reflex behavior requires therefore 8 motoneurons and 42 interneurons, each of which is represented by a non linear dynamical equation. Since I deal with nonlinear dynamical equation, particular attention should be given to system stability.

6.3 Considerations on System Stability

The subject of neural networks viewed as nonlinear dynamical systems, with particular emphasis on the stability problem is referred as *Neurodynamics* [86] [87] [88] [89] [90]. An important feature of the stability of a nonlinear dynamical system is that it is a property of the whole system. The presence of stability always implies some form of coordination between the individual parts of the system [91]. It appears that the study of neurodynamics started in 1938 with the work of Rashevsky [92], in whose visionary mind the application of dynamics to biology came into view for the first time. The stability of a nonlinear dynamical system is difficult to demonstrate. Usually, in a engineering background, stability means that the output of a system must not grow without bound as a result of a bounded input, initial condition, or unwanted disturbance. This criteria is well suited for a linear system, however it is useless for neural networks, simply because all such nonlinear dynamical systems are stable according this criteria. Indeed all neurons have an activation function that limits the neuron output under a given threshold.
When we speak of stability in the context of a nonlinear dynamical system, we usually mean stability in the sense of Liapunov. According this criterium, given a general dynamical system 6.1.

$$\frac{dx_j(t)}{dt} = F_j(x_j(t)), \quad j = 1, 2, ...N \tag{6.1}$$

where the function F_j is a non linear function of its argument. We can rewrite 6.1 in a compact form:

$$\frac{d}{dt}\mathbf{x}(\mathbf{t}) = F(\mathbf{x}(t)) \tag{6.2}$$

where $\mathbf{x}$ represents the state vector of the system which changes with time. During the life of the system its state can change defining a trajectory and sometime tend to an equilibrium point which is called equilibrium state $\overline{\mathbf{x}}$. The Liapunov theorems say:

Theorem 1 The equilibrium state $\overline{\mathbf{x}}$ is stable if in a small neighborhood of $\overline{\mathbf{x}}$ there exist a positive definite function $V(\mathbf{x})$ such that its derivative with respect to time is negative semidefinite in that region

Theorem 2 The equilibrium state $\overline{\mathbf{x}}$ is asymptotically stable if in a small neighborhood of $\overline{\mathbf{x}}$ there exist a positive definite function $V(\mathbf{x})$ such that its derivative with respect to time is negative definite in that region

The important point in using the Liapunov theorems is that they can be applied without solving the state space equation of the system.
The reflex control system, can be described using the general model proposed by Cohen and Grossberg in 1983, as a system of coupled nonlinear differential equations:

$$\frac{du_j}{dt} = a_j(u_j)[b_j(u_j) - \sum_{i=1}^{n} c_{ij}\varphi_i(u_i)], \quad j = 1, ..., N \tag{6.3}$$

According to Cohen and Grossberg, this class of neural networks admits a Liapunov function, defined as

$$E = \frac{1}{2}\sum_{i=1}^{n}\sum_{j=1}^{n} c_{ij}\varphi_i(u_i)\varphi_j(u_j) - \sum_{j=1}^{n}\int_0^{u_j} b_j(\lambda)\varphi_j^{'}(\lambda)d\lambda \tag{6.4}$$

where

$$\varphi_j^{'}(\lambda)d\lambda = \frac{d}{d\lambda}(\varphi_j(\lambda)) \tag{6.5}$$

The definition of equation 6.4 is valid if the synaptic weights of the network are "symmetric" $c_{ij} = c_{ji}$, the function $a_j(u_j) \geq 0$ and the nonlinear input-output function satisfies the condition for monotonicity $\frac{d}{du_j}\varphi_j(u_j) \geq 0$. If all these hypotheses are respected the neural network is globally asymptotically stable.
In my neural circuits the reciprocal influences between the cells are

equals, the gain for the inhibitory and the excitatory terms in the neuron state equation are in any case greater than zero, and the input-output function is monotonic. Therefore in accordance with Cohen-Grossberg the network is globally asymptotically stable.
We can also assert that the arm model and the prototype are asymptotically stable systems, nevertheless, since the control system is closed in a loop with the arm model (or real system), the global stability is not guaranteed. Rigorously we should demonstrate the stability of the closed loop system, but this requires a complex model of the whole system and moreover is not the principal goal of this work. We can be satisfied in testing the global stability empirically during the simulations.

6.4 Upper-Arm and Forearm Coordination

Every arm movement requires coordination between the joints and therefore between the arm's artificial muscles. In order to govern each muscle in an appropriate way the reflex modules should be coordinated. The system that permits this coordination is represented by the inverse kinematics module. As described in chapter four this module consists of a multilayer perceptron neural network. Given a trajectory in cartesian space this module can calculate in each instant the muscle length vector that, in turn, is sent to the path generator module. The path generator can therefore generate the appropriate signals for the reflex modules. In figures 6.1 and 6.2 we can see a straight trajectory obtained by the inverse kinematics module. In the pictures are reported some arm configurations relative the solutions that the neural network found in solving the inverse kinematic problem. The straight line that is followed by the arm is reported in a parametric form in equation 6.6.

$$\begin{aligned} x &= 19 \\ y &= 20 + (5 \cdot s) \\ z &= -5 \end{aligned} \tag{6.6}$$

As we see in figure 6.1 the line is not exactly followed, this is due to the error performed by the inverse kinematic module in calculating the muscle lengths. Although the precision of the neural network is in the order of 10^{-3}, this not sufficient, because the network is required to generalize in calculating the muscle lengths for positions never presented to it. Moreover a little error in the muscle lengths can produce an error of few centimeters in the hand positioning. This problem can be resolved by integrating the arm with a stereoscopic vision system able to apply a trajectory adjustment using the visual information.

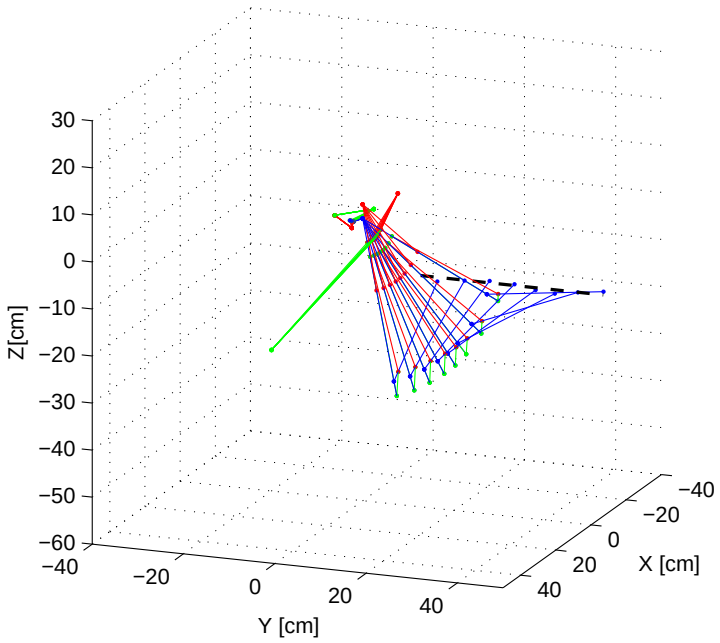

Figure 6.1: Straight trajectory generated by the Inverse Kinematic Module (**3D view**)

6.4.1 Reflex Modules Coordination

In testing the action of the all reflex modules I made a simple experiment; after connecting to the arm all the reflex modules, I flexed the elbow joint and monitored all the neuron activities and the muscle lengths error. In figure 6.3 we can see the elbow movement. Unlike one of the first experiments during the testing of the dynamic arm model, the shoulder position changes less during the movement. This is due to the shoulder's actuators that this time are active and therefore prevent the joint rotation. We can analyze the combined action of the different reflex modules observing the seven motoneuron activations reported in figure 6.4.

It is possible to see the bicep's motoneuron increases its activity in concomitance with the movement initiation. After 0.4 and 0.8 seconds the activity of the dorsal and the pectoralis motoneurons increase, in order to make a certain resistance to the shoulder flexion. It is possible to note also the potential increasing of the supraspinatus and subscapularis motoneurons in two different instants. This will cause a little rotation of the shoulder's joint, nevertheless when the elbow movement is finished all the muscles are contracted at the commanded length. In figure 6.5

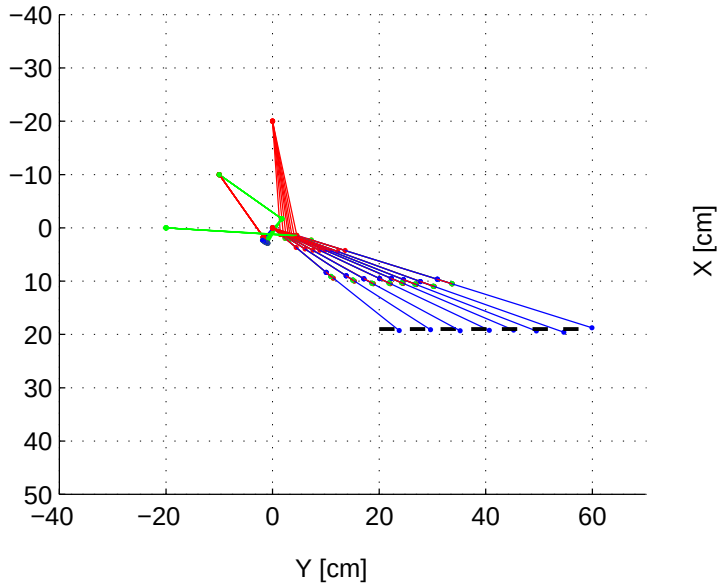

Figure 6.2: Straight trajectory generated by the Inverse Kinematic Module (**Upper view**)

we can see the trend in the length error of the muscles.

6.4.2 Path Generator Functionality

The path generator module has the main function to generate the desired trajectory for arm movements by smoothly interpolating between the initial and the final length commands coming from the inverse kinematics module. The movement starts when the volitional GO signal is sent to the module, at this time the V cells start to integrate the target length command. The output of the V cell is multiplied by the GO signal and this constitutes the velocity command for the artificial muscle spindle and the input for the A cells. When the target length command is equal to the output of the corresponding A cell the movement is terminated.

In figure 6.6 the signals that affect an elbow movement are reported . As it is possible to see, the GO signal has a sigmoidal trend, and it regulates the velocity and the duration of the whole movement. The velocity command signals have a smooth profile, in order to limit the acceleration of the joint. After 0.3 seconds the length commands for the elbow's reflex module have reached the target value and therefore the movement should be ended.

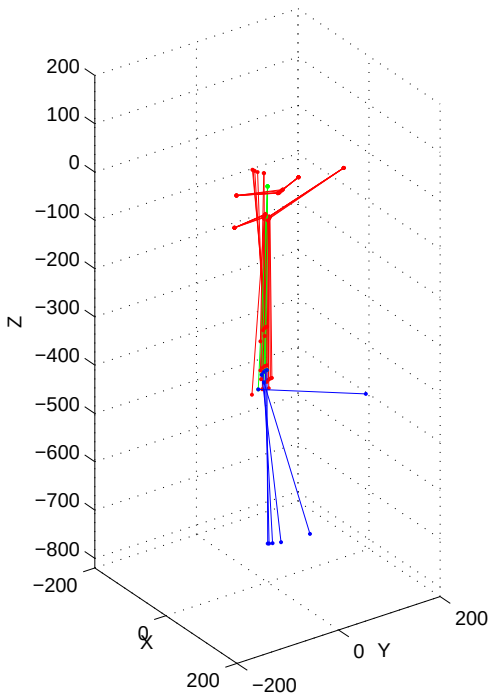

Figure 6.3: Flexion of the Elbow

6.5 Slow Reaching Movements

In human beings, we can classify as slow a movement that has an overall duration longer than 0.8 seconds. In this case inertia forces and Coriolis forces have a negligible influence on the arm motion. This is particular true for a light arm like our prototype. During a slow reaching movement in the human body the proprioceptive information can arrive on time to the superior nervous center, and therefore it possible to adjust the arm trajectory and compensate for interaction torque.
In our control system this behavior is obtained by the integration of the inverse kinematic, the path generator, and the reflex modules. Given a trajectory in Cartesian space, the inverse kinematic module generates the instantaneous target length vectors for the path generator. The path generator, in turn, calculates a smooth path for each muscle's trajectory. Finally the reflex modules, using the sensorial information, adjust the rate of contraction for each artificial muscle.
In order to verify the correct integration between this three modules, I performed an experiment where the arm should reach a target position in its workspace following a given trajectory. In figure 6.7 we can see

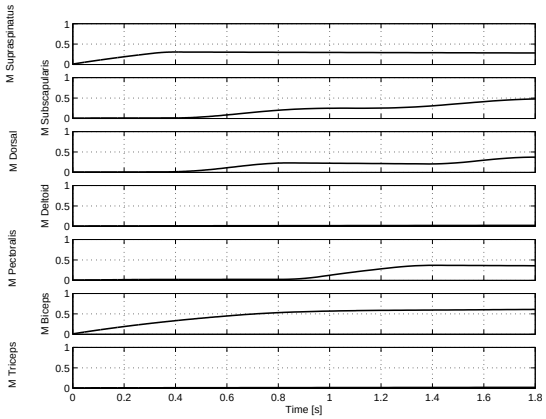

Figure 6.4: Motoneurons Coactivation

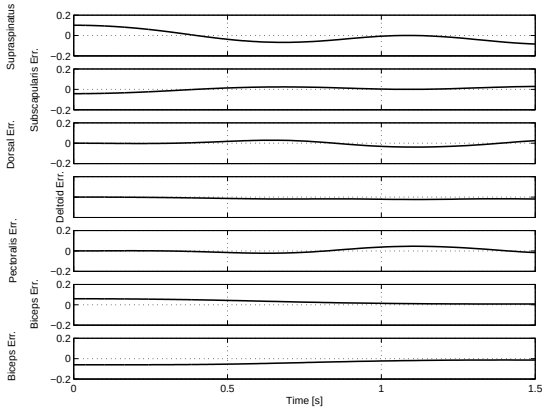

Figure 6.5: Muscles Error length, values are normalized relative the maxim length of each muscle

the results of this experiment. The trajectory that the wrist of the arm should follow is a straight line, the overall movement duration is 2,5 seconds.

As is possible to see the wrist doesn't follow a real straight line (purple line), but tends to move along an arch (black line). The final error in the wrist position is 3 centimeters and the medium error is 2 centimeters. The biggest error in the wrist positioning is due to the shoulder joint where the actuator's length error has more effect on the final arm position.

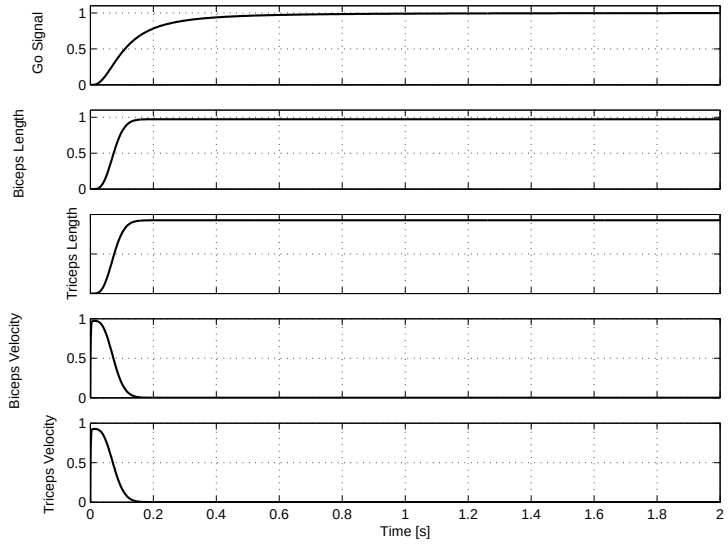

Figure 6.6: Length and Velocity command signals generated by the Path Generator

6.6 Preliminary results in Fast Reaching Movements

It is interesting to note that children during the first year of life tend to perform slow movements of exploration, in agreement with the theory [72], [73] that in order to perform rapid movement it is necessary to use the inverse dynamic model of our limbs. In the brain this inverse dynamic model is learned by the cerebellar circuits. Bastian et al. [93], [94] demonstrated that the cerebellum compensates for interaction torques that would otherwise push the arm off its desired equilibrium path during fast reaching movements. While feedback control could in principle compensate for interaction torques, it is limited by both long delays in the nervous system and the dynamic properties of muscles and proprioceptors. It was demonstrated that the cerebellum can implement a feedforward, nonlinear predictive regulation by learning part of the inverse dynamics of the arm.

6.7 Cerebellar Module Setting

In the cerebellar module the granule cell layer, composed of 100 cells, acts as an expansion encoder [95]. Each cell of this layer receives four randomly selected mossy fibers, which in turn are represented by the Gv

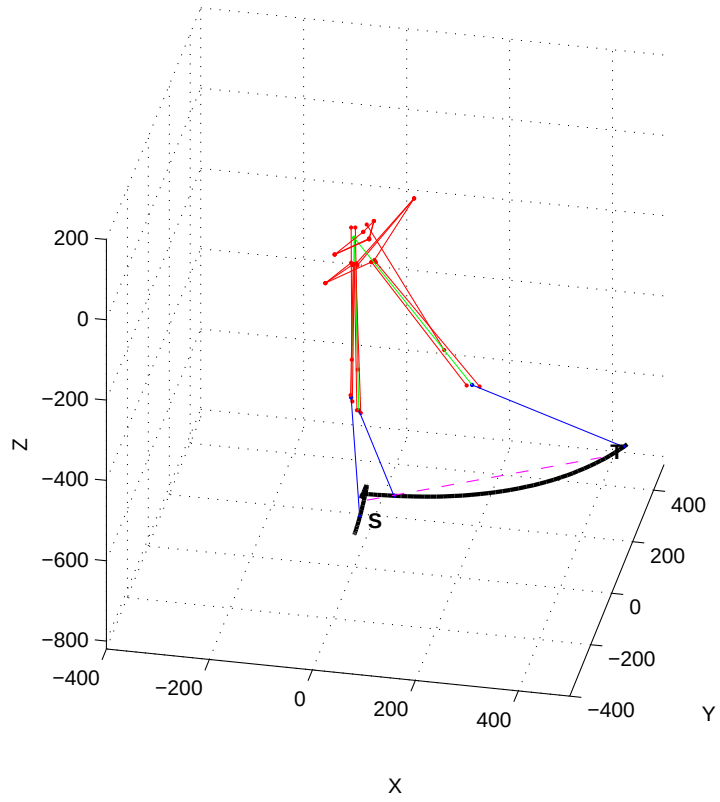

Figure 6.7: The Arm performing a slow movement, in purple the desired trajectory and in black the one performed

signal coming from the path generator module. The information that this layer codes is only the velocity command for the artificial muscles; nevertheless it is possible feed the layer also with other mossy fibers carrying different information. For example we can provide to the layer the target position command for the artificial muscles or the desired torque for the arm joint. In figure 6.8 we can see the representation of the granule cell layer connected with the seven mossy fibers.

To represent the layer activity I used a matrix where the gray intensity of each cell represent the activation level of its corresponding neuron, this permits us to take under control a big amount of data and to understand some behavior of the entire cerebellum module. An example of instantaneous activation for the granule cell layer is presented in figure 6.9.

The only Golgi cell present in the model, closed in a loop with the granule cell layer, acts as a gain controller in order to maintain the total

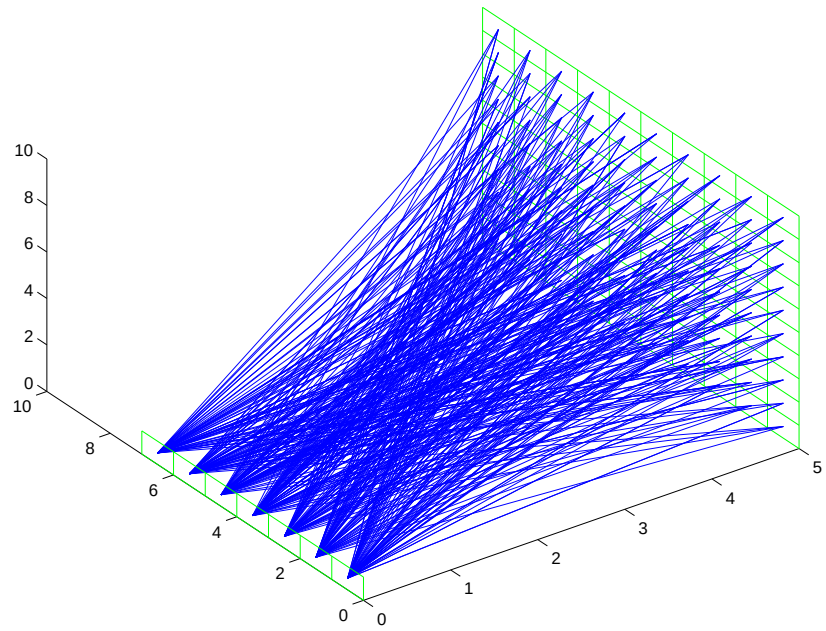

Figure 6.8: Sparse Connections between mossy fibers and Granule cells

energy in the granule cell layer at a constant level and ensure a sparse encoding.
The purkinje cells layer, formed by seven neurons, receives its inputs from the granule cell layer. These inputs are weighted by an adaptable synapses that is regulated by the activity of purkinje cells, inferior olive nuclei and parallel fibers (outputs of the granule cells layer). The output of the purkinje cell layer goes to inhibit the interposed nuclei layer, which in turn receives also excitatory inputs from the mossy fibers. The interposed nuclei activity represents the output for the cerebellum module that goes to excite the Inc interneurons and inhibit the Renshaw cell in the reflex module. A first parameter setting for the cerebellum module is presented in table 6.1, parameters represent the constants used to model the cell membrane potential.

During the first experiment, in order to verify the correct working for the cerebellum module, integrated with the other modules, of the whole control architecture, I set the learning rate to a "big value" $\alpha = 0.01$. Normally this constant should be settled to a smaller value in order to permit the artificial cerebellum to learn from trial of fast movements. Then I executed 10 straight reaching movements: at first the elbow is flexed then when it reaches an angle of 90^o the straight movement starts. The overall movement last 0.8 seconds. In figure 6.10 are reported three

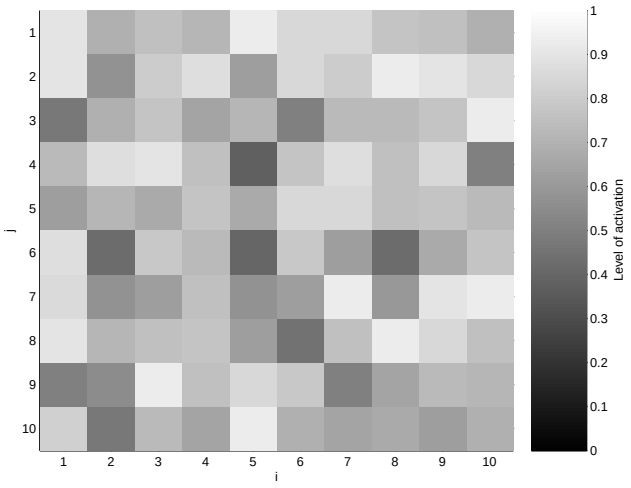

Figure 6.9: An example of instantaneous activation for the granule cells layer

Cell layer	Time constant τ	s	o	Maximum rate
Granule cells	.02	8	.5	1
Golgi cells	.05	.5	10	1
Purkinje cells	.02	.005	100	1
Interposed nuclear cells	.02	.05	-20	1
Inferior Olive	.02	.05	-20	1

Table 6.1: Cerebellum Module Parameters

of the 10 trials: the first one; the 7^{th}; and the last trial. As it is possible to see the target point is not reached, but the trajectory became more and more straight. Second a first data analysis it seems that the output signal coming from the interposed layer goes to increase the activity of the triceps and deltoid artificial muscle during the first part of the movement. Nevertheless it remain to clarify better the cerebellum-module efficacy in controlling the arm and compensating Coriolis and centrifugal force. This by intensive simulation and testing, it will be the goal of future works.

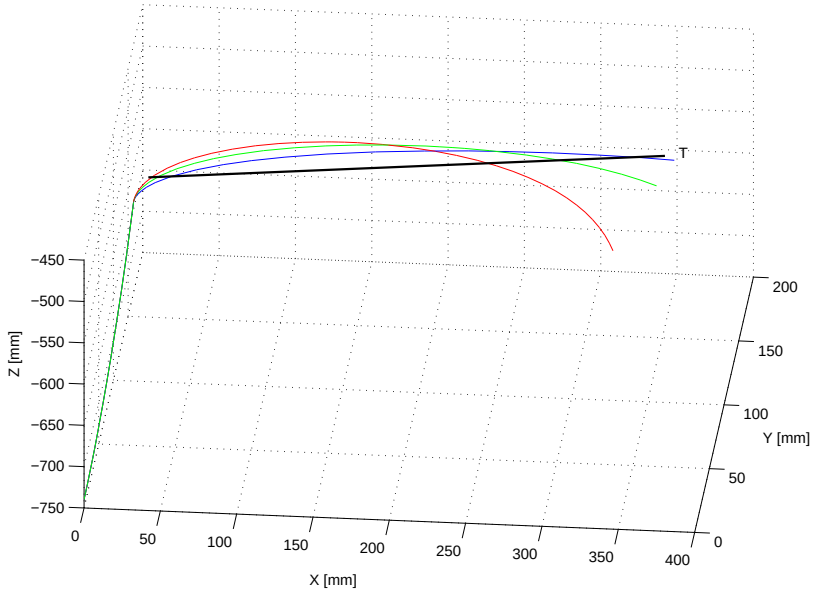

Figure 6.10: Three trials of fast reaching movements (in black the desired trajectory)

7 Experimentation on the Arm Prototype

7.1 Introduction

This chapter will describe the part of my work that deals with the construction of and experimentation on the arm prototype. Experimenting with a real system is exciting but at the same time requires a total dedication. During the time spent in the laboratory many difficulties were encountered, but at the same time many new ideas came up to solve the day by day technical problems. But as every prototype is never fully completed, and when it is, is time to move to a new implementation.
In the first section of this chapter I analyze all the parts that make up our system; I describe the implementation and the experimentation on the artificial muscles, the sensors, and the mechanical arm structure. In the second section I show the principal arm movements, like the forearm and shoulder flexion and extension, the shoulder abduction, adduction and rotation. Finally, in the last section, I report some experimental results that show the effect of a noise force on the elbow position.

7.2 Prototype Description

As introduced in the third chapter our artificial arm was designed with the principal goal to mimic the structure and the functionalities of the human arm. The artificial limb is expected to be integrated in a humanoid robot, therefore the proportions of a human arm are respected. The arm has a total of four degrees of freedom, three in the shoulder and one in the elbow. Future developments will give the arm another 2 DOF in the wrist and a 12 DOF and five fingered hand. The particularity of this arm is the shoulder joint, that has the three DOF collapsed in a single point; this allows the joint to rotate respect an arbitrary axis. The shoulder rotation is possible thanks to five artificial muscles that mimic the function of: supraspinatus, subscapularis, deltoid, pectoralis and dorsal muscles present in the human arm. Relatively to a small

size manipulator our arm is lighter, the overall weight comprising links, joints, actuators, sensor and body is only 3Kg. Although of low weight, the system can lift and move masses of 1Kg; this means that the shoulder's actuators must generate forces in the order of 300N. The physical characteristic of the prototype and artificial muscles are reported in tables 7.1 and 7.2.

Link	Length[m]	Section[m^2]	Material	Mass [Kg]
Upper Arm	0.38	$1 \cdot 10^{-4}$	Aluminium	0.21
Forearm	0.28	$1 \cdot 10^{-4}$	Aluminium	0.1
Hand	0.14	$1 \cdot 10^{-3}$	Polycarbonate	0.2

Table 7.1: Physical Properties of the arm prototype

Actuator	Min.Length[m]	Max.Length[m]	Cont.[%]	Mass[g]
Biceps	0.23	0.29	20.7	30
Triceps	0.29	0.35	17.4	40
Subscapularis	0.169	0.208	18.7	30
Supraspinatus	0.162	0.201	19.3	30
Pectoralis	0.206	0.25	17.5	30
Deltoid	0.153	0.18	15	30
Dorsal	0.32	0.403	20.7	40

Table 7.2: Artificial muscles characteristics

As we see in table 7.2, the contraction rate for each single muscle is only 20%. This obliged me to realize and install artificial muscles that are longer than human muscles. The biggest problem was encountered in mounting the dorsal actuator that has a length comparable with that of the robot's trunk. I resolved the problem by installing it along the diagonal that connects the shoulder with the opposite lower part of the trunk, in order to avoid actuator bending.
The shoulder actuators were fixed at the robot trunk with one extremity, and to the upper arm with the other. The elbow actuators are instead connected between the upper arm and the forearm. The connection between the actuator and the mechanical structure is possible thanks to tendons made of polymeric materials that are fixed with the links with micro-screws .
Before building the arm I designed it(Figure 7.1) using a 3D CAD software; this permits me to chose the best arm shape and to size each single part in view of its purpose.

The other advantages of using a 3D CAD is the possibility to calculate automatically the link mass and inertia, needed to implement a realistic

Figure 7.1: The 3D Arm design, realized using Solidage software

arm's dynamic model (described in chapter four). The entire arm and trunk structure was built using light material such as aluminum and polycarbonate, and different pieces were connected together using screws or special glues.

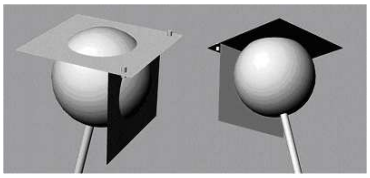

Figure 7.2: Particular in assembling the shoulder joint

Very critical was the assembly of the shoulder joint. In order to give a big mobility to the forearm , the spherical joint was surrounded by two holed laminas in posterior and lateral position (Figure 7.2). The laminas permit the spherical joint to rotate into any position but at the same time prevent the backward rotation of the upper arm. In table 7.3 are reported the rotation ranges for the shoulder and elbow joints. Rotation of the shoulder is around an absolute reference system when

the arm is in the rest position.

Joint	Rotation X axis	Rotation Y axis	Rotation Z axis
Shoulder	150	150	90
Elbow	120	0	0

Table 7.3: Range for the arm's joints

In figure 7.3 we can see the overall arm prototype *Maximum One*.

Figure 7.3: Maximum One: The humanoid Arm prototype

The position and the torque of each joint is controlled by a general purpose Analog/Digital card (Figure7.4) mounted on a dedicated PC also referred as "Target PC". This PC is governed by the XpcTarget operative system, which is a special kernel available with Simulink software (tool of Matlab) specifically for real time applications. The program that implements the modules of the overall control system runs in real time on it. The sensor signals are acquired and elaborated by the target PC with a frequency of 1Khz, then the control signals are sent to the boards that operates the actuators.
All the control software was written in Simulink and subsequently compiled and sent to the target PC via the serial port. This methodology

allows me to employ, with little modification, the same software that I used during the arm simulations.

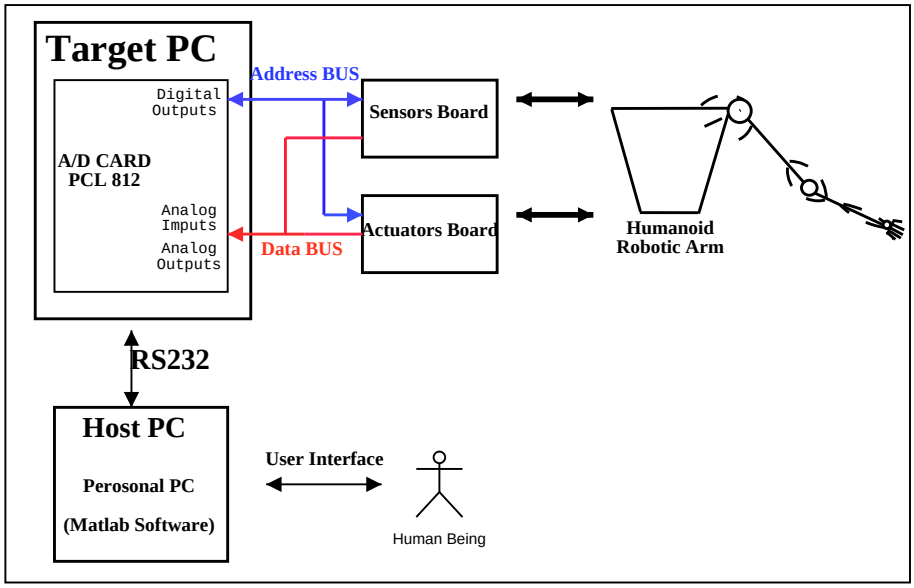

Figure 7.4: Hardware that compose the Arm Control System

The user can interact with the system using a laptop (Host PC) connected with the target PC via a RS232 serial port. During the robot operation it is possible change the control parameters on line; this permits the user to verify their effects directly when the system is operating. Experimental data can be acquired and saved using the host PC. Furthermore it is possible to monitor the system's variables using virtual probes which run on the host computer and sample the signals with a prefixed frequency.

7.2.1 Artificial Muscle

The arm's actuators, also referred to as McKibben artificial muscles, are one of the most important parts of the system. Because of this, I dedicated a lot of time to their design and experimentation. Depending on the material used for their construction, they present different static and dynamical characteristics. Choosing the right materials permits to obtain different contraction rates and different fatigue limits. Usually the thicker the inner tube, the less is the contraction at the same pressure. On the fatigue limit Hannaford et al. [17] have tested different materials and discovered that the best material to use for the inner tube is

latex; this material at 3bar can operates 6000 times without failure and therefore is suitable for this application.

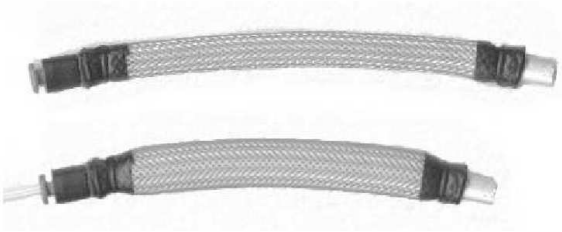

Figure 7.5: Household Mckibben actuator during the released and contracted phases

A McKibben actuator use as a primary source of energy compressed air, therefore for its operation other devices are necessary in order to control the inside pressure. Considering that the actuator should be contracted and released with high precision to be effective at least two proportional electro-valves are needed. One of those is used to increase the inside pressure and the other to decrease it.
In my experimentation I tested the homemade actuator (Figure 7.5) at different pressures in dynamical and statical conditions. To conduct the testing I built an experimental structure (Figure 7.6) where I fix the actuator extremities and measure its length and force.

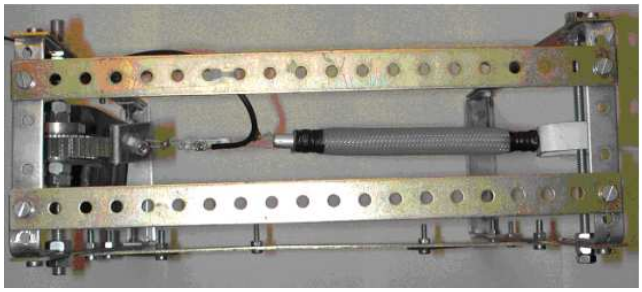

Figure 7.6: The experimental structure for testing the actuator

Static Characteristics

During the static tests, the actuator was constrained at both extremities and its inner pressure was regulated in order to reach a fixed value. The experiment consists in increasing, with a tensional device (Figure 7.7), the actuator length and at the same time measuring its force.

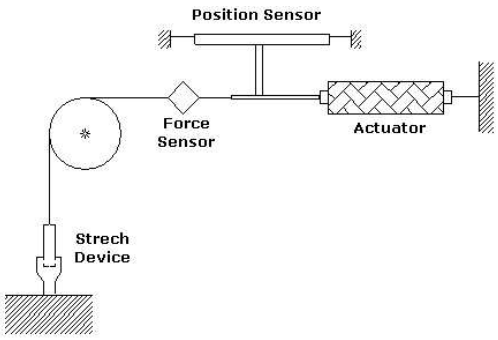

Figure 7.7: Statical testing

The experiment protocol consists in the following steps:

1. When the actuator was in its resting phase ($P = 0$) I measured the parameters l_0, α_0 and r_0.
2. The inner pressure was increased at the value P_i and in this condition I measured the actuator's length L_i and calculated the rate of contraction ε_i.
3. The actuator's length was gradually increased with the tensional device and for each length L_i I measured the correspondent F_i
4. When the actuator's length was at its maximum value ($\varepsilon = 0$) I stopped the pulling phase.
5. I started to decrease gradually the actuator's length and I measured its length and force.
6. When the actuator's length was restored to its initial value I stopped the experiment.

With this process I was able to obtain the static characteristic of the actuator at different pressures. Results are reported in figure (7.8).

As it is possible to see the more the actuator is contracted the less is the force generated; we can also note that the characteristic presents a hysteresis. Indeed the relationship between the force and the rate of contraction presents two different trends if the actuator is contracting or releasing. This behavior is not found in the model represented by the central line in the graph.

I repeated the same experiment for different pressures, and obtained the characteristics present in figure (7.9).

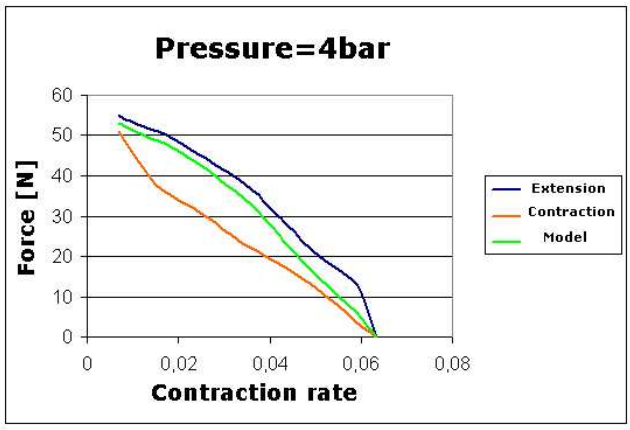

Figure 7.8: Statical characteristic at 4 bar

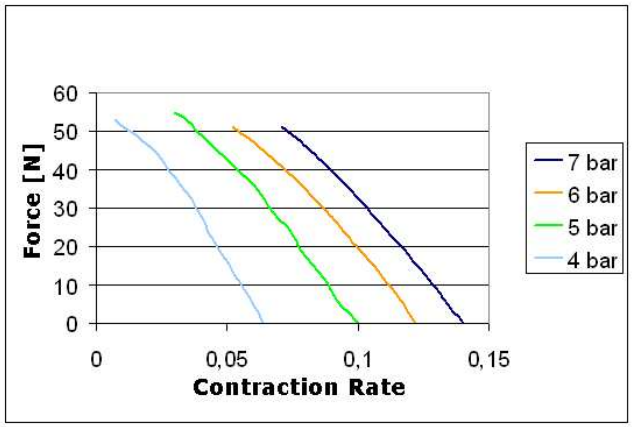

Figure 7.9: Actuator characteristic at different pressure

Observing the graph we can assert that the force in the actuator can be controlled by adjusting the inner pressure; nevertheless, as shown also by the model, this relationship is not linear.

Dynamical Characteristic

In order to test the dynamical response of the actuator, I connected a mass at one of its extremity and incremented rapidly the inner pressure. Length and force data was acquired with a frequency of 0.1Khz.

The response of the system is reported in figure 7.11, where we see that the actuator reaches the maximum contraction in only 200ms, with a trend characteristic of a non linear system.

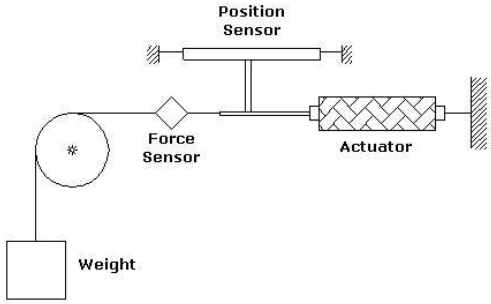

Figure 7.10: Dynamical testing

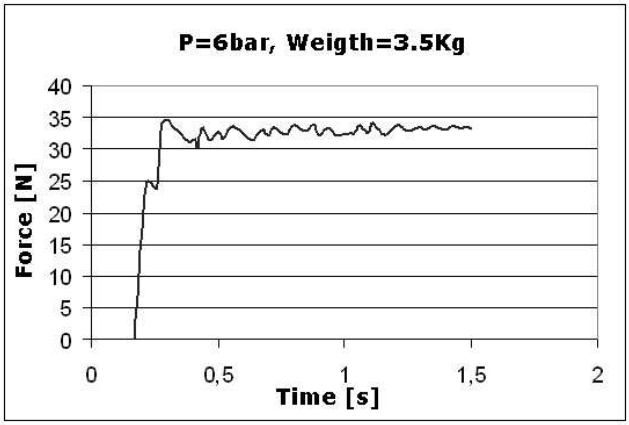

Figure 7.11: Actuator's dynamical characteristic

7.2.2 Sensory System

The proprioceptive information in the arm is acquired by two dedicated boards that I designed in order to accomplish my needs (Table 7.4).

Board	Sensorial Function	Number of channels	Output signal
1	Force measurement	16	0-5V 100mA
2	Position measurement	16	0-5V 200mA

Table 7.4: Sensory Boards Functionalities

In particular in the "force board" each channel, in order to amplify the weak signal (1-5mV)coming from the force sensor, is equipped with a Wheatstone bridge and an integrated instrumentation amplifier with an adjustable gain (0-1000). Each channel converges in an analogical mul-

tiplexer which output is sent to an A/D input of the A/D card installed on the target PC. The target PC, in turn, should generate the correct addresses in order to sample with an appropriate frequency each force sensor.

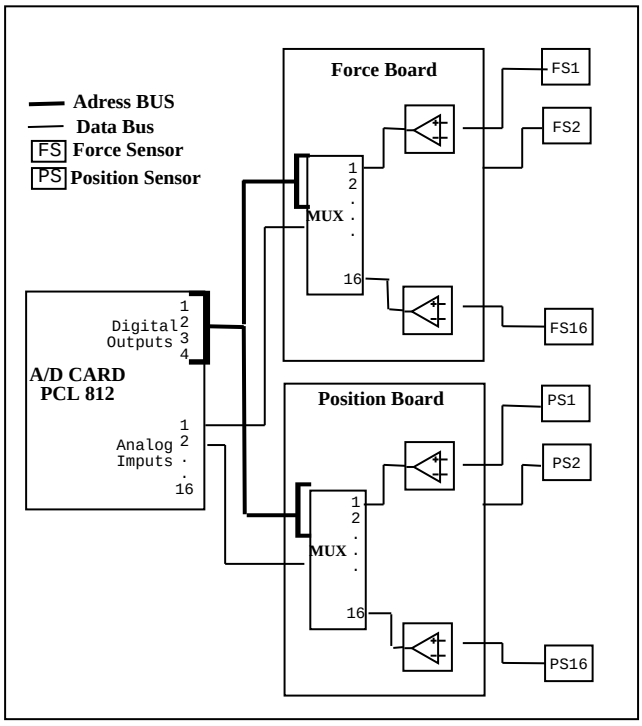

Figure 7.12: Sensorial Boards Schema

This solution permits to have virtually 16×16 channels and therefore the capability to acquire in real time the data of 256 sensors. It seems a big number of sensors, but if we think of a humanoid robot with 70 DOF (6×2 arms, 17×2 hands, 3 neck, 2×2 eyes, 6×2 legs, 5 trunk) these channels are indispensable. Indeed each degree of freedom requires at least one actuator, the actuator in turn requires at least a force and a length sensor (70×2 channels). Furthermore if we want to measure also the joint angle we need 70 other channels.
Also the "position board" has 16 channels, nevertheless this time the electronic circuit is simpler than the "Force board". Indeed the signal of the position sensor doesn't need amplification and can be sent directly to the multiplexer.

Force Sensors

As for the Golgi tendon organ, the force sensor is able to measure the tension applied by the artificial muscle on the arm's link. In commerce there are not force sensors that satisfy my needs: small size and cheap. Therefore also in this case I developed my own specific system. The force in a normal size artificial muscle can change between 0-100N, therefore I was able to realize a small sensor using a curved lamina made of aluminium and a strain gauge. The strain gauge was attached to the lamina using a special glue (Figure 7.13), therefore when this lamina is pulled it deforms the strain gauge, changing its resistance.

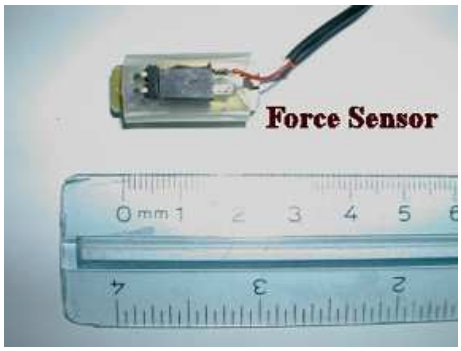

Figure 7.13: Force Sensor

The signal generated by the Wheatstone bridge is in the order of few mV therefore should be amplified at least 10^3 times. Important is the power supply for the sensor which should perfectly stabilized and noise free, otherwise after the amplification stage the noise is comparable with the signal. In figure 7.14 we can see the characteristic for a small size force sensor. As it is possible to see the characteristic is quite linear.

Muscle Length Sensors

In order to measure the muscle length we needed a sensor to be connected in parallel with the artificial muscle. This was a problem because there are some actuators, like the pectoralis, that are a little curved. Furthermore the muscle length is about 30cm and this means that the length of the sensor should be at least the same.
The artificial muscle when contracts, became shorter in the same way in each of its portions. Therefore it is possible to calculate its length measuring the length of one of its parts. The sensor that I used is called a flex sensor, it works on the piezo-resistive effect. When it is flexed

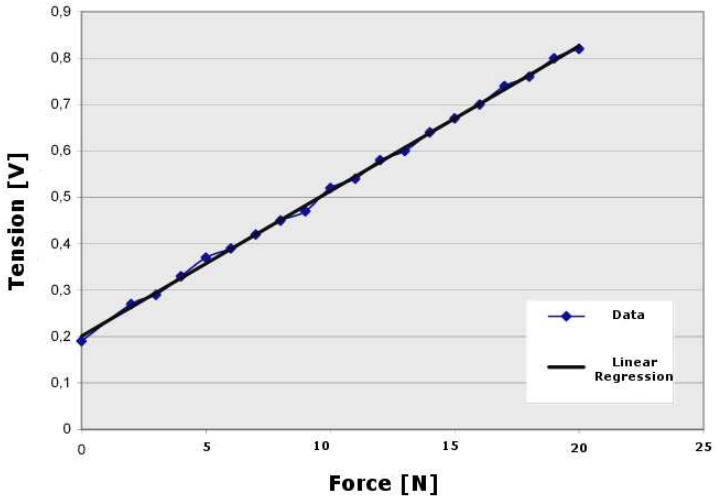

Figure 7.14: Force Sensor Characteristic

changes its resistance (Figure 7.15) in the order of Kohm, therefore the signal doesn't need amplification.

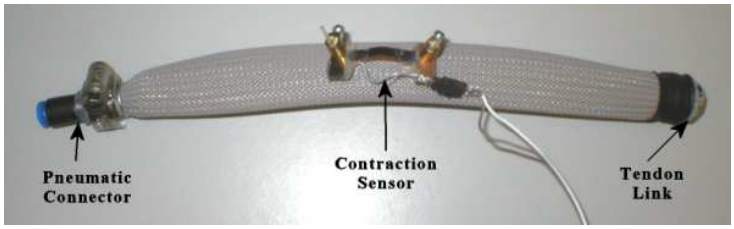

Figure 7.15: The artificial muscle with in parallel the Length Sensor

Joint Position Sensors

In the prototype the elbow position can be measured using the length measure of the triceps and biceps actuators, or using the joint sensor which is more precise. This consists in a rotative potentiometer that is connected with the body at the upper arm and with the rotor at the forearm (Figure 7.16).

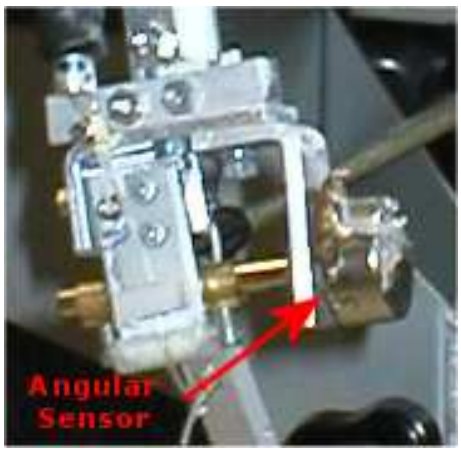

Figure 7.16: Elbow's angular Sensor

7.3 Actuation of Basic Arm Movements

In this section I will show some basic movements that can be obtained with our arm prototype. Furthermore I will show how these movements are comparable with those of the natural limb. Relative to similar systems [36], [7] our arm has a real three degrees of freedom shoulder actuated by five artificial muscles, that make it able to perform more natural movements, comparable with those of the human limb.

7.3.1 Arm Flexion and Extension

In this first movement the flexor actuators are contracted. In particular the shoulder joint is flexed by the deltoid and the elbow by the biceps. The other actuators can be partially activated, but their action should not block the joint's rotation.

Thanks to the independent actuation of the two joints, it is also possible to flex only the elbow maintaining the shoulder fixed; in this case only the biceps should be contracted and the triceps released. Or flex the shoulder maintaining the elbow extended ; for this action the deltoid should be contracted and the dorsal released. The elbow actuation differs from the natural counterpart because of triceps and biceps actuators are "monarticular", whereas the natural muscle effects both the shoulder and the elbow movements. In a robotic arm this simplifies the arm control, so the two movements can be regulated with two different reflex modules.

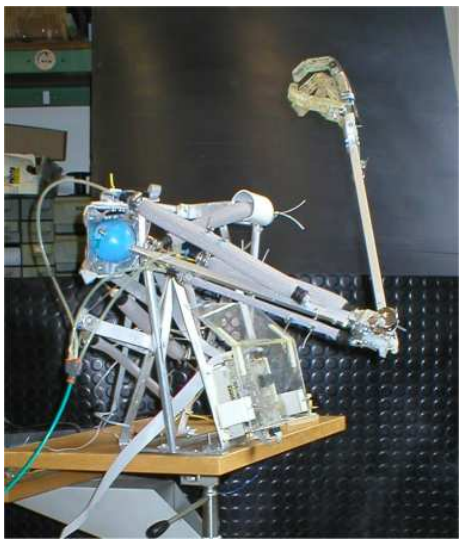

Figure 7.17: Flexion of the Arm's joints

7.3.2 Arm Abduction Adduction

In the arm adduction and abduction only the shoulder artificial muscles are involved in the movement. In particular to perform the adduction the pectoralis and the deltoid should be activated. The deltoid is partially activated and its action fixes toward which part of the trunk the arm is adducted, while the pectoralis pulls the upper arm toward the trunk.

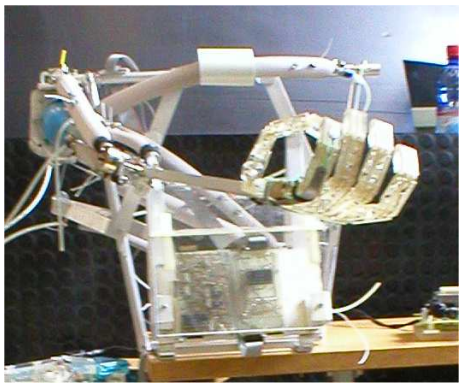

Figure 7.18: Adduction of the Arm

During the abduction movement the actuators activated are the deltoid an the dorsal. In particular to facilitate the movement it is best to flex the shoulder with the deltoid and then contract the dorsal. This

increments the torque that the dorsal actuator can apply on the shoulder joint.

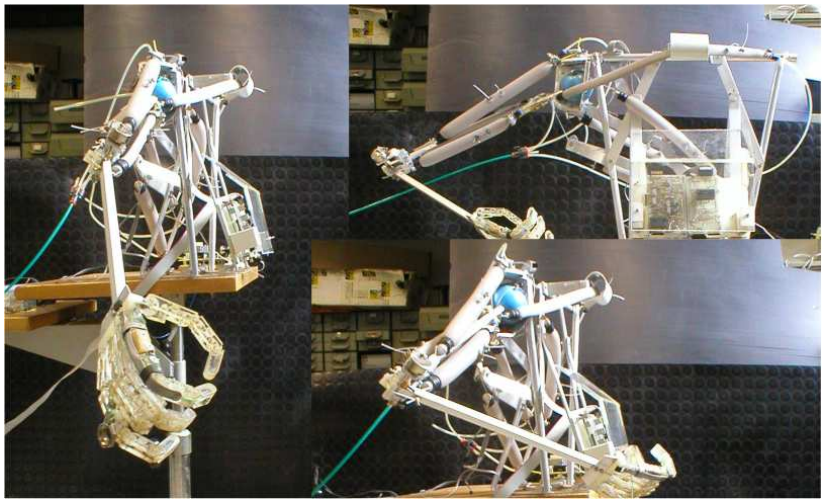

Figure 7.19: Abduction of the Arm

7.3.3 Shoulder Rotation

The shoulder rotation is possible thanks to the supraspinatus and the subscapularis actuators. Since there is not enough space to connect the actuators directly to the shoulder joint, the movement is transmitted by a tendon that is fixed to the joint by a rotative screw.

Figure 7.20: The tendon that permits the Shoulder rotation

This device permits the tendon to rotate but not slide; the action of these two muscles is independent from the action of the other shoulder's

actuators.

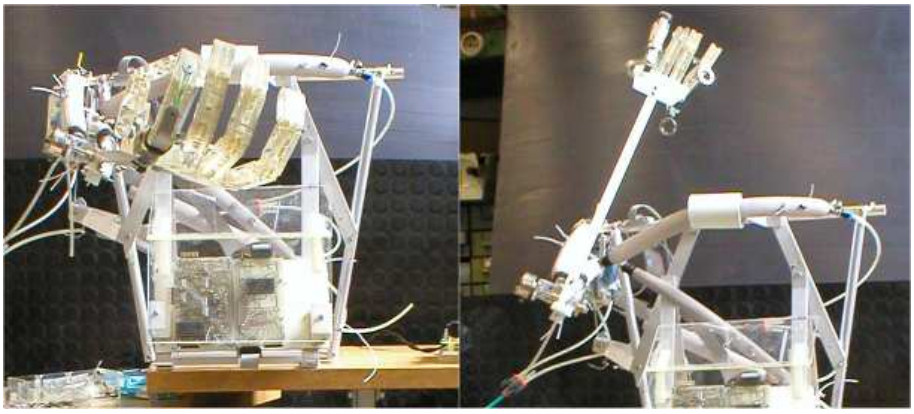

Figure 7.21: Shoulder Rotation

7.4 Preliminary Experimental Results

After having verified the movement capability of our arm, I started a series of experiments with the aim of testing:

- a single joint motion
- the effect of an external force on the joint's position
- the effect of the actuators force on the joint stiffness

In this phase of the arm experimentation I did not activate the control system, and only one joint was taken into consideration. The experiments were conducted on the elbow joint, therefore only the biceps and triceps actuators were involved the movement. Each actuator was equipped with a force sensor applied at the extremity connected with the upper arm, and with a length sensor applied at its external side. I measured also the elbow position using a supplementary angular sensor. In order to control the pressure inside the actuators I used four proportional electro-valves, two of which were connected with a pneumatic circuit. It was possible to control the pneumatic circuit pressure from zero to 7 bars using a manual regulator. The joints and the actuators velocity and acceleration were obtained by interpolating the position data and applying a numerical derivation. Data have been recorded on a personal PC for subsequent elaboration. The single experiment was repeated 5 times and the final data have been obtained by averaging the values recorded by the five experiments.

7.4.1 Single joint Motion

In this experiment I flexed and extended the elbow's joint and measured the whole system's variables. Data was sampled with a frequency of 0.1 KHz and processed directly by the target PC. In order to flex the elbow the biceps and the triceps were co-activated. The co-activation was needed in order to limit the joint velocity and to avoid over-elongations. The pressure inside the two actuators was gradually incremented with two different rates, in order to guarantee the predominance of the biceps torque over that of the triceps.

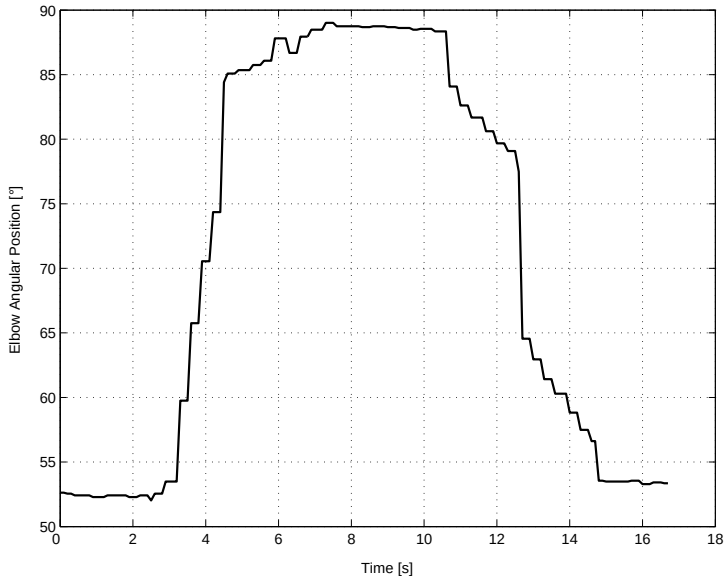

Figure 7.22: The Elbow Angular Position during the flexion-extension

In figure 7.22 we can see the trend of the elbow position; in particular the joint started from a position of 52^o and is flexed as far as 88^o. To obtain the angular velocity I interpolated with a 10^{th} order polynomial the data representing the positions and then I applied a numerical derivation. This gave me an approximation of the elbow's velocity, whose trend is shown in figure 7.23. As it is possible to see the velocity of the elbow reaches a maximum value of $17^o/s$.

In picture 7.24 the biceps and triceps lengths during the elbow movement are reported. I observe that the length variation is different for the two artificial muscles, due to the fact that they are connected in a different way to the forearm.

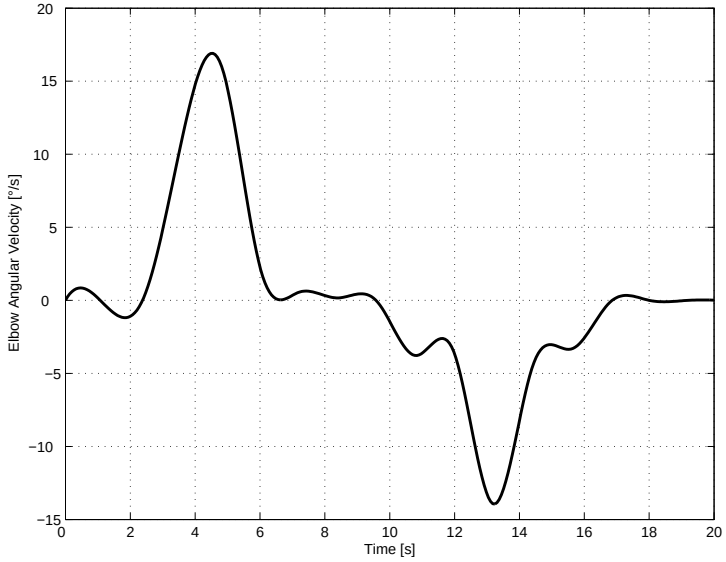

Figure 7.23: The Elbow Angular Velocity during the flexion-extension

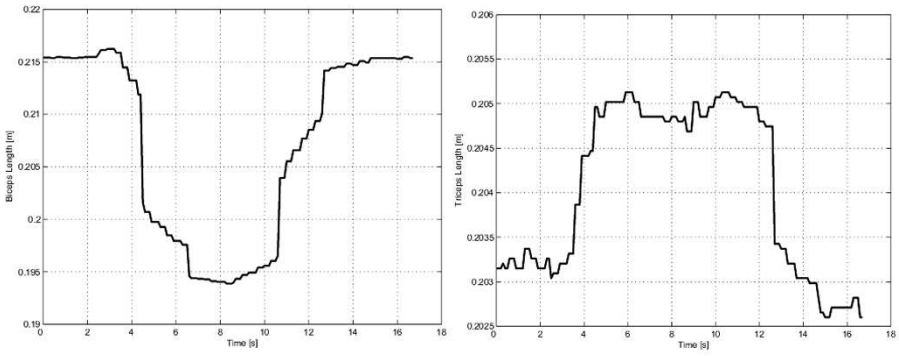

Figure 7.24: Biceps Length

7.4.2 Effect on the joint position of a Noise Force

In this experiment I moved the elbow joint to a fixed position and subsequently I applied at the wrist a noise force. Before the force application the pressure inside the two actuators was fixed at 4 bar, and the elbow flexed at 91.5^o. The force of 5N was applied two times with an interval of one second between the first and the second application.

As we see the force alters the elbow joint position of about 8^o. Between the two peaks there is a difference of 1^o, due to the fact that the force was applied manually using a dynamometer. In the graphics of figure 7.26 are

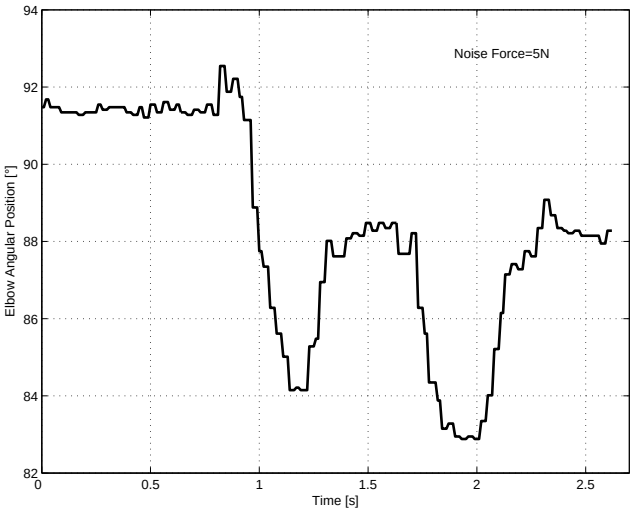

Figure 7.25: Effect on the Elbow position of a Noise force of 5N

reported the biceps and triceps forces measured with the correspondent sensors. As it is possible to see at the beginning the two actuators force are the same, because the actuators during the joint movement reached an equilibrium. After the application of the noise force, the change in the biceps and triceps forces are different, due to the fact that the McKibben actuator presents a hysteresis and therefore the force generated when the actuator decreases its length is different from the force generated when it increases its length.

7.4.3 Effect of the Actuator Co-activation on Joint Stiffness

The concomitant variation in the force of both the agonistic actuators can be used to change the joint stiffness. This permits to regulate the stiffness of the arm's joints during the execution of different tasks. In particular increasing the joint's stiffness makes the arm more immune to disturbance forces. In order to demonstrate this I conducted an experiment where was analyzed the effect of a noise force of 5N on the elbow joint settled at two different rigidities.

As it is possible to see in figure 7.27, when the actuator pressures were increased from 2 to 3Bar the same noise force altered less the elbow's position. This is due to the fact that the actuator forces were increased (Figure 7.28) and with them the joint's stiffness. This strategy is used also in the human limb [96], [49], [97] when it is required to catch an heavy object; in order to compensate the kinetic energy of the object

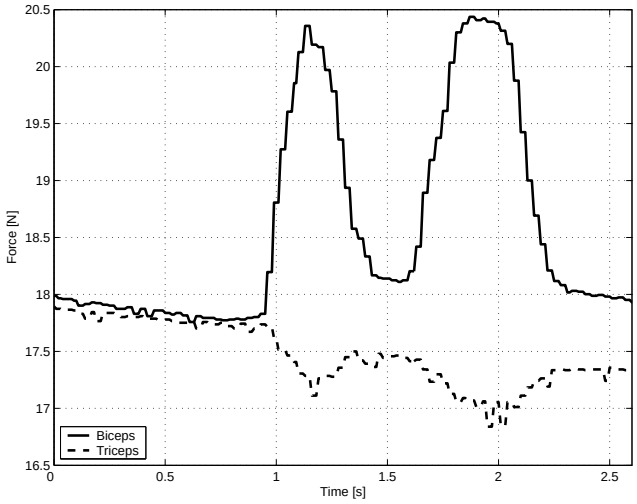

Figure 7.26: Biceps and Triceps Forces

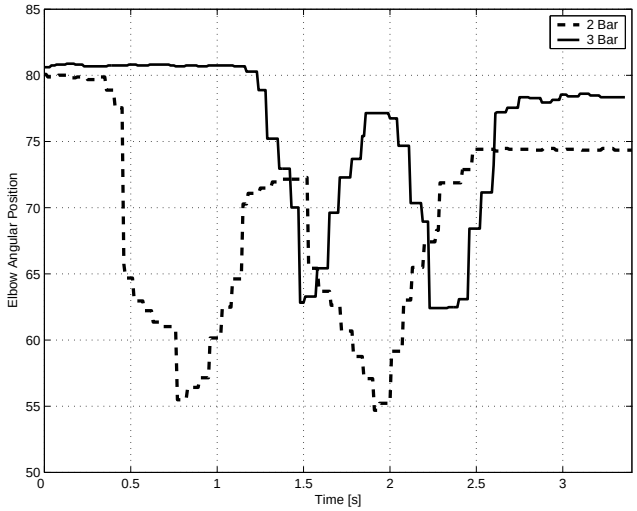

Figure 7.27: Effect of the same noise force (5N) on two different stiffness values

the articulations should change their viscose-elastic characteristic. This is possible by changing the relationship between the muscle's force and length during a isometric contraction (muscle length constant).

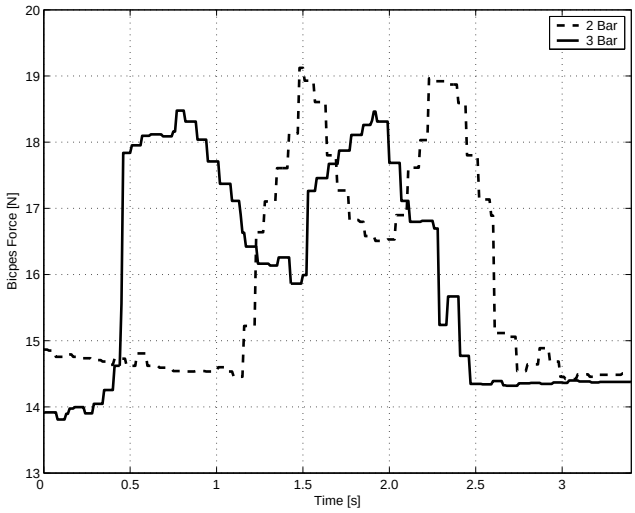

Figure 7.28: Reaction Force in the Biceps actuator during the application of a Noise Force

7.4.4 Myotatic Reflex and Adaptation

In chapter five I have tested the behaviors of the reflex module in controlling the arm model. It was shown that the neural circuit is suitable to regulate the joint's position and to compensate external noise forces. In the reflex module artificial motoneurons set the pressure inside the actuators connected with the joint. This allows to regulate the forces and therefore the torque and the stiffness of the joint. I have also noted the importance of the Ia-interneuron in regulate the activity of the antagonistic motoneuron. Thanks to this cross inhibition when an actuator increases its contraction, due to its length error, the antagonist is released. This behavior allows to save energy during the joint movement and at the same time maintains the joint stiffness under control.
I have done the same testing also on the arm prototype. In this experiment, again, I considered only the elbow joint and therefore the action of the biceps and triceps actuators. As a reference position for the elbow I chose a square function with a period of one second. The signals were sampled every 0.04s and recorded on the Host Pc. We can see the testing results in figure 7.29.

In this experiment the synapses that Ia-interneurons form with the biceps and triceps motoneurons are adaptable. The rule that describes their dynamical behavior was presented in chapter three. The more the synapse is excited the more it increases its efficiency, this in accordance with the Hebbian learning role. In figure 7.30 are reported the weights

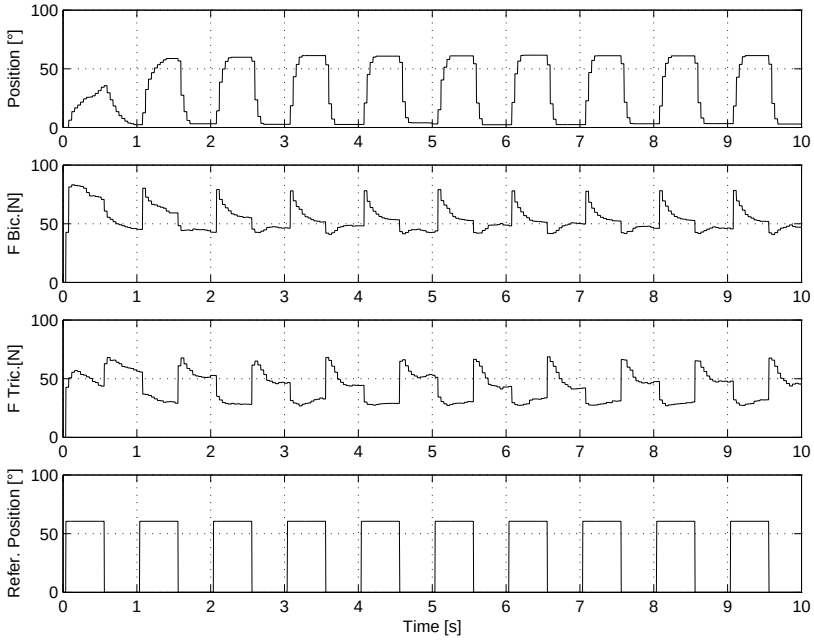

Figure 7.29: Testing of the Reflex Module (Myotatic Reflex)

for the two cross inhibitions. The two weights are initially set to the minimum value, this means that during the first elbow flexion there are not cross inhibition.

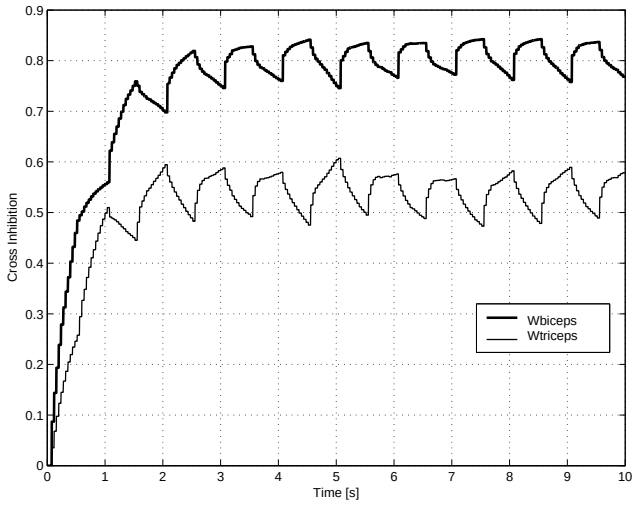

Figure 7.30: Cross inhibition weights in the Elbow Reflex Module

As is possible see in figure 7.30 the two weights reach a stable value after four second. In particular the weight which correspond to the synapse between the biceps Ia-interneuron and the triceps motoneuron reaches a value of 0.8, and the weight of the antagonist counterpart a value of 0.55. These values correspond to the "optimal" control strategy, indeed if we look to the elbow position, after four seconds it follow the reference position quite well. From the graph of picture 7.29 it is possible to note the effect of the cross inhibition, indeed when the elbow is flexing the biceps increases its force and this inhibits the triceps activity and so its force.

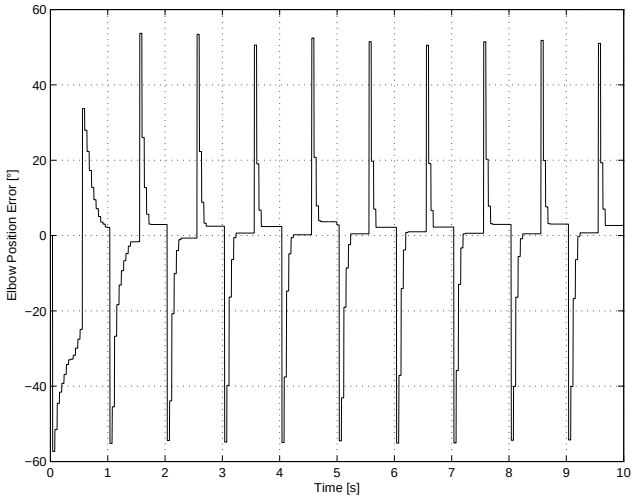

Figure 7.31: Position Error of the Elbow

In figure 7.31is reported the elbow position error. As it is possible see during the first elbow flexion the average error assumes its maximum value.
During the simulations described in chapter five, I demonstrated that the reflex module can compensate for disturbance forces. A similar experiment was done also on the real system. At first the elbow was flexed at 60^o (figure7.32), then at the third second a force of 30N was applied at the wrist in order to increase the elbow flexion. As is possible see in the graph, due to the disturbance force, the elbow changes its position, but at the same time also the triceps and biceps forces change. In particular, to compensate the noise force and extend the elbow, the triceps force increased and the biceps force decreased. We can compare these results with those of figure 7.25, as is possible see without reflex control the elbow position depends strongly on the noise force.

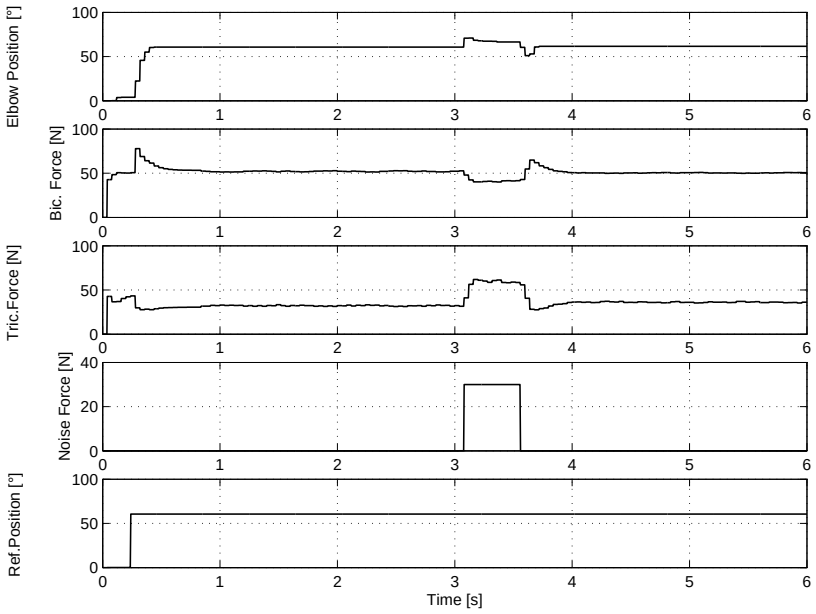

Figure 7.32: Noise Force compensation

In figure 7.33 is reported the trend for the error position in the elbow. As it is possible see, at first there is a big peak due to the fact that the elbow initially is complete extended and it is necessary a certain time to reach the reference position (60^o). After three second the noise force is applied and the position error increases again until it reaches 10^o, at this point the reflex control compensates the noise force and annuls the error. We can also observe that when the noise force is removed there is a negative peak in the position error, this is due to the fact that the reflex control needs a certain time to decrease the triceps force and increase the biceps force. An additional delay in the control loop is due to the fact that the artificial-muscle pressures are regulated by electro-valves that have their own dynamic.

In the last experiment I verified the ability of the reflex control in regulating the elbow stiffness. As underlined before, the capacity to regulate the joint stiffness during the arm operation is crucial in order to execute certain tasks. This is particular true when the robot is expected to collaborate with a human being. In this experiment the elbow was flexed at the angular position of 60^o, but the activity of the biceps and triceps motoneuron were reduced. In figure 7.34 we can see that the reference position was reached again, but the biceps and triceps forces were reduced (in comparison with picture 7.32). This action permits to

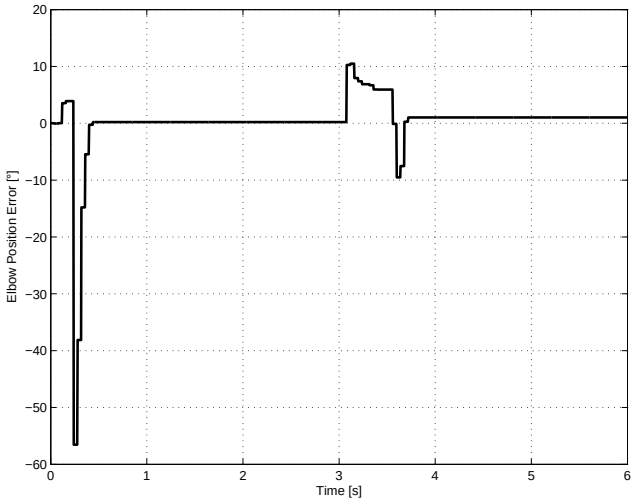

Figure 7.33: Position Error of the Elbow due to the noise force

reduce the elbow stiffness from $3\frac{N}{degree}$ to $1.5\frac{N}{degree}$, indeed when the noise force was applied, this time the elbow had a bigger position variation (figure 7.35).

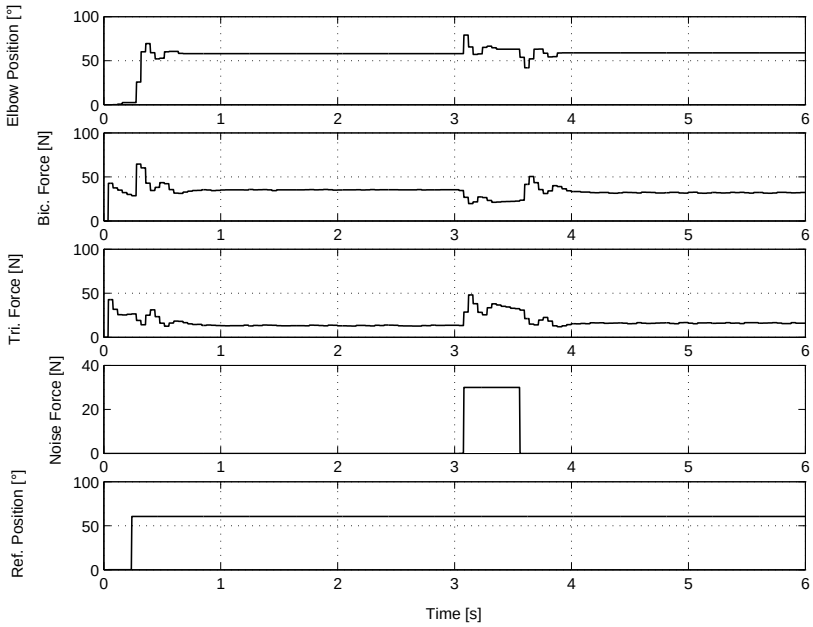

Figure 7.34: Stiffness regulation

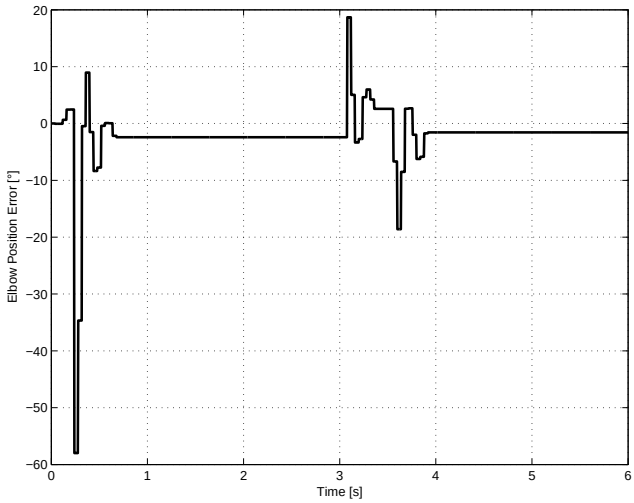

Figure 7.35: Position Error of the Elbow at lower stiffness

8 Conclusion

8.1 Thesis Summary

The main aim of this work was the development of a human-like artificial arm for application in the field of humanoid robotics. Because mimicking the human arm from the mechanical and functional point of view was one of my principal research aims, I conducted an intensive study of the natural limb. Not only did I analyze its physiological characteristics, but because interested in emulating also the strategy of control, I studied the human central nervous system with particular attention to the spinal and cerebellar neural circuits. After this study I concentrated my attention to the design and the implementation of a real human-like robotic arm, and at the same time, to developing a possible control model based on the actual knowledge that neurophysiologists have of the human nervous system.
Our arm differs from other analogous systems [36], [7], [11], by the presence of a full 3DOF shoulder joint moved by five artificial muscles. Furthermore, thanks to the employment of light materials, the system can be integrated with a whole humanoid robot.
During the laboratory activity I was involved in solving many technical and implementation problems. This required me to face the design of new sensors and actuators, and the development of dedicated electronic hardware. In order to experiment with the control architecture and compare its behavior with the human being, I developed also a kinematic and dynamic model of our arm prototype, and used it to conduct different simulations. In particular I concentrated my work on testing a realistic artificial spinal circuit, that showed the capacity to replicate the human myotatic and inverse myotatic reflexes. Furthermore my experiments showed how it is possible apply a bio-inspired control architecture also to an artificial system like our robotic arm. I tested the reflex controller on the elbow joint of our robot and verified its ability to regulate the position also in presence of external noise forces.
During the simulations the control system presented behavior comparable with those of the natural limb, like the tremor that appears in a

human limb when there is a big isotonic co-contraction of the articulation muscles.
I introduced also an innovative reflex controller able to operate on three agonistic artificial muscles that is not based on a biological knowledge of its counterpart, but only on an engineering speculation. Furthermore, I posed a conjecture on a plausible structure for the natural circuit.
After testing the artificial reflexes, I integrated into the control architecture two other modules: the inverse kinematic module, based on a standard multi layer perceptron neural network, and the path generator module. The path generator module evidenced the behavior of generating desired arm movements by smoothly interpolating between a initial and a final target length command for the artificial muscle.
Relative to the Kawamura et al. [36] approach in controlling the bio-inspired arm, based on the studies conducted directly the muscle myoelectric activity, I face the problem of reproducing the internal behavior of the human spinal and cerebellar neural circuits. This permits me to study a general model of the natural reflexes, that can be applied also to control an artificial system like our robotic arm. Furthermore by the simulated experiments I was able to better understand the behavior of the natural limb.
Relative to the Hannaford et al. research [15], [19], [7] I expanded the control architecture in order to operate a four degree of freedom arm moved by seven artificial muscles. Furthermore I integrated it also with an inverse kinematic module and a cerebellar module. The cerebellar model, relative to the research of Grossberg-Bullock et al. [37], [38], [39], [40] is expanded using a layer of 100 granule cells and a layer of 7 purkinje cell,in order to control the seven motoneurons activity during fast movements.
Relative to more standard approaches [85], [98]in controlling the McKibben actuated artificial arm, I showed that a bio-inspired controller has comparable performance and its architecture can be applied to very complex kinematic robotic systems, and therefore is suitable for humanoid robotics. Nevertheless the control architecture is intrinsically parallel, therefore in order to be competitive with standard control systems, needs an hardware implementation. This in order to speed up the solving of the differential equations that represents the natural cells dynamic.

8.2 Future Work

Future works will complete the model and the simulations of the cerebellar module integrated within the whole control architecture. It remains

also to clarify its effectiveness in predicting the arm dynamic and improve the fast reaching movements. Also the performances of the whole system in following a predefined trajectory should be improved, maybe considering a single reflex module in order to govern the shoulder joint. The control architecture should be implemented and tested on the arm prototype and the performances should be compared with the model predictions. In order to perform a reaching grasp it is necessary furnish the arm with an anthropomorphic artificial hand (actually under development) and a stereoscopic vision system. Indeed vision in humans holds an important role in coordinating the arm movements and adjusting the hand trajectory.
In real, the true hope and dream of the visionary author of this manuscript is to work, in the future, on a full size intelligent humanoid robot, able to help humans being in their everyday life and to contribute to the humanity progress.

Bibliography

[1] A. V. Hill, "The heat of shortening and the dynamic constants of muscle," *Proceedings of the Royal Society London*, vol. B 126, pp. 136–195, 1938.

[2] L. Massone and E. Bizzi, "A neural network model for limb trajectory formation," *Biological Cybernetics*, vol. 61, pp. 417–425, 1989.

[3] Milos Zefran, Vijay Kumar, Greg Garvin, and Jaydev Desai, "Experimental investigation of human two-arm manipulation," *International Conference on Mechanics in Medicine and Biology*, 1996.

[4] Walter Maurel and Daniel Thalmann, "A case study on human upper limb modelling for dynamic simulation," *Computer Methods in Biomechanics and Biomedical Engineering*, vol. 2, no. 1, pp. 65–82, 1999.

[5] R.D. Beer, H.J. Chiel, R.D. Quinn, and R.E. Ritzmann, "Biorobotic approaches to the study of motor systems," *Current Opinion in Neurobiology*, vol. 8, no. 6, pp. 777–782, 1998.

[6] Giorgio Metta, *Babyrobot A Study on Sensori-motor Development*, Ph.D. thesis, University of Genoa, 1999.

[7] Blake Hannaford, Jack M. Winters andChing Ping Chou, and Pierre-Henry Marbot, "The anthroform biorobotic arm: A system for the study of spinal circuits," *Annals of Biomedical Engineering*, vol. 23, pp. 399–408, March 1995.

[8] K. Kawamura, R.A. Peters II, D.M. Wilkes, W. Alford, and T. Rogers, "Isac: Foundations in human-humanoid interaction," *IEEE Intelligent Systems*, vol. 15, no. 4, pp. 38–45, Jul/Aug 2000.

[9] B. Webb, "Can robots make good models of biological behaviour?," *Behavioural and Brain Sciences*, vol. 24, no. 6, pp. 1033–1094, 2001.

[10] P. Dario, E. Guglielmelli, V. Genovese, and M. Toro, "Robot assistant: Application and evolution," *Robotic and Autonomous Systems*, vol. 18, no. 1-2, pp. 225–234, July 1996.

[11] Rodney Brooks, Cynthia Breazeal, Matthew Marjanovic, Brian Scassellati, and Matthew Williamson, "The cog project: Building a humanoid robot," *Computation for Metaphors, Analogy and Agents*, vol. LNCS 1562, pp. 52–87, January 1999.

[12] Robert Ambrose, Scott Askew, William Bluethmann, Myron Diftler, and Martin Lockheed, "Humanoids designed to do work," *Proc. IEEE-RAS Humanoids2001 Conference,Tokyo,Japan*, pp. 173–180, November 2001.

[13] Stefan Schaal, "Is imitation learning the route to humanoid robots?," *Trends in Cognitive Sciences*, vol. 3, no. 6, pp. 233–242, June 1999.

[14] Mourad El. Gamal, Atsusshi Kara, Kazuhiko Kawamura, and Mobolaji Fashoro, "Reflex control for an intelligent robotics system," *Proceeding of the 1992 IEEE/RSJ Intelligent Robots and System*, vol. 2, pp. 1347–1354, July 1992.

[15] Blake Hannaford and Ching-Ping Chou, "Study of human forearm posture maintenance with a physiologically based robotic arm and spinal level neural controller," *Biological Cybernetics*, vol. 76, pp. 285–298, 1997.

[16] G. K. Klute and B. Hannaford, "Accounting for elastic energy storage in mckibben artificial muscle actuators," *ASME Journal of Dynamic Systems, Measurement, and Control,*, vol. 122, no. 2, pp. 386–388,, 2000.

[17] Ching-Ping Chou and Blake Hannaford, "Measurement and modeling of mckibben pneumatic artificial muscles," *IEEE Transactions on Robotics and Automation*, vol. 12, no. 1, pp. 90–102, 1996.

[18] Glenn K. Klute, Joseph M. Czerniecki, and Blake Hannaford, "Mckibben artificial muscles: Pneumatic actuators with biomechanical intelligence," *IEEE/ASME 1999 International Conference on Advanced Intelligent Mechatronics*, 1999.

[19] Blake Hannaford, Kristen Jaax, and Glenn Klute, "Bio-inspired actuation and sensing," *Robotics*, vol. 11, pp. 267–272, November 2001.

[20] Kristen Nicole Jaax, *A Robotic muscle spindle: neuromechanics of individual and ensemble response*, Phd thesis, University of Washington, 2001.

[21] King sun Fu, Rafael C. Gonzalez, and C.S. George Lee, *Robotics: Control, Sensing, Vision, and Intelligence*, McGraw-Hill, 1987.

[22] Patrick van der Smagt, "Cerebellar control of robot arms," *Connection Science*, vol. 10, no. 3-4, pp. 301–320, September 1998.

[23] T. Yabuta and T. Yamada, "Neural network controller characteristics with regard to adaptive control," *IEEE Transactions on Systems, Man, and Cybernetics*, vol. 22, no. 1, pp. 170–177, 1992.

[24] K. S. Narendra and K. Parthasarathy, "Identification and control of dynamical systems using neural networks," *IEEE Transactions on Neural Networks*, vol. 1, no. 1, pp. 4–27, 1990.

[25] A.G. Barto, "Reinforcement learning," *The Handbook of Brain Theory and Neural Networks, The MIT Press, Cambridge, Massachusetts*, pp. 804–809, 1995.

[26] Jun Izawa, Toshiyuki Kondo, and Koji Ito, "Biological robot arm motion through reinforcement learning," *IEEE International Conference on Robotics and Automation*, pp. 3398–3403, May 2002.

[27] C.G. Atkeson, J. Hale, M. Kawato, S. Kotosaka, F. Pollick, M. Riley, S. Schaal, S. Shibata, G. Tevatia, and A. Ude, "Using humanoid robots to study human behaviour," *IEEE Intelligent Systems*, vol. 15, no. 4, pp. 46–56, 2000.

[28] S. Schaal, *Learning from demonstration*, MIT Press, 1997.

[29] D. M. Gorinevsky, "Modeling of direct motor program learning in fast human arm motions," *Biological Cybernetics*, vol. 69, pp. 219–228, 1993.

[30] R. A. Jacobs and M. I. Jordan, "Learning piecewise control strategies in a modular neural network architecture," *IEEE Transactions on Systems, Man, and Cybernetics*, vol. 23, no. 2, pp. 337–345, 1993.

[31] H. Gomi and M. Kawato, "Recognition of manipulated objects by motor learning with modular architecture networks," *Neural Networks*, , no. 4, pp. 485–497, 1993.

[32] Mitsuo Kawato, Y. Uno, M. Isobe, and R. Suzuki, "Hierarchical neural networkmodel for voluntary movement with application to robotics," *IEEE Control Systems Magazine*, pp. 8–16, 1988.

[33] Mitsuo Kawato and M. Katayama, "Virtual trajectory and stiffness ellipse during multijoint arm movement predicted by neural inverse models," *Biological Cybernetics*, vol. 69, pp. 353Ű362, 1993.

[34] M. Folgheraiter and G. Gini, "Blackfingers an artificial hand that copies human hand in structure, size, and function," *Proc. IEEE Humanoids 2000,MIT, Cambridge*, September 2000.

[35] Marek Perkowski Mikhail Pivtoraiko. Michele Folgheraiter, Giuseppina Gini, "Blackfingers a sophisticated hand prosthesis," *Proc. ICORR 2003, International Conference on Rehabilitation Robotics, Korea*, April 2003.

[36] K. Kawamura, R.A. Peters II, D.M. Wilkes, W.A. Alford, and T.E. Rogers, "Isac: Foundations in human-humanoid interaction.," *IEEE Intelligent Systems*, vol. 15, no. 4, pp. 38–45, July/August 2000.

[37] J.L. Contreras-Vidal, Sephen Grossberg, and D. Bullock, "A neural model of cerebellar learning for arm movement control: Cortico-spino-cerebellar dynamics," *Learning and Memory*, vol. 3, pp. 475–502, 1997.

[38] Stephen Grossberg and Daniel Bullock, "A cortico-spinal model of reaching and proprioception under multiple task constraints," *Journal of Cognitive Neuroscience*, vol. 10, no. 4, pp. 425–444, 1998.

[39] J.L Contreras-Vidal, Stephen Grossberg, and Daniel Bullock, "A neural model of cerebellar learning for arm movement control: Cortico spino cerebellar dynamics," Tech. Rep. $CAS/CNS-TR97/003$, Boston University, 677 Beacon Street, Boston, Massachusetts,USA, April 1997.

[40] D. Bullock, J. C. Fiala, and S. Grossberg, "A neural model of timed response learning in the cerebellum," *Neural Networks*, vol. 7, no. 6/7, pp. 1101–1114, 1994.

[41] M. Ito, *The Cerebellum and Neural Control*, Raven Press, New York, 1984.

[42] Peter L. Williams and Roger Warwick, *Anatomia del Gray*, 1985.

[43] Cesare Casella and Vanni Taglietti, *Principi di Fisiologia*, La Guliardica, 1996.

[44] A. J. Vander, J. H. Sherman, and D. S. Lugiano, *Fisiologia dell'Uomo*, Il Pensiero Scientifico, 1980.

[45] Aurelio Bairati, *Anatomia Umana*, Minerva Medica, IV Edizione.

[46] A. A Thomson, *Handbook of anatomy for art students*, Dover publications, New York, 1964.

[47] Luciana Porcher Nedel, *Anatomic Modeling Of Human Bodies Using Phuysically-Based Muscle Simulation*, Phd thesis, Ecole Polythecnique Federale De Lausanne, 1998.

[48] Werner Platzer, *Anatomia Umana, apparato locomotore*, Casa Editrice Ambrosiana, 2000.

[49] AS Bahler, "Series elastic component of mammalian skeletal muscle," *American Journal of Physiology*, vol. 213, no. 6, pp. 1560–1564, 1967.

[50] Arthur E. Chapman, "The mechanical properties of human muscle," *Exercise and Sport Sciences Reviews*, vol. 13, pp. 443–501, 1985.

[51] A.M. Gordon, A.F. Huxley, and F.J. Julian, "The variation in isometric tension with sarcomere length in vertebrate muscle fibres," *Journal Physiology*, vol. 184, pp. 170–192, 1966.

[52] Oswald Steward, *Functional Neuroscience*, Springer, 2000.

[53] O. Oscarsson, "Functional organization of the spino- and cuneocerebellar tracts," *Physiology Review*, vol. 45, pp. 495–522, 1965.

[54] H. C Diener, J. Hore, and J. Dichgans, "Cerebellar dysfunction of movement and perception," *The Canadian Journal of Neurological Sciences*, vol. 20, pp. 62–69.

[55] M. Kawato and H. Gomi, "A computational model of 4 regions of the cerebellum based on feedback-error learning," *Biological Cybernetics*, vol. 68, no. 2, pp. 95, 1992.

[56] J. G. Keating and W. T. Thach, "Nonclock behavior of inferior olive neurons interspike interval of purkinje-cell complex spike discharge in the awake behaving monkey is random," *Journal of Neurophysiology*, vol. 73, no. 4, pp. 1329–1340, 1995.

[57] A. J. Bastian and W. T. Thach, "Cerebellar outflow lesions a comparison of movement deficits resulting from lesions at the levels of the cerebellum and thalamus," *Annals of Neurology*, vol. 38, no. 6, pp. 881–892, 1995.

[58] M. Folgheraiter and G. Gini, "Simulation of reflex control in an anthropomorphic artificial hand," *Proc. VIII ISCSB 2001 (Int Symposiumon Computer Simulation in Biomechanics), Milan, Italy,*, July 2001.

[59] M. Folgheraiter and G. Gini, "Human-like hierarchical reflex control for an artificial hand," *Proc. IEEE Humanoids 2001, Waseda University, Tokyo*, November 2001.

[60] David C. Sterratt, "Locust olfaction synchronous oscillations in excitatory and inhibitory groups of spiking neurons," *Emergent Neural Computational Architectures*, vol. 2036, pp. 270–284, 2001.

[61] G. Kuntimad and H. S. Ranganath, "Perfect image segmentation using pulse coupled neural networks," *IEEE Transaction on Neural Network*, vol. 10, no. 3, pp. 591–598, May 1999.

[62] Y. Omura, "Neuron firing operations by a new basic logic element," *IEEE Electron Device Letters*, vol. 20, no. 5, pp. 226–228, May 1999.

[63] Paul Cisek, Stephen Grossberg, and Daniel Bullock, "A corticospinal model of reaching and proprioception under multiple task constraints," *Journal of Cognitive Neuroscience*, vol. 10, no. 4, pp. 425–444, 1998.

[64] D.O. Hebb, "The organization of behavior: A neuropsychological theory," *New York:Wiley*, 1949.

[65] Daniel Bullock and Stephen Grossberg, "Neural dynamics of planned arm movements:emergent invariants and speed-accuracy properties during trajectory formation," *Psychological Review*, vol. 95, pp. 49–90, 1988.

[66] F. Rosenblatt, *Principles of neurodynamics*, Spartan, 1962.

[67] J.Albus, "A new approach to manipulator control: The cerebellar model articulation controller (cmac)," *Journal of Dynamic Systems, Measurement and Control, Transactions of the ASME*, vol. 97, pp. 270–277, 1975.

[68] W. T. Miller, F. H. Glanz, and L. G. Kraft, "Cmac: An associative neural network alternative to backpropagation," *Proceedings of the IEEE, Special Issue on Neural Networks*, vol. 78, pp. 1561–1567, 1990.

[69] J. C. Houk, "Model of the cerebellum as an array of adjustable pattern generators," *Cerebellum and Neuronal Plasticity*, vol. 148, pp. 249–260, 1986.

[70] N. Schweighofer, M. A. Arbib, and M. Kawato, "Role of the cerebellum in reaching movements: distributed inverse dynamics control.," *European Journal of Neuroscience*, vol. 10, pp. 86–94, 1998.

[71] D. Bullock, J. L. Contreras-Vidal, and S. Grossberg, "Speed scaling and adaptive cerebellar control of renshaw cell and motoneuron gain," *23rd Annual Meeting of the Society for Neuroscience, Washington, DC*, 1993.

[72] Mitsuo Kawato, "Internal models for motor control and trajectory planning," *Current Opinion in Neurobiology*, vol. 9, pp. 718–727, 1999.

[73] Hiroshi Imamizu, Satoru Miyauchi, Tomoe Tamada, Yuka Sasaki, Ryousuke Takino, Benno Putz, Toshinori Yoshioka, and Mitsuo Kawato, "Human cerebellar activity refecting an acquired internal model of a new tool," *Nature*, vol. 403, pp. 192–195, January 2000.

[74] Hiroshi Imamizu, Tomoe Kuroda, Satoru Miyauchi, Toshinori Yoshioka, and Mitsuo Kawato*, "Modular organization of internal models of tools in the human cerebellum," *Neuroscience*, vol. 100, no. 9, pp. 5461–5466, April 2003.

[75] D.M. Wolperta and M. Kawato, "Multiple paired forward and inverse models for motor control," *Neural Networks*, vol. 11, pp. 1317–1329, 1998.

[76] Etienne Burdet, Rieko Osu, David W. Franklin, Theodore E. Milner, and Mitsuo Kawato, "The central nervous system stabilizes unstable dynamics by learning optimal impedance," *Nature*, vol. 414, pp. 446–449, November 2001.

[77] C. Ghez, *Principles of Neural Science*, Appleton and Lange, Norwalk, Conneticut, third edition, 1991.

[78] C. Ghez, J. Gordon, M. F. Ghilardi, C. N. Christakos, and S. E. Cooper, "Roles of proprioceptive input in the programming of arm trajectories," *In Cold Spring Harbor Symposium of Quantitive Biology*, vol. 55, pp. 837Ű847, 1990.

[79] T. Kohonen, "An introduction to neural computing," *Neural Networks*, vol. 1, pp. 3–16, 1988.

[80] T. Kohonen, *Self-Organization and Associative Memory*, New York:Springer-Verlag, 1988.

[81] G.S Stent, "A physiological mechanism for hebb's postulate of learning," *Proceedings of the National Academy of Sciences of the USA*, vol. 70, pp. 997–1001, 1973.

[82] M. Ito, "The cellular basis of cerebellar plasticity," *Current Opinion in Neurobiology*, vol. 1, pp. 616–620, 1991.

[83] Simon Haykin, *Neural Network A Comprensive Foundation*, Macmillan College Publishing Company, 1994.

[84] J.J. Craig, *Introduction to Robotics: Mechanics and Control*, Addison-Wesley, 2nd edition, 1989.

[85] B. Tondu and P. Lopez, "Modeling and control of mckibben artificial muscle robot actuators," *IEEE Control Systems Magazine*, vol. 20, no. 2, pp. 15–38, April 2000.

[86] M. W. Hirsch, "Convergent activation dynamics in continuos time networks," *Neural Networks*, vol. 2, pp. 331–349, 1989.

[87] M. W. Hirsch and S. Smale, "Differential equations, dynamical systems, and linear algebra," *New Yourk: Academic Press*, 1974.

[88] M. W. Hirsch, "Convergence in neural nets," *1st IEEE International Conference on Neural Networks, San Diego, CA*, vol. 2, pp. 115–125, 1987.

[89] F. J. Pineda, "Dynamics and architecture in neural computation," *Journall of Complexity*, vol. 4, pp. 216–245, 1988.

[90] F. J. Pineda, "Generalization of back-propagation to recurrent neural networks," *Physical Review Letters*, vol. 59, pp. 2229–2232, 1987.

[91] W. R. Ashby, *Design for a Brain*, Wiley, 2nd edition, 1960.

[92] N. Rashevsky, "Mathematical biophysics," *University of Chicago Press*, 1938.

[93] A. J.Bastian and W. T. Thach, "Cerebellar outflow lesions a comparison of movement deficits resulting from lesions at the levels of the cerebellum and thalamus," *Annals of Neurology*, vol. 38, no. 6, pp. 881–892, 1995.

[94] A. J. Bastian, J. W. Mink, and W. T. Thach, "A specific movement deficit due to focal lesion of the inferior cerebellar vermis in children," *Annals of Neurology*, vol. 40, no. 2, pp. 121–121, 1996.

[95] J.Albus, "A theory of cerebellar function," *Mathematical Bioscience*, vol. 10, pp. 25–61, 1971.

[96] AS Bahler, "Modeling of mammalian skeletal muscle," *IEEE Transactions of Bio-Medical Engineering*, vol. 15, pp. 249–257, 4 1968.

[97] HJ Ralston, MJ Polissar, VT Inman, JR Close, and B Feinstein, "Dynamic features of human isolated voluntary muscle in isometric and free contractions," *Journal of Applied Physiology*, vol. 1, no. 7, pp. 526–533, 1949.

[98] Giovanni Tonietti and Antonio Bicchi, "Adaptive simultaneous position and stiffness control for a soft robot arm," *Proc. IEEE Int. Symp. Intelligent Robots and Systems*, pp. 1992–1997, October.